STIFTELSEN SVENSK BERGTEKNISK FORSKNING
SWEDISH ROCK ENGINEERING RESEARCH

OCH SVENSKA BERGMEKANIKGRUPPEM
AND SWEDISH NATIONAL GROUP ISRM

SVENSKA BIDRAG TILL ISRM:s TIONDE INTERNATIONELLA BERGMEKANIKKONGRESS GAUTENG 2003

Swedish Contributions to 10th International Congress on Rock Mechanics Gauteng 2003

Reprinted from the 10th ISRM Congress Proceedings
held from 8 – 12 September 2003 in Sandton, South Africa.

CONTENTS page

Ansell, A., Malmgren, L. The response of shotcrete to blast induced vibrations in mining.
ISRM 2003–Technology roadmap for rock mechanics, South African Institute of Mining and Metallurgy, 2003.

The response of shotcrete to blast induced vibrations in mining

Anders Ansell*, Lars Malmgren**
* Concrete Structures, Royal Institute of Technology (KTH), Stockholm, Sweden
** LKAB R&D, Sweden and Division of Rock Mechanics, Luleå University of Technology, Luleå, Sweden

This paper deals with the influence from blast induced stress waves on the performance of shotcrete support in the Kiirunavaara mine. Time histories of stress waves from blasting were obtained from measurements during production blasts in the mine, followed by failure mapping. A finite element model, consisting of beam and spring elements, was used to calculate the shotcrete response to vibrations from blasting. The modelling approach was similar to that of a building during an earthquake, with accelerations measured in-situ used as loads. The analysis showed that the calculated adhesive stresses exceeded the strength in the interface between rock and shotcrete near to the blasted ring. It also indicated that tensile rock failure did occur. These types of failure will presumably result in ejection of joint defined rock blocks or rock slabs and will require a ductile support, such as fibre reinforced shotcrete. The predicted failure was confirmed by the mapping, which also showed that the zone of failed shotcrete was much larger in areas with plain shotcrete compared to areas with reinforced shotcrete.

L'influence de l'onde de pression générée par les sautages à la mine de fer de Kiruna sur la performance du béton projeté est étudiée dans le présent article. Les ondes créées par les sautages ont été enregistrées et les domages résultants ont été cartographiés. La réponse du béton projeté aux vibrations de sautage est étudiée à l'aide d'un modèle d'éléments finis, constitué de poutres et de ressorts. L'approche est similaire à celle d'un immeuble subissant un tremblement de terre, avec les accélérations internes utilisées comme charges. L'analyse montre qu'à proximité des sautages, la contrainte adhésive dépasse la résistance de l'interface roche-béton. L'analyse confirme aussi l'existence de ruptures en tension. Ces types de rupture induisent probablement l'éjection des blocks définis par les structures du massif rocheux et requierent un support ductil, comme du béton projeté renforcé par exemple. Le type de rupture est confirmé par les observations de terrain, qui montrent aussi une extension plus importante des domages lorsque le béton projeté n'est pas renforcé.

In diesem Konferenzbeitrag geht es um den Einfluss, der aus einer Sprengung hervorgerufenen Schwingungswellen auf die Ausführung der Spritzbetonverstärkung in dem Kiirunavaara Bergwerk. Die Aufzeichnungen der Schwingungswellen von Sprengungen gemäß einer Fehlerkartierung beziehen sich auf Messungen, die während der Sprengungen durchgeführt wurden. Ein Finite Elemente Modell, bestehend aus Stab- und Federelementen, wurde für die Berechnung der Spritzbetondeformation in Bezug auf die Schwingungen aus Sprengungen angewendet. Die Modellierungsmethode war ähnlich der eines Gebäudes während eines Erdbebens anhand der gemessenen Beschleunigungen vor Ort, die als Lasten benutzt wurden. Die Untersuchung hat gezeigt, dass die berechnete Haftspannung größer war als die Festigkeit in der Verbindung zwischen Gestein und Spritzbeton in der Nähe des Sprengungscentrums. Die Analyse hat gezeigt, dass die Zugfestigkeit des Gesteins versagte. Diese Arten von Versagen werden als Folge der Herausnahme von Gesteinsbrocken oder Gesteinsplatten erklärt und benötigen eine faserverstärkte Spritzbeton. Das vorausgesagte Versagen bestätigte sich beim Kartieren, welches auch zeigte, dass die Zone des versagenden Spritzbetons in Bereichen mit unverstärktem Spritzbeton viel größer war als in Bereichen mit armierten Spritzbeton.

Background

In many mines, the openings are subjected to dynamic loads that can give serious damage to underground structures. Important examples are rock bursts and vibration loads from detonation of explosives. Close to the drawpoint, the dynamic influence from the production blasting is significant. It is therefore important to secure the profile of the cross cut to provide a safe working environment for the miners and to allow mining of the right ore quality with a proper mass flow. The Kiirunavaara mine, situated in Kiruna in the northern of Sweden, has an annual production of approximately 20 million tonnes of iron ore. The ore body is 4000 m long, 80–100 meters wide and extends to an estimated depth of 2000 m, striking nearly North-South and dipping 60° to the East. The mining method used is large scale sublevel caving, as shown in Figure 1. One ring for the production blasting normally consists of 11 blasting holes with the diameter of 115 mm, as shown in Figure 2. The distance between each ring is 3 m. Detailed descriptions of important features of the large scale sublevel caving in the Kiirunavaara mine are given by Quintero et al.[1]

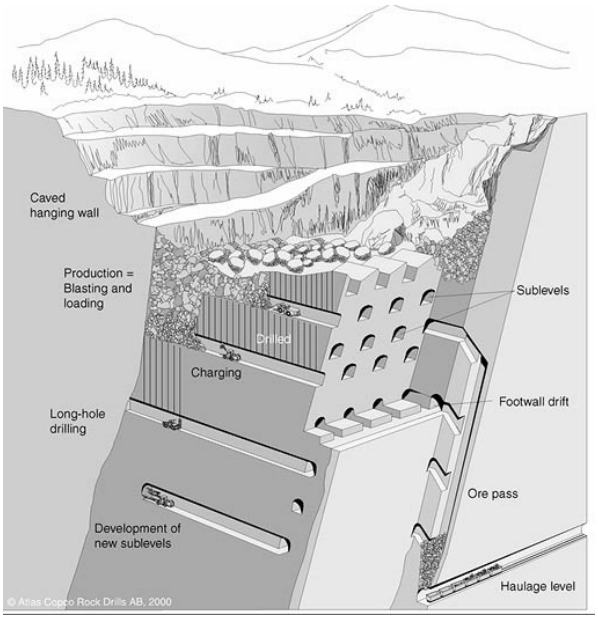

Figure 1. Principles of large scale sublevel caving. From Atlas Copco.[2]

This paper deals with the influence from blast induced stress waves on the performance of shotcrete support in the mine. Acceleration time histories of stress waves from blasting were obtained from measurements during production blasts.[3] The vibration measurements were done 4.5 to 14 m from the blast holes as shown in Figure 3. Two accelerometers were assembled in one hole with the measurement directions as shown in Figure 4. The vibration measurements showed a wide scatter of magnitudes of the particle accelerations, which was expected. The maximum particle velocity was 1.1 m/s at a horizontal distance of 4.5 m away from the blast holes. Furthermore, field observations[3] showed that failures in steel fibre reinforced shotcrete could be observed from the drawpoint and to a horizontal distance of 1–4 m away from that point. Failures in plain shotcrete occurred over a larger area, with a limit at 3–9 m. This was also confirmed by a numerical study[3] of the dynamic response of a rock prism supported by shotcrete, as seen in Figure 5. The recorded vibrations were used as external loads in the analyses. The adhesive strength between shotcrete and rock has been investigated several times, indicating that normal values for the adhesive strength in the mine are 0.3–0.4 MPa.

The vibration resistance of young, plain shotcrete was investigated through a series of accelerometer-instrumented tests.[4] The measured accelerations were later used as input to a numerical, elastic stress wave model for predicting shotcrete damage.

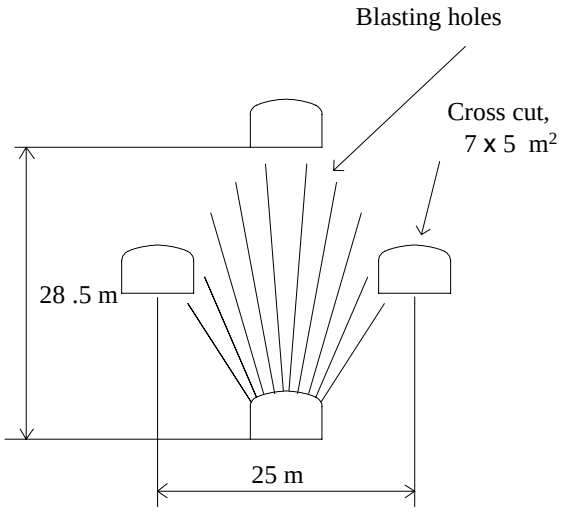

Figure 2. One ring for production blasting in large scale sublevel caving.

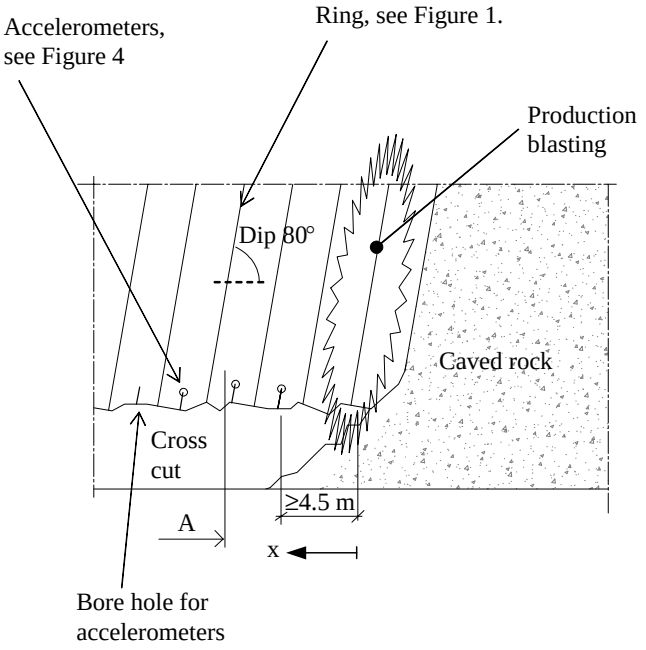

Figure 3. Arrangement of the accelerometers in the cross cut. From Malmgren.[3]

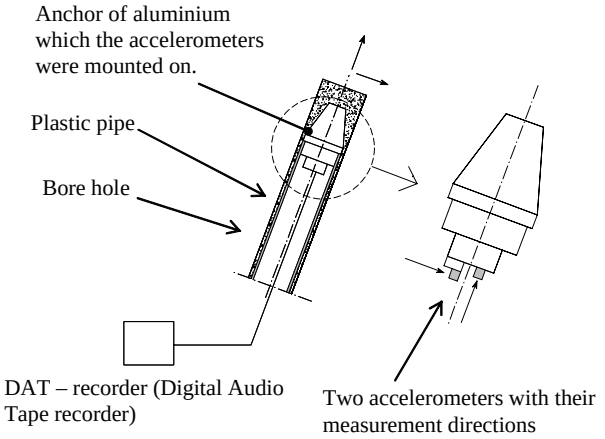

Figure 4. Accelerometers in the bottom of the borehole. From Malmgren.[3]

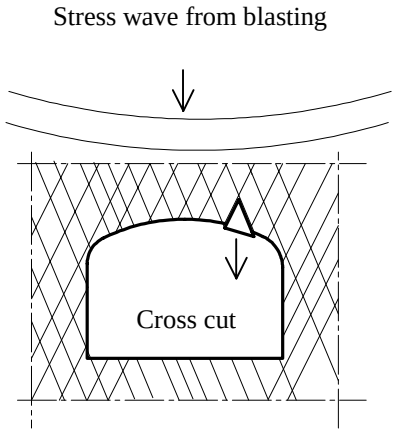

Figure 5. Ejection of a rock prism. From Malmgren.[3]

Finite element model

As a complement to the stress wave model,[4] a finite element model was used to calculate the shotcrete response to vibrations from blasting.[5–6] The fundamentals of the model are shown in Figure 6 where a section of rock with shotcrete is modelled using beam elements that represent flexural stiffness and mass. The beams are attached to the ground through elastic springs, also accounting for movement parallel to the rock surface. The maximum allowed spring elongations are governed by the flexural strength of rock and the adhesive strength between shotcrete and rock. The stresses that appear on the adhesive interface between rock and shotcrete are thus proportional to the elongation of the springs. The modelling approach was similar to that of a building during an earthquake, where ground accelerations induce inertia forces. The load was here applied at the degrees of freedom inside the rock as measured time histories of accelerations. Figure 7 shows an example of measured accelerations used in the analyses.

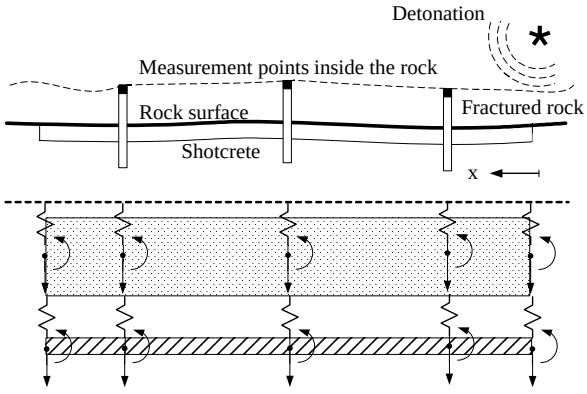

Figure 6. Finite element model of shotcrete and fractured rock, vertical section. Beam elements with transversal and rotational degrees of freedom, interconnected by springs.

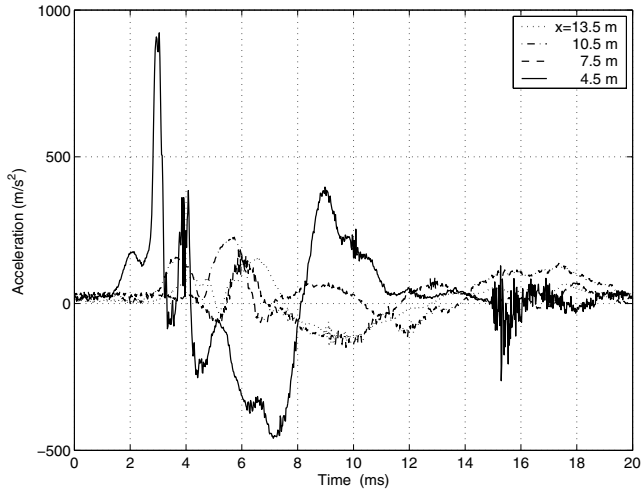

Figure 7. Example of measured accelerations from one production blast sequence in the Kiirunavaara mine.

The response of shotcrete and rock is obtained through mode superposition analysis. For the examples presented, the displacements were calculated using a routine based on Duhamel's integral. The number of possible degrees of freedom, i.e. the number of beam elements, is theoretically unlimited.

The finite element model was used to calculate the shotcrete–rock response to accelerations from eight of the recorded production blasts from the Kiirunavaara mine. The modelled shotcrete was assumed to be 40 mm thick and have a length given by the placement of the measurement points, typically 10–20 m. The shotcrete density was 2100 kg/m^3 and the dynamic Young's modulus was assumed to be 37 GPa with an internal damping of 2.5 %. The spring stiffness was calculated as stress per length or practically as E/h where E is Young's modulus and h the thickness of shotcrete. In the direction parallel to the rock surface, this was replaced by G/h where the modulus of shear was chosen as $G = 0.4E$. The effect of 500 mm fractured rock was accounted for through the choice of material parameters. Due to the heterogeneous nature of rock with discontinuities in the rock mass,[7] the stiffness (Young's modulus) and the strength of the rock was difficult to predict. For the examples presented, the density of rock (iron ore) was 4700 kg/m^3 and Young's modulus assumed to be within 16–40 GPa. The higher limit value corresponds to intact rock while the lower was estimated according to Bieniawski[8] and Serafim and Pereira,[9] corresponding to a RMR value of 58 which is a common value in the mine. To investigate the effect of various choices of Young's modulus was each case first modelled with E = 16 GPa and then with E = 40 GPa. The stiffness of the springs between fractured and intact rock was calculated by inserting rock properties in E/h and G/h. The strength of the rock varies depending on the quality of the intact rock and the properties of the rock joints. When a stress wave arrives at the free surface of an opening, it can cause movement of roof, walls and also the floor. Due to tensile failures of intact rock or separation of (natural) joints, the reflected tensile pulses at the free rock surface can eject pieces and blocks of rock. The tensile strength of the intact rock was assumed to be 15 MPa, or approximately 10 % of the compressive strength of the intact rock. In the case of ejection of rock blocks formed by a joint set, the strength to resist ejection will mainly depend on the strength and orientation of the joints, the (static) stress state and the mass of the block. To predict this strength and to model this behaviour in a continuous model is difficult. Therefore, the tensile strength in this study was assumed to be equal to the strength of intact rock, i.e. 15 MPa which must be assumed to be the upper level of the tensile strength of the rock mass.

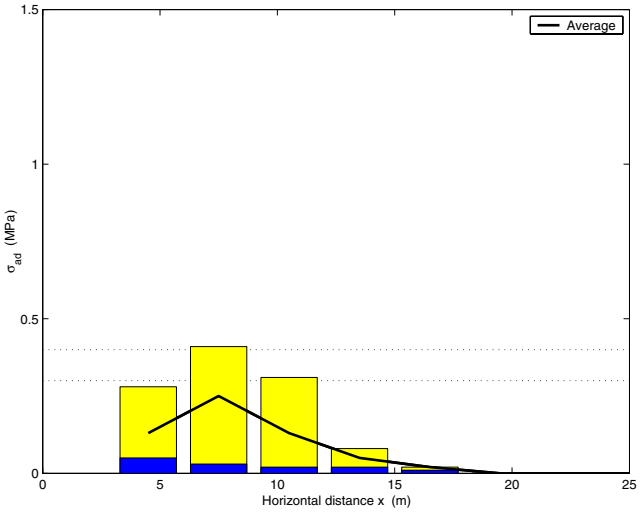

Figure 8. The maximum, minimum and average adhesive stresses σ_{ad} between shotcrete and rock and perpendicular to the rock surface. From eight finite element calculations.

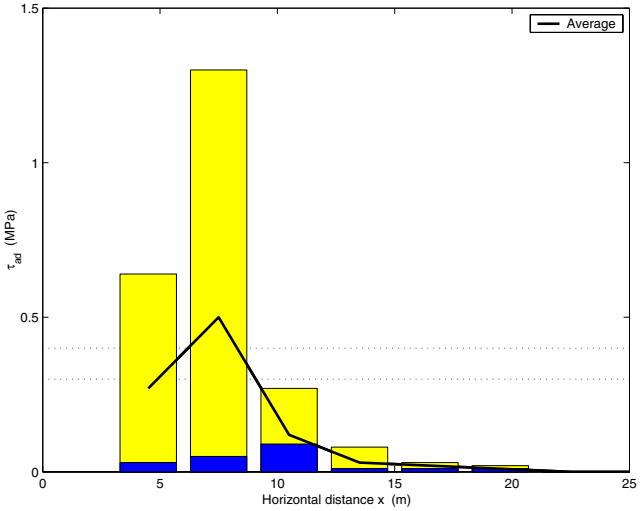

Figure 9. The maximum, minimum and average adhesive stresses τ_{ad} between shotcrete and rock and parallel to the rock surface. From eight finite element calculations.

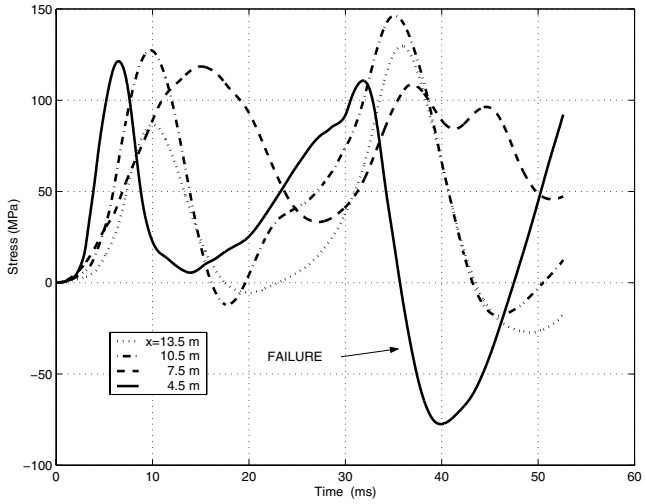

Figure 10. Example of calculated rock stresses, perpendicular to the roof of the cross cut with E = 40 GPa.

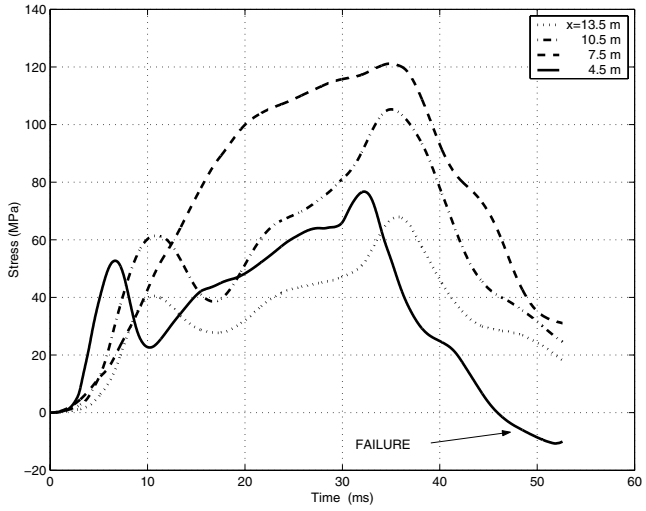

Figure 11. Example of calculated rock stresses, perpendicular to the roof of the cross cut with E = 16 GPa.

Numerical results

The calculated response from the acceleration measurements in the mine were given as vectors of node displacement vs. time. The adhesive stress loads between rock and shotcrete was calculated by use of the stiffness of the elastic springs in the model. The results from eight sets of measurement data are compiled in Figures 8–9. The adhesive stresses between shotcrete and rock, perpendicular to and parallel with the rock surface, are shown as one bar representing each measurement point, i.e. x = 4.5, 7.5, . . . , 22.5 m from the drawpoint, in accordance with Figures 3 and 6. The light area of each bar shows the range of the calculated results while the lines represent average values. The results that were calculated with Young's modulus for rock chosen as 16 and 40 GPa, respectively, only showed minor differences when compared. The shotcrete beams showed very low tensile bending stresses in the order of 20 kPa.

Examples of calculated rock vibrations are given in Figures 10–11, showing rock stresses perpendicular to the roof of the cross cut. The two figures show results calculated from the same acceleration load case but with different choices of Young's modulus for the rock. The initial compressive normal stresses (positive sign) are due to compression of the rock mass caused by incoming stress waves. The calculated tensile stresses >15 MPa indicate that tensile rock failure did occur 4.5 m from the drawpoint for both cases.

Conclusions

It was found that a shotcrete lining partly has the necessary bearing capacity to support rock exposed to blast induced vibrations of the observed type. The calculated results were compared to field observations which showed that the tested finite element model was able to predict adhesive stresses in the interface between rock and shotcrete. In some sections of the tunnel, the stresses exceeded the adhesive strength, as can be seen in Figures 8–9. The results show that it is necessary to anchor the shotcrete lining with rock bolts to prevent adhesive failure close to the drawpoint.

As already mentioned, the calculated tensile bending stresses in the shotcrete were relatively small which indicate that the adhesive strength between rock and shotcrete is crucial for the survivability of shotcrete close to vibrations. The modelling showed that stresses exceeding the adhesive strength of 0.3–0.4 MPa are to be expected within x < 10 m behind the drawpoint. The compiled results in Figures 8–9 show larger stresses at x = 7.5 m than at x = 4.5 m. This may be due to that none of the cases modelled had a shotcrete lining, or included rock, that stretched closer to the drawpoint than 4.5 m. This limit was due to that no measurement points had been placed close to the drawpoint in risk of damaging accelerometers and other equipment. A free end of a spring supported beam gives less resistance to applied forces, whereas an inner section of such a beam is more rigid. Less adhesive stress is thus necessary for the end of the shotcrete to follow the motion of the end of the rock beam. On the other hand, the large scatter of results indicate that there are large variations in the magnitudes of the measured accelerations, especially at x = 7.5 m. This may be an effect of the stress wave propagation between the detonation and point of observation. Stress waves in the shape of P and S waves interact to produce the acceleration components that have been measured in two orthogonal directions. This was not investigated within the project.

The calculated shear stresses in the rock–shotcrete interface τ_{ad} are higher compared to the stresses σ_{ad} perpendicular to the surface. This indicates that a shotcrete lining exposed to this type of vibration loads will, for high magnitudes, fail in shear at the rock–shotcrete interface. On the other hand, there are no reliable in-situ results that give the adhesive shear strength between rock and shotcrete.

Results from other studies[10] have shown that the shear strength in the interface between old concrete and shotcrete may be up to two times higher than that in the perpendicular direction. It can therefore be assumed that the average stress curve in Figure 9 may well be situated below the adhesive shear strength limit.

In some cases, the rock showed large calculated displacement approximately 4.5 m away from the blasted ring, which indicate rock failure as in Figures 10–11. These figures also demonstrate the changes in the rock vibrations that occur as the Young's elastic modulus is changed from 16 to 40 GPa, thus changing the stiffness and natural frequencies of the elastic system. This type of failure will possibly result in ejection of joint defined rock blocks or rock slabs. The results were confirmed by the failure mapping and the dynamic analyses of rock prisms.[3] The conclusion is that this type of load conditions will require a ductile support, such as fibre reinforced shotcrete.

Further research

The further development of the finite element model will include rock bolts, introduced as stiff springs concentrated to some of the nodes in the model. It will be possible to model the reinforcing effect of installation of bolts and this will most certainly lead to larger bending stresses in the shotcrete.

The effect of stress wave propagation from the detonation must be investigated. Stress waves interact with the rock geometry and imperfections in the rock which may give reflection, damping or amplification of the propagating stresses.

More reliable data for estimating the adhesive and shear strength between rock and shotcrete is required. Large scale in-situ testing will preferably be done at the same time as rock and shotcrete mapping, to also get an overview of rock properties and tunnel geometry. Today, there is a problem to obtain reliable data for estimation of the strength at the shotcrete–rock interface. Therefore, the Division of Rock Mechanics at Luleå University of Technology in Sweden and LKAB have started a project to increase the understanding of shotcrete–rock interaction. In laboratory tests, the shear and adhesive strengths will be studied, followed up by in-situ testing and mapping of rock and shotcrete.

References

1. Quinteiro, C., Quinteiro, M., Hedström, O., 'Underground Iron Ore Mining at LKAB, Sweden, Underground Mining Methods', *Engineering Fundamentals and International Case Studies*, Society for Mining, Metallurgy, and Exploration Inc., Editor Hustrulid and Bullock, 361–368, 2001.
2. http://www.atlascopco.com, Atlas Copco AB, Sweden.
3. Malmgren, L., *Shotcrete Rock Support Exposed to Varying Load Conditions*, Licentiate Thesis, Department of Civil and Mining Engineering, Division of Rock Mechanics, Luleå University of Technology, Sweden, 2001.
4. Ansell, A., *Dynamically Loaded Rock Reinforcement*, Doctoral thesis, Bulletin 52, Dept. of Structural Engineering, Royal Institute of Technology, Stockholm, 1999.
5. Ansell, A., *Material Properties for Dynamic Analysis of Shotcrete on Rock*, Technical report 2002:7, Dept. of Civil and Architectural Engineering, Royal Institute of Technology, Stockholm, 2002.
6. Ansell, A., *Finite Element Models for Dynamic Analysis of Shotcrete on Rock*, Technical report 2002:8, Dept. of Civil and Architectural Engineering, Royal Institute of Technology, Stockholm, 2002.
7. Sjöberg, J., *Analysis of large Scale Rock Slopes,* Doctoral thesis, Department of Civil and Mining Engineering, Division of Rock Mechanics, Luleå University of Technology, Sweden, 1999.
8. Bieniawski, Z.T., 'Determining Rock Mass Deformability: Experience from Case Histories', *International Journal of Rock Mechanics and Mining Sciences*, **15**, 237–247 (1978).
9. Serafim, J.L., Pereira, J.P., 'Considerations on the Geomechanical Classification of Bieniawski', *the Int. Symposium on Engineering Geology and Underground Construction*, Lisbon, 1983.
10. Silfwerbrand, J., *Lagning av betongskador med sprutbetong. Försök med balkar under statisk och utmattande last* (*Concrete repair with shotcrete. Tests on beams under static and fatigue load*, in Swedish), Bulletin no 153, Department of Structural Engineering, Royal Institute of Technology (KTH), Stockholm, Sweden, 1988.

Ask, D., Cornet, F.H., and Stephansson, O., Integration of CSIR- and CSIRO-type of overcoring rock stress data at the Zedex Test Site, Äspö HRL, Sweden. ISRM 2003–Technology roadmap for rock mechanics, South African Institute of Mining and Metallurgy, 2003.

Integration of CSIR- and CSIRO-type of overcoring rock stress data at the Zedex Test Site, Äspö HRL, Sweden

Ask, D., Cornet, F.H., Stephansson, O.
Royal Institute of Technology*/Luleå University of Technology*, Institut de Physique du Globe de Paris**, GeoForschungZentrum Potsdam***

We have conducted a stress analysis of overcoring stress measurements undertaken at the Zedex Test Site (ZTS) in the Äspö HRL, Sweden. Two different types of overcoring cells have been used at the site: the 9-gauge Borre Probe (CSIR-type) and the 12-gauge CSIRO HI cell. Inversion programs based on the least-squares criterion were developed and calibrated. The primary and secondary stress field in the ZTS were back-calculated using strain data from individual cells as well as from combining data from both cells. We propose that the combination of strain data from the two cells significantly improves the determination of the stress field. A striking result is the good agreement between the re-analysed overcoring data and the existing hydraulic fracturing data. The deviations for the horizontal stresses between the re-analyzed overcoring data and the existing hydraulic fracturing data are approximately 3 MPa. The deviation in the orientation of maximum horizontal stress is approximately 10-20°.

Nous avons analysé les résultats de mesures de contrainte par surcarottage réalisées sur le site Zedex, du laboratoire souterrain HRL d'Aspö, en suède. Deux types de cellule de mesure ont été utilisés sur ce site : la cellule à 9 jauges (du type CSIR) et la cellule à 12 jauges (du type CSIRO HI). Un programme d'inversion mettant en œuvre une norme par moindres carrés a été développé et validé. Les champs de contrainte primaires et secondaires du site Zedex ont été évalués d'une part en considérant chaque mesure isolément, d'autre part en intégrant l'ensemble des données de déformation dans une inversion unique. Nos résultats suggèrent que l'association des diverses mesures dans une intégration unique améliore nettement la détermination du champ de contrainte. Un résultat intéressant est le bon accord entre ces nouveaux résultats et les résultats des mesures par fracturation hydraulique. Les écarts sur l'amplitude des contraintes horizontales est de l'ordre de 3 Mpa, les écarts sur les orientations de l'ordre de 10-20°.

Auf dem Zedex Test Gelände im Äspö Festgesteinslabor (HRL) wurde eine Spannungsanalyse mittels Overcoring Spannungsmessungen durchgeführt. Hierzu wurden zwei verschiedene Methoden verwendet: das 9-kanal Borre Gerät (CSIR- Ausführung) und die 12-Kanal CSIRO HI Zelle. Inversionsprogramme, die auf dem "least-squares"- Kriterium basieren, wurden entwickelt und kalibriert. Das primäre und sekundäre Spannungsfeld des Zedex Test Geländes wurde sowohl aus Verformungsdaten individueller Zellen als auch aus Kombination beider Zellen ermittelt. Wir nehmen an, daß die Kombination der Messergebnisse beider Geräte die Bestimmung des Spannungsfeldes signifikant verbessert. Überzeugender Beweis hierfür ist die gute Übereinstimmung der überprüften Overcoring Daten und Ergebnisse aus existierenden Hydraulic Fracturing Versuchen. Die Abweichungen der horizontalen Spannungen aus beiden Datensätzen ist etwa 3 MPa und Abweichungen der Orientierung der größten Horizontalspannung liegen bei etwa 10-20°.

Introduction

The Äspö Hard Rock Laboratory (HRL) of the Swedish Nuclear Fuel and Waste Management Co. (SKB), Fig. 1, has been a geoscientific research area since 1986. Among the vast number of research projects conducted are a large number of rock stress measurements. In total, about 250 hydraulic fracturing, overcoring, and hydraulic tests on pre-existing fractures have been made in the region (e.g. [2-6]).

Existing studies indicate a non-linear stress distribution versus depth, which is strongly influenced by existing discontinuities (e.g. [1]; [7-10]). There is also a significant difference between the different measuring techniques used. Thus, despite the large number of measurement collected in this limited area, the stress field is not accurately known.

In this paper we will concentrate on the strain data collected at the Zedex Test Site (ZTS) using the Borre Probe (e.g. [11]) and the CSIRO HI cell (e.g. [12]). All Borre Probe data from the Äspö HRL were recently re-analysed using a new interpretation technique ([13]), which will be briefly presented here. The same analysis is currently being applied on the data from the CSIRO HI cell ([14]).

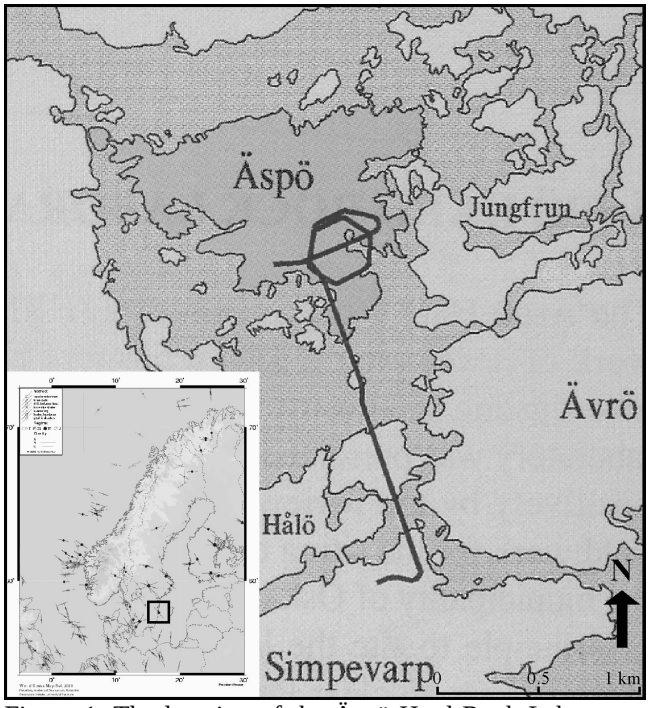

Figure 1. The location of the Äspö Hard Rock Laboratory (HRL), South-eastern Sweden, encircled in the European World Stress Map in the lower left corner. The HRL reaches a depth of about 450 m under the central part of the Äspö Island (After [1]).

The Zedex Test Site

General

The ZTS is located at about 415 m depth in the HRL (Fig. 2). The overcoring data consists of Borre Probe and CSIRO HI measurements in thee and two boreholes, respectively.

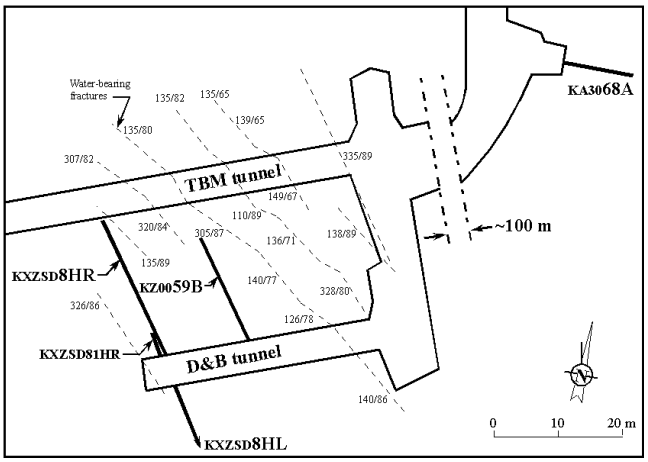

Figure 2. The ZTS with mapped fractures and overcoring rock stress measurement boreholes. Note the cut in the figure between the ZTS and borehole 68A. (Modified after [3] and [17]).

The two cells indicated large differences and the data were therefore analyzed by Myrvang[15], who concluded that the differences between the cells were mainly due to poorly conducted biaxial tests for the CSIRO HI cells. Further, Ask[1] suggested that the CSIRO HI data suffer from boundary yield between the cell and the rock.

General geology at the Zedex Test Site

The dominating rock type in the ZTS is the grey, medium-grained Äspö diorite. The diorite is slightly anisotropic but the anisotropy is not strong enough to require corrections according to Amadei's rule of thumb (e.g. [16]). Geological mapping at the site identified two main discontinuous fracture sets, NW and NNE, both steeply dipping. Steeply dipping NW-SE striking fractures are the most dominant set, and these fractures are also the most water-bearing, which is in accordance with the determination of maximum horizontal stress in the region (NW-SE striking; [17]).

Stress data

Table 1 presents the available overcoring data of this study. The data provides information of the primary and secondary stress fields. From now on, the boreholes in Table 1 will be referred to as 8HL, 68A, 8HR, and 59B.

Table 1. Summary of analyzed overcoring data at the ZTS.

Borehole, abbreviation	Depth [m]	No. of points	Stress field	Cell, reference
KXZSD8HL 8HL	~406.4	4	P	BP, [4]
KA3068A, 68A	~407.6	4	P	CHI, [3]
KXZSD8HR, 8HR	~418.5	8	S	BP, [4]
KZ0059B, 59B	~416.1	6	S	CHI, [3]

Keys: BP and CHI are the Borre Probe and CSIRO HI cells, respectively. P and S denote data measuring primary and secondary stress fields, respectively.

Analysis of overcoring data

Determination of strain

The initial strain gauge readings are taken at a stable point before flushing is initiated (poorly glued rosettes are recognized when flushing is turned on/off). The post overcoring strain reading is taken close to core break/flushing stop, which is normally done a few minutes after drilling stop (Fig. 3). This implies that temperature effects are also minimized. Only one test in borehole 8HL required temperature correction. Appropriate temperature correction factor the Borre Probe have been derived in Ask et al.[13].

The data sampling frequency during overcoring for the CSIRO HI cell was poor, which make it difficult to identify possible malfunctioning strain gauges. Consequently, we used the CSIRO HI strain data of the original reports ([3]; [5]). The results from all the CSIRO HI measurements in the entire Äspö HRL indicate a large stress component parallel to the direction of the borehole ([1]; [14]). In total, 32 out of 49 tests have the major principal stress less than 30° from the borehole direction. Most boreholes are oriented close to the strike of maximum horizontal stress, thus one would indeed

expect to find major principal stress in that direction. However, it is remarkable that 15 out of 49 measurements points have the major principal stress less than 10° from the borehole direction.

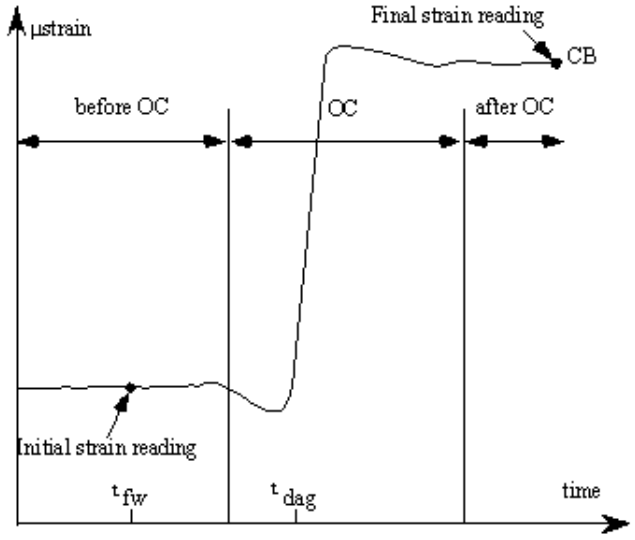

Figure 3. Schematic response of a tangential strain gauge during overcoring. The strongest strain gauge response occurs at t_{dag}, i.e. when the **d**rill bit is **a**t the **g**auge position. t_{fw} and CB denote the time when flush-water is turned on and core break, respectively (Modified after [1]).

Irvin et al.[18] suggested that similarity in borehole direction and major principal stress orientation could be an effect of boundary yield between the cell and the rock. If yield occurs at the boundary between the cell and the rock in either the adhesive grout or the rock substrate, the cell will allow longitudinal expansion of the cell during overcoring, i.e. giving too high values on axial and 45°/135°-gauges. In the stress calculation this is visualized by a large component parallel to the borehole and larger stresses than expected in the plane perpendicular to the borehole.

The small distance between CSIRO HI and Borre Probe data at the ZTS, especially in the pillar between the D&B and TBM tunnels, allows comparison between the axial strains from the two cells. The result indicates that the axial strains in the pillar are approximately the same and equal to 186 and 240 μstrains for the two cells. However, three measurements in borehole 59B indicate too large axial strains. The boreholes measuring the primary stress field are located about 130 m from each other, which makes the comparison doubtful. Yet, the comparison yields that the axial strains are 50% larger for the CSIRO HI cell compared to the Borre Probe. The two boreholes also have slightly different strikes (102° and 146° for 68A and 8HL, respectively), i.e. with 8HL oriented closer to the average orientation of maximum horizontal stress of all data at the Äspö HRL (131±19°; [1]). This implies that the measurements in borehole 8HL should result in larger axial strains compared to borehole 68A. It was concluded that borehole 68A suffer from yielding because: (1) too large axial strains are recorded; (2) the average orientation of maximum horizontal stress is only 7° from the borehole direction; (3) the stresses perpendicular to the borehole are larger than expected. To test the boundary yield hypothesis, the strains in three tests in borehole 59B were corrected based on the results from the surrounding stress data in the same borehole (218 μstrain). For borehole 68A, the correction was based on the minimum recorded strain in the borehole (202 μstrain). As an example, a reduction of 80 μstrain of the axial gauges gives a 40 μstrain reduction of the 45°/135°-gauges.

Determination of elastic parameters

The determination of the elastic parameters has been made only for the Borre Probe data ([13]). The determination of the elastic parameters for the thin-walled Borre Probe cores includes biaxial testing and cyclic loading up to 10 MPa. Generally, the unloading curves between 3-10 MPa are used. Thus, this may be considerably less than the measured magnitudes. In this study (and in [13]), the unloading curves between 8-10 MPa were used (secant modulus), which are closer to the measured magnitudes. In addition, all doubtful strain rosettes were excluded when calculating the elastic parameters. The poorly conducted CSIRO HI biaxial tests were discarded. Instead, we used the average values of the elastic parameters obtained from adjacent measurements with the Borre Probe.

Results

The results from the stress calculations of the primary and secondary stress fields are presented as individual measurement points (including questionable gauges) and combined result for each borehole and for combined boreholes (excluding questionable gauges). For the calculation of the average stresses, the empirical Chauvenet's criterion has been used to remove illegitimate strain gauges. This means that an iterative procedure has been undertaken until all strains are accepted or when erroneous gauges no longer affect the calculated stresses.

Individual measurement points

Primary stress field

The re-calculated stresses in boreholes 8HL and 68A are significantly different compared to the original results (Fig. 4), especially regarding the magnitudes. Two measurement points in 8HL and all measurement points in 68A include doubtful strain data that affect the results that are excluded in the calculation of the average stress field. The stresses in borehole 68A are, when using average values on the elastic parameters from 8HL and corrected for boundary yield, comparable with the Borre Probe data. The horizontal stresses may be compared with the results from hydraulic fracturing stress measurements ([2]) giving these indicate maximum and minimum horizontal stresses equal to 19.6 and 7.9 MPa, respectively. The orientation of the maximum horizontal stress is N130°E. The vertical stress may be compared with the theoretical vertical stress at this level, which is approximately 10.8 MPa. The re-calculated stresses in boreholes 8HL (the two deeper measurement points) and 68A agree reasonably well with the hydraulic

data. The Borre Probe raw data in 8HL fits better to the hydraulic fracturing data and to the theoretical vertical stress (see [1] and [13] for details).

Secondary stress field

The re-calculated stresses in boreholes 8HR and 59B are again significantly different compared to the original result (Fig. 5), especially regarding the magnitudes. In borehole 8HR and 59B, three and two measurement points, respectively, include doubtful data affecting the results. The stresses in borehole 59B are, when using average values on the elastic parameters from 8HR and corrected for boundary yield, comparable with the Borre Probe data. Both cells agree reasonably well with modelled stresses ([19]) giving stress magnitudes in the N-S, E-W and vertical directions the stresses equal to about 18, 9, and 8 MPa, respectively.

Combined result from each borehole and for borehole combinations

Primary stress field

In the calculation of the primary stress field from each borehole and combined boreholes (Figs. 4 and 9), all suspect strain gauges have been omitted (9 and 5 gauges in 8HL and 68A, respectively). Note that the average result for borehole 68A as well as the combined result with borehole 8HL only includes the two shallower measurement points in borehole 68A. The horizontal stresses are very similar to the hydraulic fracturing data, especially when combining both cells. All combinations seem to underestimate the vertical stress, at least when comparing with the theoretical vertical stress.

Secondary stress field

The calculated secondary stress field in the pillar between the D&B and TBM tunnels (Figs. 5 and 9) is comparable to both modelled stress field and hydraulic fracturing data (omitting all suspect gauges). The minimum horizontal stress is slightly underestimated while the vertical stress is in good agreement with the theoretical vertical stress.

Discussion

Results

The integration of the two cells was a fruitful approach, especially regarding the secondary stress field in the pillar between the D&B and TBM tunnels. We believe that the reliability of the CSIRO HI measurements have been improved when correcting for elastic parameters and boundary yield, at least when compared with the data from the Borre Probe, the hydraulic fracturing stress data, and the theoretical stress from the weight of the overburden. One may argue that the CSIRO data have been adjusted to fit the data from the Borre Probe, when using the elastic parameters from the Borre Probe. This is true in the sense that the analysis assumes that the Borre Probe data are fully reliable and that the state of stress is constant in the rock volumes investigated. On the other hand, it is clear that the CSIRO HI data suffer from poor biaxial results (too high pressures leading to fracturing of the core during loading) and boundary yield and a rigid analysis thus requires some sort of correction. The corrections for boundary yield, based on the minimum recorded axial strain in the borehole, which is similar to the recorded axial strains from the nearby Borre Probe boreholes, are judged reliable.

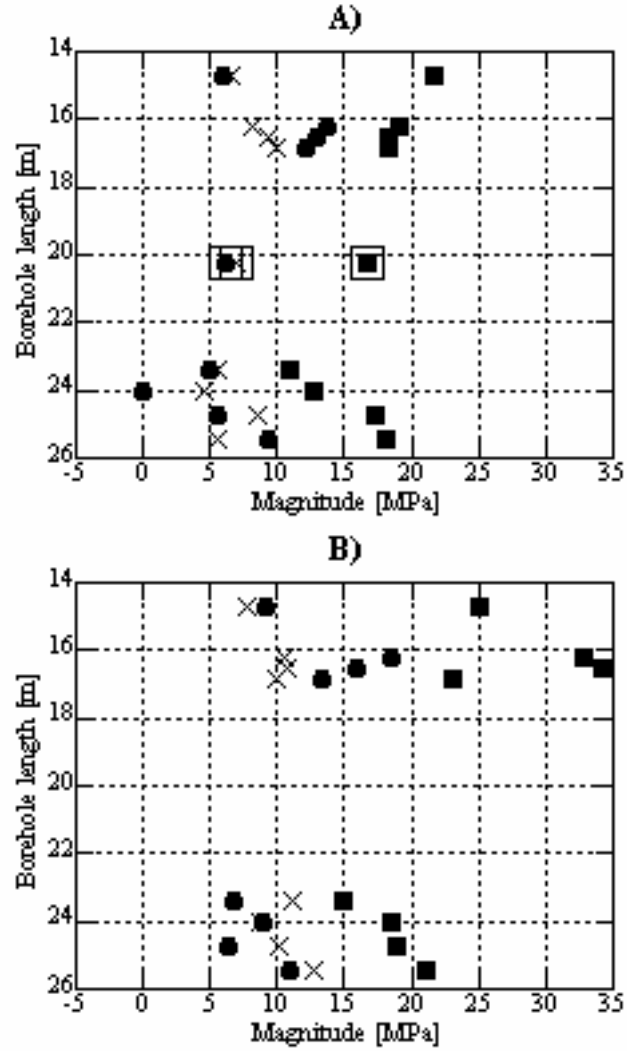

Figure 4. Horizontal stresses versus borehole length in boreholes 8HL and 68A. A) Result using re-analysed data, and B) Result using raw data ([3]; [4]). Filled squares, circles, and crosses are maximum and minimum horizontal, and vertical stresses, respectively. In A, the average result using both cells and using re-analyzed data is visualized with large unfilled squares as background.

The reason for the non-linear stress field versus depth in borehole 68A is not fully understood and may reflect: (1) influence of the excavation; (2) microcracking of the core; and (3) boundary yield between the cell and the rock ([17]). It has been estimated that the geometry at the site would tend to lower major principal stress with only about 5%. Further, the measurements are located over a short section (2.2 m) which is unlikely long enough to record an excavation-induced stress gradient, considering the accuracy of the method. The biaxial test results display slightly non-linear curves but not more than normal and the effect of

microfractures in the core is judged as small. The boundary yield effect has been tested, and the result still includes a strong rotation of major principal stress.

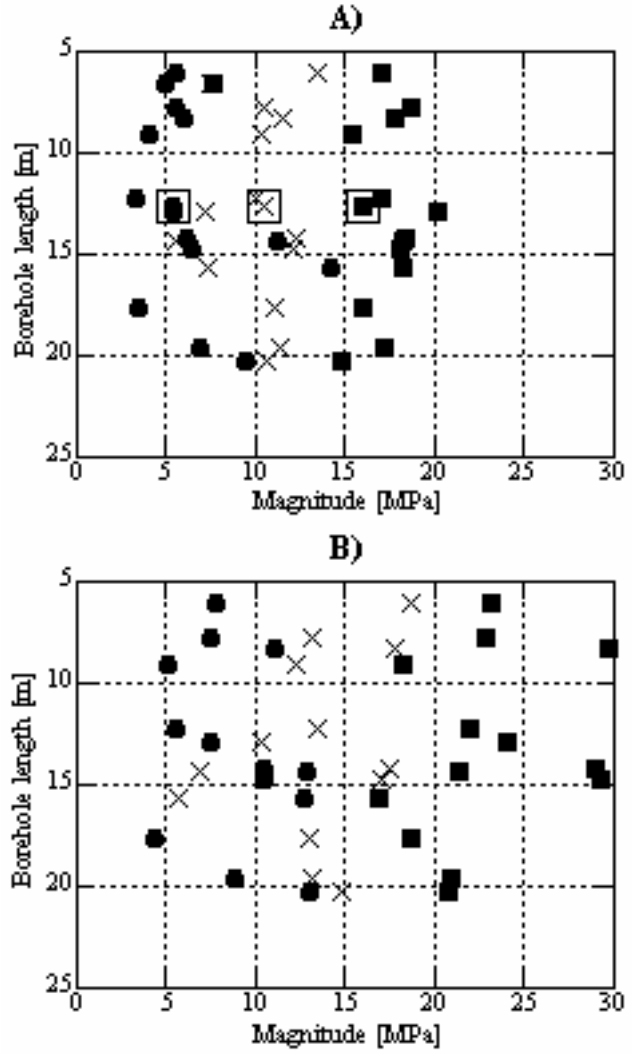

Figure 5. Horizontal stresses versus borehole length in borehole 8HR and 59B. A) Result using re-analysed data, and B) Result using raw data ([3]; [4]). Filled squares and circles, and crosses are maximum and minimum horizontal, and vertical stresses, respectively. In A, the average result using both cells and using re-analyzed data is visualized with large unfilled squares as background.

Thus, if the mentioned explanations may be ruled out, the most plausible explanation may be the influence of a water-bearing fracture located about 2-4 metres from the test points. The stress data from the measurement points closest to the fracture indicate that major and minor principal stresses are oriented NW and NE, respectively, which corresponds well with the dominant, water-bearing and NW-striking fracture set.

The inclined principal stresses at the ZTS may be influence of a major geological structure. Recent modelling work suggests that the non-linear stress versus depth at the Äspö HRL is caused by the NE-2 fracture zone ([10]; [20]). The effect is clearly visible when plotting the results from hydraulic fracturing stress measurements, see Fig. 9. Another explanation for the inclined principal stresses at the ZTS could be influence of the dominant NW-oriented fracture set. These fractures are likely to intersect or are closely located to the overcoring stress measurement points. At the ZTS, a majority of the tests indicate such an influence of the fracture set (i.e. major and minor principal stresses are parallel and perpendicular, respectively, to the NW-oriented fracture set).

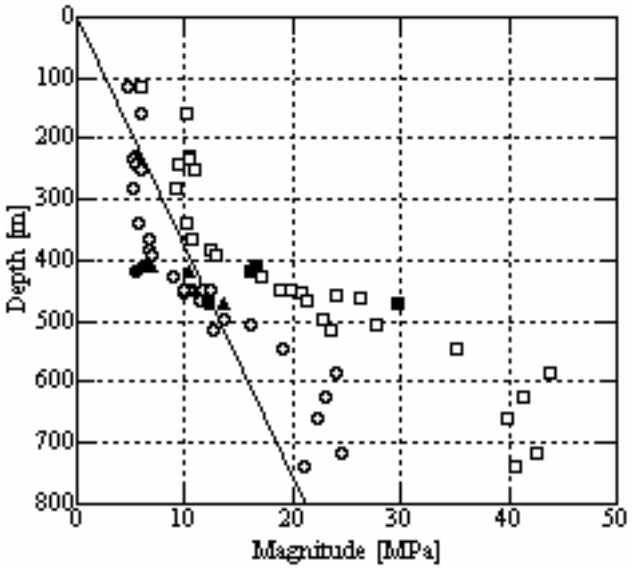

Figure 9. Results from hydraulic fracturing stress measurements in boreholes KAS02, KA2599G01, KF0093A01 ([2]; [6]), unfilled symbols. The results presented as filled symbols are the integrated results from the primary and secondary stress fields in this study (at about 415 m depth) and a previous study using Borre Probe data from borehole KA3579G, at 470 m depth in the Prototype Repository ([21]). The squares and circles are maximum and minimum horizontal stresses, respectively. Theoretical vertical stress is represented by a solid line and calculated vertical stress from this study with filled triangle.

Uncertainties in the study

The applied study has not considered natural uncertainties, e.g. anisotropy. The application of the average elastic parameters from the Borre Probe to the CSIRO HI data does probably not induce large errors in the pillar between the D&B and TBM tunnels, where the measurements are closely spaced, but may be questioned for the primary stress field boreholes. Further, the correction for boundary yield in boreholes 68A and 59B lead indisputably to large uncertainties.

Conclusions

We have developed an inversion method for integration of CSIR- and CSIRO-type of overcoring data based on the least-squares criterion. The integrated results indicate a good agreement with hydraulic fracturing stress data, theoretical vertical stress, and modelled stresses. The most deviating result concerns the vertical stress for the primary stress field, which is slightly underestimated compared to the theoretical vertical stress. The modelling result, indicating a similar stress field in the centre of the pillar as

the primary stress field, was confirmed in this study. The most striking result from this study is the good agreement between the re-analysed overcoring data and the existing hydraulic fracturing data. Comparing average stress data from the site, the deviation for maximum and minimum horizontal stress is only about 3 MPa. The deviation in the orientation of maximum horizontal stress is approximately 20°. The integrated result for the primary and secondary stress fields indicates that the minimum horizontal stress is rather similar in magnitude with the vertical stress. The orientation of maximum horizontal stress is NW-SE. The CSIRO HI data from the Äspö HRL are currently being re-analysed ([14]) and some of the biaxial test results omitted in this study may be used.

Acknowledgements

The Swedish Nuclear Fuel and Waste Management Co. and the Swedish Research Council (1999-2001) financially supported this work. We would like to thank Maria Ask, Luleå University of Technology, Rolf Christiansson, SKB, and Lennart Ekman, LE Geokonsult, for reviewing the manuscript. Tobias Backers, GFZ Potsdam, is acknowledged for translating the abstract to German.

References

1. ASK, D. Evaluation of measurement-related uncertainties in the analysis of overcoring rock stress data from Äspö HRL (a case study), in prep. 2003.
2. BJARNASON, B., KLASSON, H., LEIJON, B., STRINDELL, L. and ÖHMAN, T. Rock stress measurements in boreholes KAS02, KAS03 and KAS05 on Äspö. SKB Progress Report 25-89-17, Stockholm, 1989.
3. LITTERBACH, N., LEE, M. STRUTHERS, M. and STILLBORG, B. Virgin stress measurement results in boreholes KA2870A and KA3068A. SKB Progress Report 25-94-32, Stockholm, 1994.
4. LJUNGGREN, C. and KLASSON H. Rock stress measurements at Zedex test area, Äspö HRL. Äspö Hard Rock Laboratory, Technical Note TN-96-08z, Stockholm, 1996.
5. NILSSON, G., LITTERBACH, N., LEE, M. and STILLBORG, B. Virgin stress measurement results, borehole KZ0059B. Äspö Hard Rock Laboratory, Technical Note TN-97-25g, Stockholm, 1997.
6. KLEE, G. and RUMMEL, F. Rock stress measurements at the Äspö HRL. Hydraulic fracturing in boreholes KA2599G01 and KF0093A01. SKB International Progress Report IPR-02-02, Stockholm, 2002.
7. LEIJON, B. Summary of rock stress data from Äspö HRL. SKB Progress Report 25-95-15, Stockholm, 1995.
8. ASK, D. Inversion and interpretation of hydraulic and overcoring stress measurements in the Äspö region, Sweden. Lic. Thesis, Royal Institute of Technology, Div. Engineering Geology, Stockholm, 2001.
9. ASK, D., STEPHANSSON, O. and CORNET, F.H. Integrated tress analysis of hydraulic stress data in the Äspö region, Sweden. Analysis of hydraulic fracturing stress data and hydraulic tests on pre-existing fractures (HTPF) in boreholes KAS02, KAS03 and KLX02. SKB International Progress Report, IPR-01-26, Stockholm, 2001a.
10. HAKAMI, E., HAKAMI, H., and COSGROVE, J. Strategy for rock mechanics site descriptive model. Development and testing of an approach to modelling the state of stress. SKB Report R-02-03, Stockholm, 2002.
11. SJÖBERG, J. and KLASSON, H. Stress measurement in deep boreholes using the Borre (SSPB) probe. Submitted to *Int. J. Rock Mech. & Geomech. Abstr.,* 2003.
12. WOROTNICKI, G. CSIRO triaxial stress measurement cell. *Comprehensive Rock Engineering*, Vol. **3**. (J. Hudson, Ed.) Pergamon Press, Oxford: 329-394, 1993.
13. ASK, D., CORNET, F.H. and STEPHANSSON, O. Analysis of overcoring stress data at the Äspö HRL, Sweden. Analysis of overcoring rock stress measurements performed using the Borre Probe, SKB Report in press 2002.
14. ASK, D., CORNET, F.H. and STEPHANSSON, O. Analysis of overcoring stress data at the Äspö HRL, Sweden. Analysis of overcoring rock stress measurements performed using the CSIRO HI cells, SKB Report in prep. 2003.
15. MYRVANG, A. Evaluation of in-situ rock stress measurements at the Zedex Test Area. SKB Progress Report HRL-97-22, Stockholm, 1997.
16. AMADEI, B. *Rock anisotropy and the theory of stress measurements*, Lecture notes in Engineering, Springer-Verlag, 1983.
17. HERMANSSON, J., LEIJON, B., MARKSTRÖM, I., MUNIER, R. and STANFORS, R. Geological interpretation of the Zedex rock volume. SKB Technical Note 25-95-06z, Stockholm, 1995.
18. IRVIN, R.A., GARRITTY, P., and FARMER, I.W. The effect of boundary yield on the results of in situ stress measurements using overcoring techniques. *Int. J. Rock Mech. Min. Sci. & Geomech. Abstr.*, Vol. **24**, No. 1: 89-93, 1987.
19. SKB. Numerical modelling, acoustic emission and velocity studies of the excavation disturbed zone at the hard rock laboratory. SKB Technical Note TN-97-02z, Stockholm, 1996.
20. HUDSON, J.A. Strategy for rock mechanics site descriptive model. A test case based on data from the Äspö HRL. SKB Report R-02-04, Stockholm, 2002.
21. ASK, D., STEPHANSSON, O. and CORNET, F.H. Analysis of overcoring rock stress data in the Äspö region. *Proc. from the 38th US Rock Mech. Symp.*, Washington, USA. A.A. Balkema Publ.: 1401-1405, 2001b.

Fardin, N., Stephansson, O., Jing, L., Scale effect on the geometrical and mechanical properties of rock joints
ISRM 2003–Technology roadmap for rock mechanics, South African Institute of Mining and Metallurgy, 2003.

Scale effect on the geometrical and mechanical properties of rock joints

Nader Fardin, Ove Stephansson, Lanru Jing
Engineering Geology and Geophysics, Department of Land and Water Resources Engineering,
Royal Institute of Technology, KTH, Sweden.

A pair of silicon rubber replicas of size 250 mm by 250 mm, from a natural rock joint, was used to produce several high strength concrete fracture replicas of different sizes, from 50 mm by 50 mm to 200 mm by 200 mm. The morphology of the concrete fracture replicas were digitized at the laboratory using a 3D-laser-scanning machine with high accuracy and resolution. The scale dependency of the geometrical properties, including surface roughness and aperture, of the samples were investigated using fractal method. The investigation was extended to study the scale effect on the mechanical properties of the concrete fracture replicas. Four concrete replicas having same geometry from each sampling size were sheared under four different normal loads. The results show that normal and shear stiffness and peak shear strength decrease with increasing sample size and decreasing normal stress. It is concluded that for accurate determination of geometrical and mechanical properties of rock joints in the laboratory and field scales, samples with size equal to or larger than stationarity limit are required.

Silikongummiabdrücke der Größe 250 mm x 250 mm einer natürlichen Kluft dienten als Vorlage für mehrere Hochfestbeton Rissreplikas verschiedener Größe. Die Morphologie der Beton Rissreplikas wurde mittels eines 3D-Laserscanners hoher Genauigkeit und Auflösung im Labor digitalisiert. Die Skalenabhängigkeit der geometrischen Eigenschaften, dies inklusive Oberflächenrauhigkeit und Öffnungsweite, wurden mittels Fraktalen bestimmt. Die Studie wurde durch die Untersuchung der mechanischen Eigenschaften der Betonrepliken erweitert. Hierbei wurden vier Betonrepliken der selben Geometrie jeder Probengrösse unter vier verschiedenen normalen Belastungen abgeschert. Die Ergebnisse zeigen das sowohl Normal- und Schersteifigkeit als auch die Spitzenscherfestigkeit mit zunehmender Probengrösse und abnehmender Normalspannung abnehmen. Es hat sich gezeigt, daß für eine genaue Bestimmung der geometrischen und mechanischen Eigenschaften von Felsklüften im Labor und im Feld Proben einer Größe gleich oder größer des stationären Limits verlangt werden.

Deux répliques en gomme de silicone d'une fracture naturelle, de dimension 250 mm par 250 mm, ont été utilisées pour produire des répliques en béton de haute résistance de dimensions allant de 50 mm par 50 mm à 200 mm par 200 mm. La morphologie de ces répliques a été digitalisée au laboratoire à l'aide d'un laser-scanner 3D haute résolution et haute précision. L'influence de l'échelle des propriétés géométriques, incluant rugosité et ouverture, a été étudiée en utilisant la méthode des fractales. Des essais complémentaires ont été réalisés afin d'étudier l'effet d'échelle sur les propriétés mécaniques des répliques de fracture en béton. Quatre répliques béton de même géométrie pour les différentes tailles d'échantillons ont été cisaillées sous quatre valeurs de contrainte normale. Les résultats montrent que la rigidité normale et tangentielle ainsi que la résistance de pic diminuent en proportion de l'augmentation de la taille de l'échantillon et de la diminution des contraintes normales. On peut en conclure que, pour une détermination précise des propriétés géométriques et mécaniques des fractures au laboratoire et sur le terrain, des échantillons de taille égale ou supérieure à la limite stationnaire sont nécessaires.

Introduction

The hydraulic and mechanical behaviours of rocks strongly depend on the geometrical characteristics of rock joints. The hydro-mechanical properties of rock joints are also scale-dependent. For obtaining large-scale geometrical and mechanical properties of rock joints, a method for extrapolating laboratory data to field scale is needed.

During past decades, many researchers have investigated the effect of scale on the surface roughness and shear strength of rock joints. In their works, rock joint samples of different sizes were characterized and sheared and from the obtained results, relationships were established to extrapolate rock joints properties to the field scale from laboratory samples.

However, recent studies by authors[1] show that there exists a stationarity threshold for the roughness of rock joints, so that for a joint of a size larger than stationarity limit the surface roughness of rock joints remains almost constant and can be used to define the field scale properties of the rock joints. This stationarity threshold may be different for different types of rock joints with respect to their geometrical and mechanical properties. Therefore, it is necessary to determine the maximum stationarity limit for rock joints and then apply the obtained properties of samples at this size to the large rock joints at the field scales.

Sample preparation

To study the scale effect on both geometrical and mechanical properties of rock joints, it is necessary to perform several mechanical shear tests on the rock joints samples having the same geometrical features. However, it is impossible to find rock joints with same geometrical features in nature. Therefore, replicas of a natural rock joint from a quarry (in Töre, Northern of Sweden) made by Lindfors[2] (1996), was used as the parent joint sample and a pair of silicon-rubber moulds were made from its surfaces consisting of both lower and upper surface parts.

High-strength concrete replicas of the parent joint sample with decreasing size, from 200 mm by 200 mm to 50 mm by 50 mm, were made in order to study scale effect on the mechanical properties of rock joints. In total, 16 concrete fracture replicas were casted and tested.

The concrete used to produce the replicas is a premixture high strength concrete, Densitop ST, which is normally used for very high strength industrial floors. The water cement ratio is between 0.2-0.5, according to the manufacturer, which is rather low compared with normal concrete. The concrete samples were casted carefully to avoid entrapment of air near the joint surface and conditioned with moisture of 100%. Fig 1 shows the method of sample preparation.

The mechanical properties of the replicas, determined by Olsson[3] (1998) through different uniaxial and Brazilian tests on dry core material with a diameter of 42 mm and direct shear tests on saw-cut dry surfaces are listed in Table 1.

Table 1. Mean values and standard deviations of the mechanical parameters for dry Densitop T2 used for replicas (after Olsson[3], 1998)

Parameter	dry samples
Young's modulus *E*, GPa	57±3
Poisson's ratio ν	0.25
Uniaxial compressive strength σ_c, MPa	215±13
Tensile strength σ_t, MPa	9.1±1.1
Density ρ, Kg/m^3	2600-2650
Basic friction angle ϕ_b, Degree	32.5±2.5

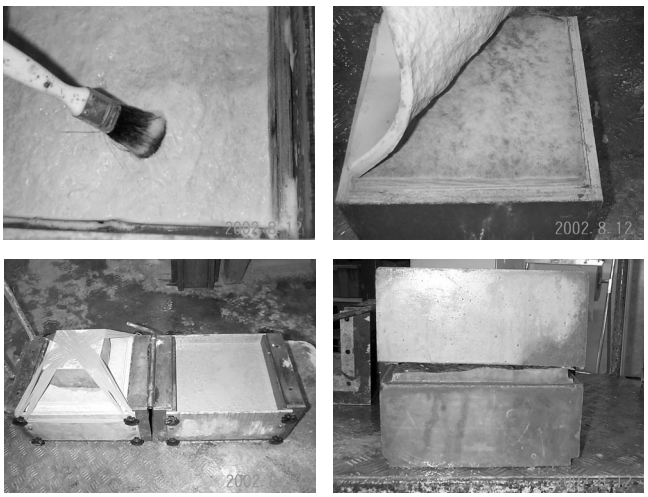

Figure 1. Method of producing the concrete fracture replicas in the laboratory.

Topographical measurement at the laboratory

A 3D-laser scanner with an accuracy of ±20 μm and a resolution of 10 μm was used to measure the topography of the replicas. The 3D-laser scanner is described by Lanaro[4] (1999).

The concrete fracture replicas were digitized with a high accuracy of 0.2 mm using the 3D-laser scanner. To characterize the void geometry of the samples, the relocation method used by Lanaro[4] (1999) was applied, as it is shown in Fig. 2. In this method, a set of calibrated spheres (7mm in diameter) were attached onto the two concrete replica blocks and used as reference objects. Firstly, the concrete replica joint was closed and all reference spheres were scanned. Secondly, the joint was opened and the two surfaces were scanned individually including the attached spheres.

Since scanner produces a large number of data points for each sphere, the central position of spheres could be accurately calculated by computer programs. The final step is to rotate and translate the digital replica of the individually scanned surfaces with respect to the original position of the spheres, where the reference spheres coincide with the position they had before opening the samples. In this way, the joint geometry can be re-constructed with high accuracy and void volume can be calculated using Surfacer software package by Imageware[5] (2000).

A 3-dimensional isometric view of the digital replicas obtained from 3D-laser scanner and reconstructed by Imageware software package, before and after relocation is shown in Fig. 3.

Figure 2. 3D-laser measuring of the concrete replica at the Laboratory.

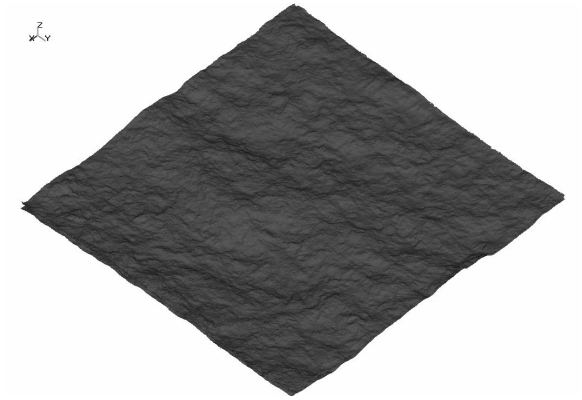

Figure 3. 3-Dimensional isometric view of a digital replica reconstructed by Surfacer Imageware code.

Geometrical characterization of the joint samples

After scanning the joint sample surfaces, before and after relocation, their geometrical characteristics such as surface roughness and aperture were characterized using special programs written in Surfacer.

Since the geometrical features of concrete fracture replicas of same size are the same, made from same silicon-rubber mould, therefore, just one sample from each group was characterized before conducting the shear tests.

In the following sections, surface roughness, aperture and contact areas are characterized followed by study on the effect of scale on the geometrical characteristics of the fractures.

Surface roughness characterization of the joint samples

Surface roughness of the concrete fracture replicas was characterized on basis of fractal concept. fractal dimension D and amplitude parameter A, describe roughness of rock joint surfaces. Since Roughness Length Method (Malinverno[6], 1990) has the main advantages, comparing to other methods, to remove a planar global trend of a profile, this method was used to calculate the fractal parameters of the concrete fracture replicas.

To calculate fractal parameters, D and A, of each fracture surface, different series of window sizes of 1%, 2%, 4%, 5% and 10% of the total sample length were considered with respect to the sample size.

For both surfaces of each concrete fracture replica, the standard deviations of reduced asperity height, $S(w)$, were calculated as functions of the window sizes, w, using the Imageware code. The results show very good linear relationships between the standard deviations of the reduced asperity height and the window sizes for the fracture surfaces with different sizes.

Therefore, the fractal parameters, D and A, of both surfaces of joints were estimated by a power law regression analysis. The calculated D and A of the both surfaces of all concrete fracture replicas are listed in Table 2, and implies that fractal parameters increase with increasing sample sizes.

Table 2. The estimated fractal dimension D and amplitude parameter A for concrete fracture surfaces of increasing sizes.

Sample size (mm × mm)	Lower surface		Upper surface	
	D	A, mm	D	A, mm
45×45	2.0041	0.0153	1.992	0.0214
99×99	2.0359	0.016	2.0568	0.0185
149×149	2.0457	0.0168	2.0331	0.0162
194×194	2.0891	0.0179	2.0804	0.0172

Scale effect on the surface roughness of the joint samples

To study the scale effect on the fractal parameters of the samples, the calculated D and A values are plotted in Figs. 4a and b, respectively as a function of the sample size.

The figures show that for the lower surfaces, both the fractal dimension and amplitude parameter increase with the increasing sample size. However, there is a very small difference between the obtained parameters. For the upper surfaces, the fractal dimension generally increases with increasing sample size but the amplitude parameter is almost constant.

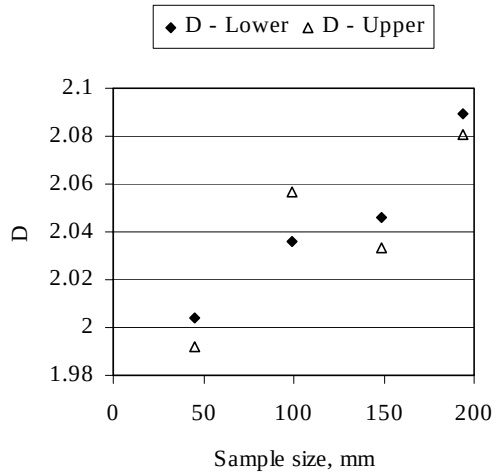

(a)

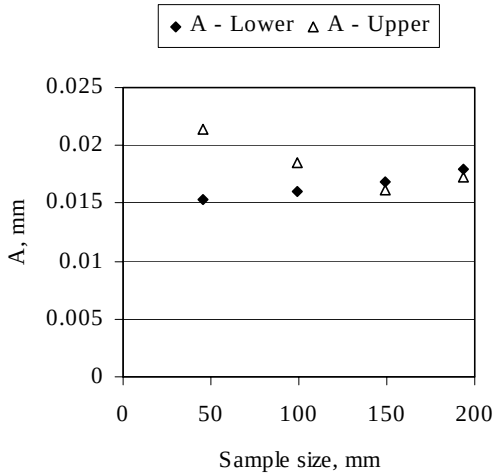

(b)

Figure 4. Fractal dimension (a) and amplitude parameter (b) for both surfaces of all concrete fracture replicas as a function of the sample size.

Aperture characterization of the joint samples

Geometrical aperture, defined as the separation distance between two fracture surfaces along the direction perpendicular to the surfaces was calculated, with only the self-weight of the upper block after scanning and relocation of the two surfaces of each fracture.

The frequency histograms of the aperture of the concrete fracture replicas are plotted together in Fig. 5. This figure shows that although there is little difference in the aperture histograms, mainly due to relocation error, all samples have generally the same aperture distribution irrespective of their size.

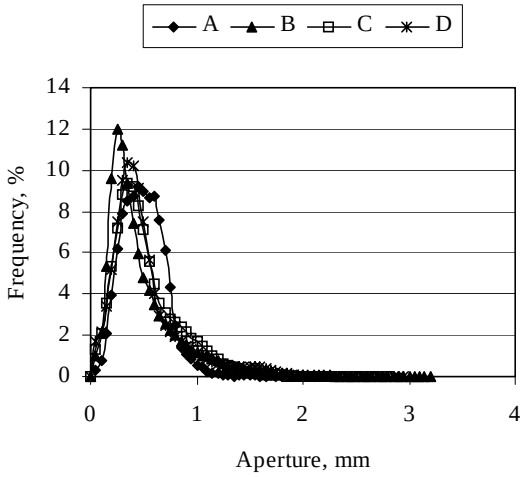

Figure 5. Frequency distribution of the fracture aperture for all sample sizes (A: 45, B: 99, C: 149 and D: 194 mm).

The standard deviation of the aperture for a series of the window size of 1.03%, 2.5%, 4%, 6.6% and 10% of the total sample length were also plotted for each sample size, which shown very good linear relationships.

Therefore, the aperture can also be characterized by a power law, where the power of the equation is equal to the Hurst exponent of the aperture, H_a, and its constant is defined as aperture proportionality constant, G_a.

The calculated H_a and G_a of all concrete fracture replicas are listed in Table 3.

Table 3. The estimated H_a and G_a for concrete fracture aperture of increasing sizes.

Sample size (mm × mm)	H_a	G_a
45×45	0.498	0.069
99×99	0.495	0.048
149×149	0.357	0.061
194×194	0.310	0.061

Scale effect on the aperture of the joint samples

To study the scale effect on the aperture of the joint samples, the calculated H_a and G_a are plotted in Figs. 6a and b as a function of the sample size, respectively. The figures show that both H_a and G_a decrease with increasing sample sizes.

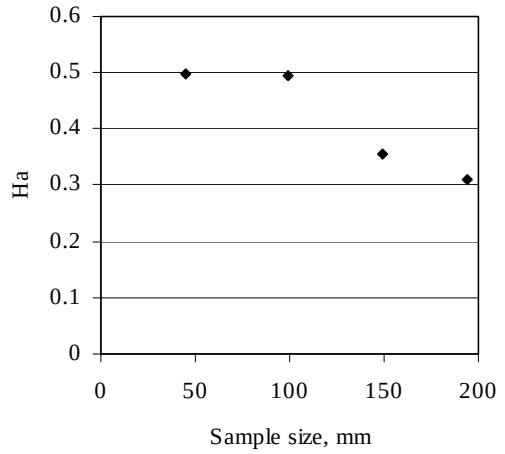

(a)

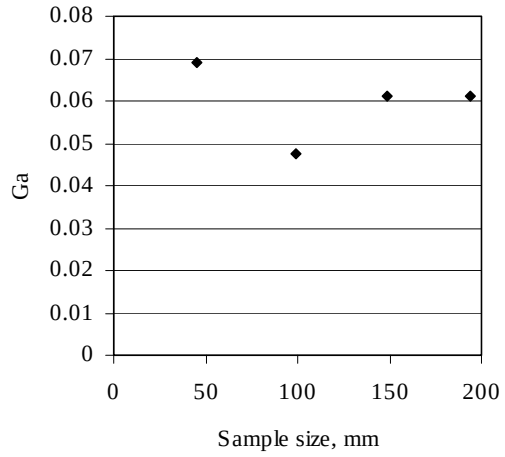

(b)

Figure 6. Obtained Hurst exponent H_a (a) and aperture proportionality constant G_a (b) for aperture distribution of the all concrete fracture replicas as a function of the sample size.

Mechanical tests

The experimental study of the scale effect on the mechanical properties of the concrete replicas was based on direct shear tests under constant normal load conditions, using direct shear test equipment at the TESTLAB of Luleå University of Technology.

In this section, the mechanical normal and direct shear tests are described and the results obtained from mechanical tests are discussed.

Normal loading tests

The concrete replicas were tested under different normal loading condition, in order to study their normal deformation behaviour. Two normal loading-unloading cycles were conducted on each sample, followed by a loading phase up to the desired normal stress to be used during the shear phase. Each concrete replica was tested at one specific normal test, and four direct shear tests were performed for each sample size under normal stresses of 1, 2.5, 5 and 10 MPa, respectively. In total, 16 normal and shear tests were performed during this series of experiment.

Scale effect on the normal deformation of the joint samples

To investigate the scale effect on the normal deformation of the concrete fracture replicas, the normal stiffness of the samples, K_{nn}, under each specific normal load were calculated at the linear part of the third loading cycle. The calculated normal stiffness of the concrete fracture replicas is plotted in Fig. 7 as a function of the sample size. Under the same normal stress, the samples of smaller sizes show larger normal stiffness, and the normal stiffness of the samples increases with increasing the normal stresses.

It is concluded that with increasing sample sizes, the normal stiffness decreases and has the lowest value for sample with the largest size.

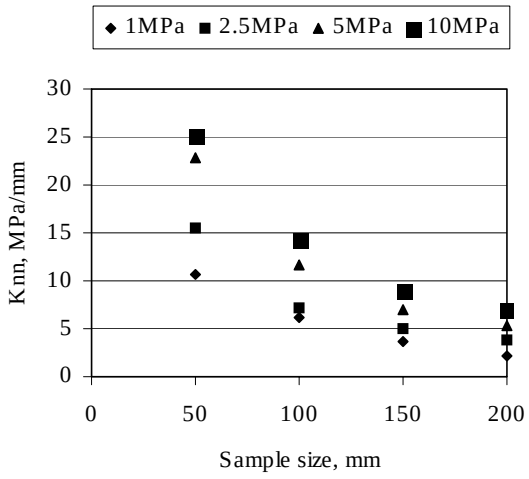

Figure 7. The estimated normal stiffness as a function of the sample size under different normal stress for all concrete fracture replicas.

Direct shear tests

After conducting the normal loading tests, the shear tests were performed on the samples. The purpose was to study the shear behaviour of the concrete fracture replicas at different scales and under different loading condition. The applied normal load was halted in the third loading cycle at its maximum desired value and the shear force was then applied to the upper block, while the lower block was held in place.

The shear velocity was kept constant at about 1 mm/min during the shear tests, with a maximum shear displacement of about 20 mm.

Scale effect on the shear behaviour of the joint samples

The scale effect on the shear behaviour of the concrete fracture replicas was investigated by plotting the estimated shear stiffness, K_{ss}, of all samples as functions of the sample size and normal load. Figure 8 shows that under the same normal stress, the samples of smaller size have larger shear stiffness, and the shear stiffness of the samples increases with increasing the normal stress.

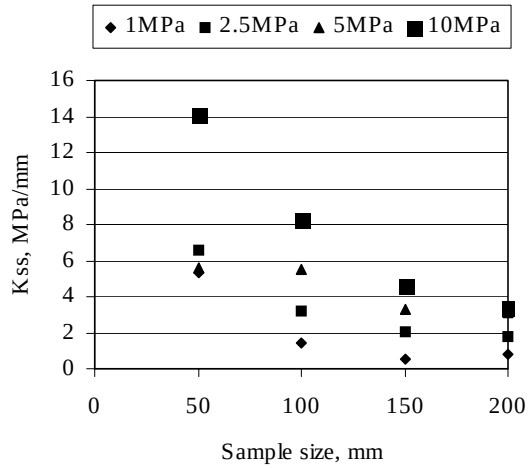

Figure 8. Shear stiffness as a function of sample size under different normal stress for all concrete fracture replicas.

Scale effect on the peak shear stress

The scale effect on the peak shear stress, defined as shear strength of the concrete fracture replicas, were investigated by plotting the maximum shear stress versus samples size with different applied normal stresses (Fig. 9). This figure shows that the maximum shear stress of the samples decrease with increasing sample size with all normal loading conditions.

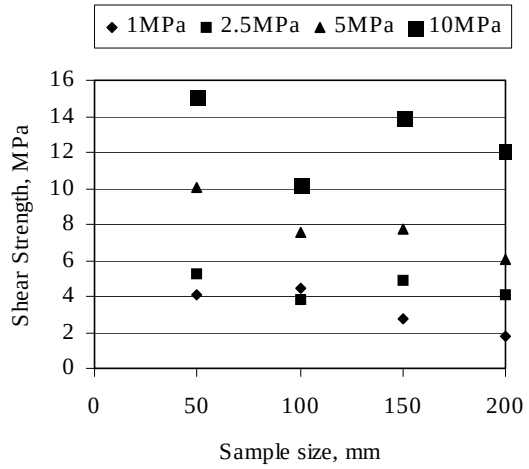

Figure 9. The maximum shear stress as a function of the sample size under different normal stress for all concrete fracture replicas.

Discussion and conclusion

Scale effect on the geometrical and mechanical properties of a rock fracture was investigated. The results obtained from the geometrical characterisation showed that both fractal dimension and amplitude parameters of the fracture surface are scale dependent and their values increase with increasing sample sizes. The aperture histograms of the joints show little difference with respect to sample size, however, both Hurst exponent H_a and aperture proportionality constant G_a decrease with increasing of the sample size. Comprehensive study on the scale effect on the surface roughness of a planar rock fracture of size 1000 mm by 1000 mm by an early study of the authors[1], showed that the scale dependency of roughness was limited to a certain size, 500 mm by 500 mm, defined as stationarity threshold. In this study the sample size was limited to the maximum size of the shear box, i.e. 200 mm by 200 mm for the upper blocks, and may still be below a possible stationarity limit of the joint surface.

The mechanical tests on the concrete fracture replicas of different size, showed that mechanical properties of the joint samples are all scale dependent and their values decrease with increasing sample size and decreasing normal stress. It is concluded that stationarity threshold is different for different types of rock joints with respect to their geometrical and mechanical properties, and must be considered in characterization of the hydro-mechanical behaviour of rock joints for either theoretical models or experimental investigations.

Acknowledgements

The author thanks Dr. Björn Lagerblad and his colleagues at the "Swedish cement and concrete reasearch Institute" (CBI), and the staff of the TESTLAB at Luleå University of Technology for their great help during sample preparation and performing the mechanical tests, respectively.

References

FARDIN, N., STEPHANSSON, O. and JING, L. The Scale Dependence of Rock Joint Surface Roughness. Int. J. of Rock Mech. & Min. Sci., 38(2001), 659-669.

LINDFORS, U. Experimental Study of the Mechanics of Rock Joints. Licentiate Thesis, Division of Rock Mechanics, Luleå University of Technology, Publ. 1996:01L, Luleå, Sweden.

OLSSON, R. Mechanical and Hydromechanical Behaviour of Hard Rock Joints - a Laboratory Study. Ph.D. Thesis, Chalmers University of Technology, Gothenburg, Sweden, 1998. P. 197.

LANARO, F. and STEPHANSSON, O. A Unified Model for Fracture Characterization. Proc. 3rd Euroconference on Rock Physics and Rock Mechanics, Bad Honnef, Germany, H.J. KÜMPEL (ed.), 2001.

IMAGEWARE, Inc., 2000. Surfacer User's Guide, Ver. 10. Ann Arbor, Michigan, USA.

MALINVERNO, A. A Simple Method to Estimate the Fractal Dimension of a Self Affine Series. *Geophys. Res. Lett*. (1990), 17: 1953-6.

Hakami, E. Fracture displacement due to thermal load from nuclear waste at a repository
ISRM 2003–Technology roadmap for rock mechanics, South African Institute of Mining and Metallurgy, 2003.

Fracture displacement due to thermal load from nuclear waste at a repository

Eva Hakami
Itasca Geomekanik AB

The objective of the study was to estimate the largest shear displacement that could be expected on a pre-existing fracture located in the repository area, due to the heat release from deposited waste. Two-dimensional numerical analyses using UDEC have been performed. The maximum shear displacement, at the fracture centre, amounts to 0.2 – 13.8 cm depending on fracture parameters. The fracture extension, friction angle and shear stiffness are found to be the most important.

Le but de cette étude est de déterminer le déplacement maximal en cisaillement qui puisse se développer le long d'une fracture préexistante en réaction à la chaleur dégagée par les déchets radioactifs enfouis dans la roche. Les analyses numériques ont été réalisées à l'aide du code 2D UDEC. Le déplacement maximal en cisaillement enregistré au centre de la fracture varie entre 0.2 et 13.8 cm en fonction des propriétés de la fracture. L'ouverture, l'angle de friction et la rigidité au cisaillement semblent avoir une influence dominante sur les résultats.

Zielsetzung der Studie war die Abschätzung der maximalen Scherverschiebung, die auf einer innerhalb des Endlagergebietes existierenden Rissfläche infolge der Wärmeabstrahlung des eingelagerten Materials zu erwarten war. Es wurden zwei-dimensionale numerische Berechnungen mit UDEC durchgeführt. Die maximale Scherverschiebung im Zentrum der Rissfläche beträgt 0.2-13.8 cm, abhängig von den Risseigenschaften. Dabei hat sich herausgestellt, dass Rissgrösse,Reibungswinkel und Schersteifigkeit den grössten Einfluss haben.

Introduction

The primary function of a deep repository for spent nuclear fuel is to isolate the waste. If this isolation should be breached, a second function is to retard the transport of radionuclides from the fuel. The canister, the buffer and the host rock work in conjunction to provide these two functions. This study relates to the requirement of having mechanical stability of the rock around the repository. One of the concerns in this respect is the possibility of a large displacement occurring on a pre-existing fracture intersecting a deposition hole. Such a large displacement might jeopardise the intactness of a waste canister, i.e. break the isolation. A large fracture displacement might also result in increased ground water transport from the deposition hole to the surrounding rock mass, i.e. reduce the retardation.

The main difficulty in estimating the movements of large rock discontinuities, such as fracture zones or minor faults, is the lack of knowledge concerning their mechanical properties (Leijon, 1995). For the purpose of safety analyses it thus makes it inevitable to choose parameter values within wide ranges.

If it is assumed that a discontinuity can be approximated as a singular planar structure where the shear displacement is mainly controlled by friction, the most conservative case is a zero friction angle. An analytical calculation of a two-dimensional case (Figure 1) indicates that, with the most unfavourable orientation, the size of a discontinuity should be on the order of 100 m to get a displacement of 0.1 m. The intention with the analyses performed in this study was to add to the current state of knowledge by performing numerical analyses of a two-dimensional case, in principle similar to that in Figure 1, but with assumptions somewhat closer to the real repository situation.

The thermal load due to the temperature development from the canisters has been calculated and the corresponding mechanical response with time determined in a thermo-mechanically coupled model has been evaluated.

Numerical Modelling

The actual geometry of a future repository site will be complex and truly three-dimensional. Nevertheless, for this generic study, the approach to the problem has been to simplify the problem by looking at only one single, continuous and planar fracture. This simplification can be regarded as conservative, since in reality it can be expected that the thermally induced shear stresses would be released by deformations along many fractures, resulting in less shear deformation on each individual fracture.

The fracture is also assumed to have the most disadvantageous location, i.e. with the central part intersecting the repository horizon, and conservative assumptions are made concerning the fracture properties. Two-dimensional analyses using UDEC (Itasca, 2000) have been performed. UDEC is a distinct element code with the ability to explicitly represent discontinuities.

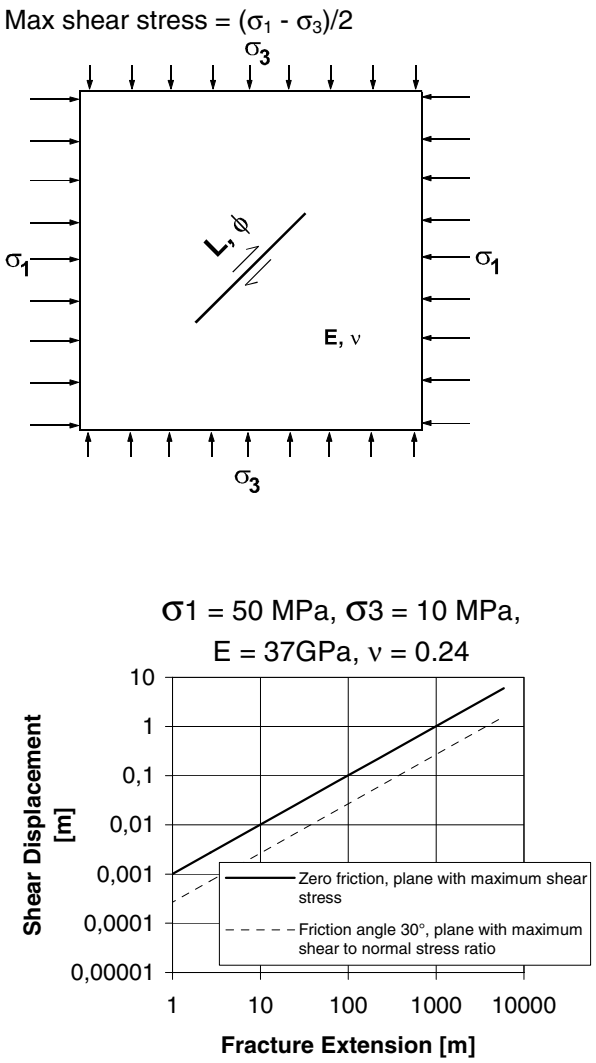

Figure 1. Fracture with extension L, and friction angle ϕ in elastic medium with the elastic parameters E and ν. The shear deformation is maximum at the centre of the fracture and zero at the edges (after Pollard and Segall, 1987).

Model geometry

The UDEC model represents a vertical cross section of the repository and has a width of 1400 m and a height of 900 m (Figure 2). The waste repository is assumed to have 25 tunnels with 40 metres spacing. The fracture (or fault) under study intersects a deposition hole in the central part of the repository.

Mechanical properties

The rock mass surrounding the fracture was modelled as a homogeneous, isotropic and elastic material, with a Young's modulus of 40 GPa and a Poisson's ratio of 0.22.

The fracture was modelled with a Coulomb slip criterion and the fracture parameters used were altered between different models to evaluate their influence on fracture shear displacements. The fracture was simulated with no cohesion and no dilation.

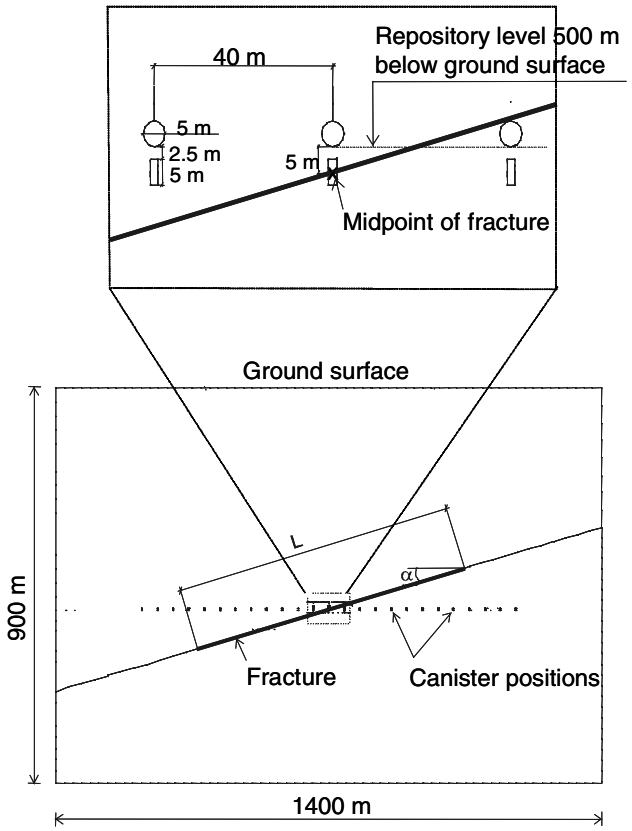

Figure 2. UDEC model geometry. In the figure the fracture length, L, is 719 m and the fracture dip angle, α, is 15°.

Thermal properties

The thermal properties are assumed to be isotropic, homogenous and constant throughout the rock mass, and only heat transfer by conduction in the rock mass is modelled. This means that the presence of the fracture does not influence the calculated thermal field, and that effects of heat convection by fluid flow or fluid buoyancy were neglected. The contribution from convection is very small and it is also conservative to neglect it. The thermo-mechanical calculations performed involve a one-way coupling, such that changes in the temperature field affect the stress field through the linear expansion coefficient. Thermal properties for the rock mass are given in Table 1.

A time period up to 1000 years after deposition was simulated by using the heat decay function suggested by thunvik and Braester (1991). The initial heat release for each canister, i.e. heat release at the time of waste deposition, was set to 1200 W. With a canister spacing of 25 m by 6 m, the corresponding initial heat release per unit repository area will then be 8.0 W/m2. A corresponding initial heat release per meter tunnel was assigned to the canister blocks in the two-dimensional model. Since the thermal effects are only due to temperature increase, the initial temperature was set to zero in the entire model.

Adiabatic boundary conditions were used for the outer boundaries, i. e. no heat transfer occurs across these boundaries. These thermal boundary conditions give slightly overestimated temperatures. The interior of the

tunnels was assumed to have the same thermal properties as the surrounding rock mass.

Table 1 Thermal properties for the rock mass.

Property	Value
Specific heat [J/kg°C]	741
Thermal conductivity [W/m°C]	3.0
Linear expansion coefficient [1/°C]	8.5E-6

Modelling Sequence

The modelling sequence consisted of three major stages:

1. Initiation of initial stresses and pore pressures in fracture. (Calculation to equilibrium).
2. Excavation of the three central tunnels in the repository. (Calculation to equilibrium).
3. Simultaneous emplacement of all waste canisters. Coupled thermo-mechanical calculations to a maximum time of 1 000 years after deposition.

Models with different fracture properties were analysed. Other conditions were kept constant between models.

Results

The temperature distribution in the rock mass will develop identically in all models. As an example, the temperature distribution after 200 years is shown in Figure 3. The temperature development with time may be better understood by looking at Figure 4 which shows the temperature for three locations in the model (marked in Figure 3).

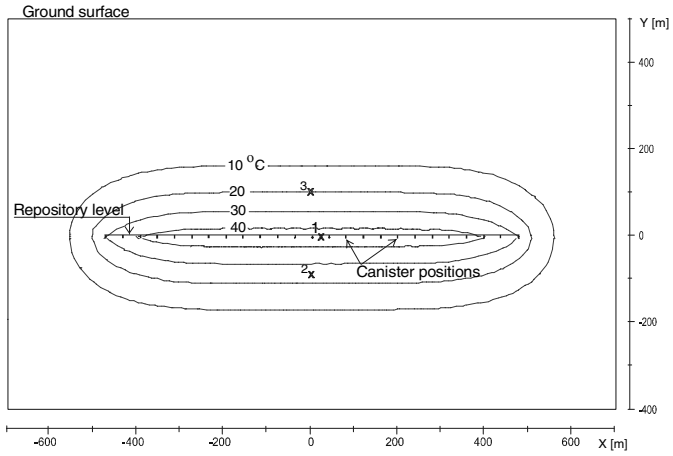

Figure 3. Temperature increase after 200 years of deposition. To get the expected total temperatures, the initial in-situ depth dependent temperatures must be added.

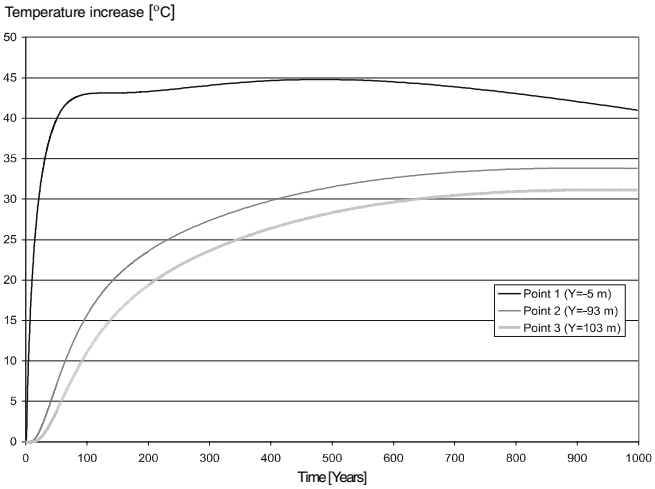

Figure 4. Temperature development at three points in the model (see Figure 3).

The shear displacement of the fracture will become largest at the centre of the fracture, because the movements are constrained at the ends, and because the load is largest at the centre where the repository is located. Figure 5 shows the shear displacement distribution along the fracture of model M3 at 1000 years after deposition. The shear displacement will develop differently at different locations along the fracture. Figure 5 also shows positions in which shear displacement data were collected during the calculation. These time histories are shown in Figure 6. (This diagram may be compared to the temperature development diagram in Figure 4).

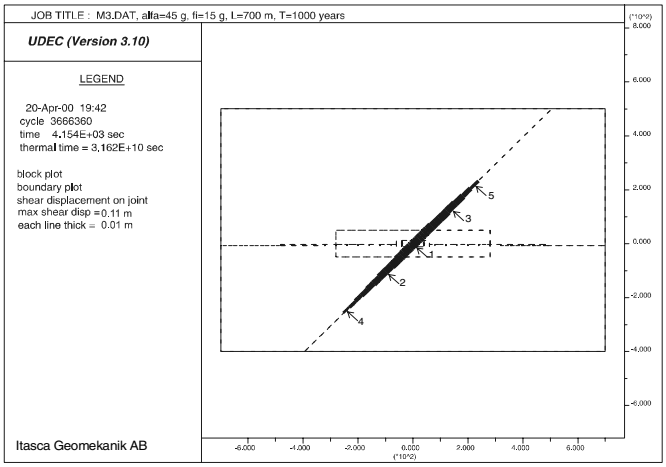

Figure 5. Shear displacement distribution along fracture at 1000 years after deposition (Model M3).

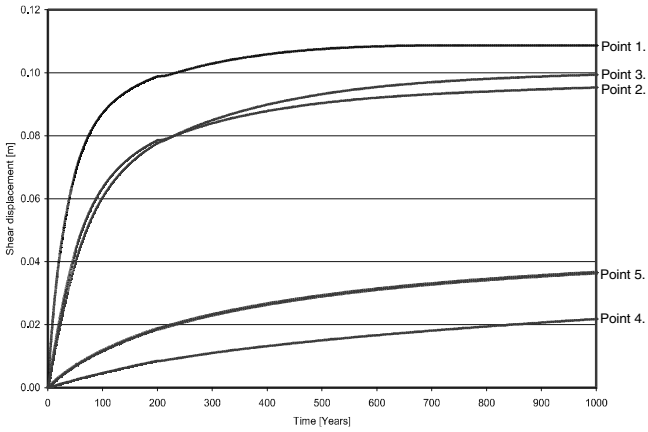

Figure 6. Shear displacement development with time for five points. Point locations are shown in Figure 5.

In Figure 7 a diagram with calculated maximum shear displacements from six models illustrates the influence of fracture length. All these fractures have the same dip angle, 30°, which is the angle at which the displacement is largest. The maximum shear displacement is approximately proportional to the fracture length, which is consistent with the analytically obtained results shown in Figure 1.

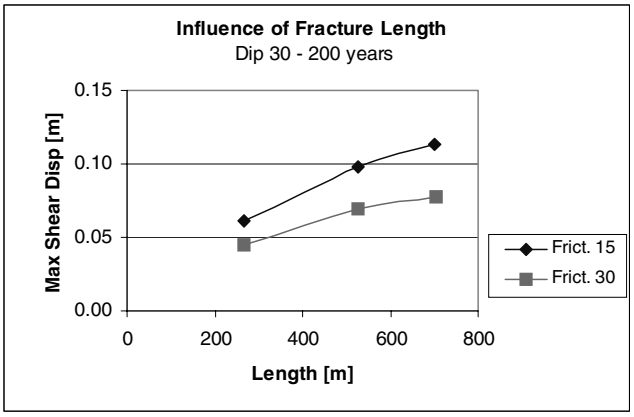

Figure 7. Influence of fracture length, L, on maximum shear displacement after 200 years of deposition.

Similarly, results are compiled in a diagram to present the influence of fracture dip, see Figure 8. The influence of dip becomes significant when the friction angle is fairly high. The maximum lies around a dip angle of 30°. For fractures of very low friction the dip angle has less importance.

The influence of the friction angle on maximum shear displacement is further illustrated in the diagram of Figure 9. For the high friction angle no slip occurs for the thermal load and the shear displacement are in the elastic regime The difference in maximum shear displacement between a model with ϕ=5° and ϕ=15° is only 1.8 cm (for L=500 m and α=30°).

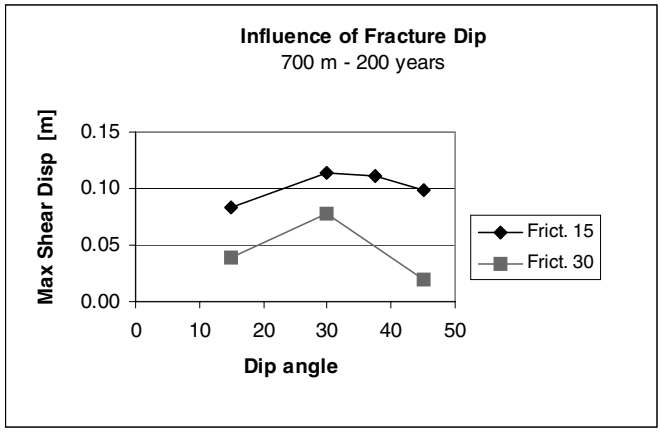

Figure 8. Influence of fracture dip angle, α, on maximum shear displacement after 200 years of deposition.

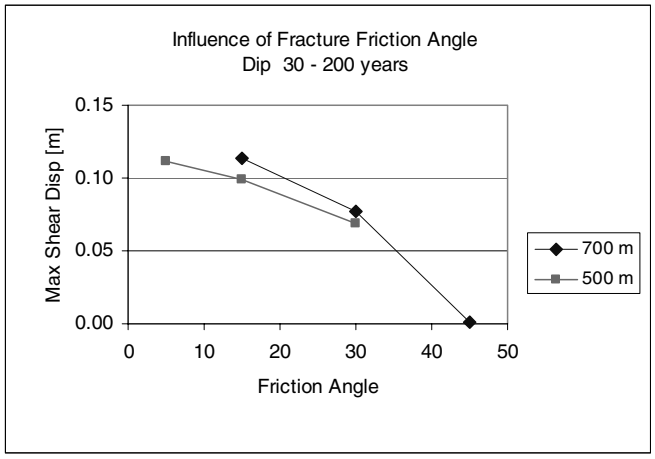

Figure 9. Influence of fracture friction angle, ϕ, on maximum shear displacement after 200 years of deposition.

Models with different shear stiffness, K_s, and different normal stiffness, K_n, were also analysed. The results showed that if the shear stiffness is sufficiently low it will control the shear deformation, but with higher shear stiffness level the fracture will slip and the shear strength (friction angle) controls the amount of deformation obtained. The effect of the normal stiffness is expected to be less on the shear deformation since the dilation is assumed to be zero in these models.

Discussion

Fracture extension and fracture shape

The extension of a fracture, fracture zone or fault is not easy to determine. A definition of what is “start" and "end" points is needed. Also the question of what constitutes one fracture and what is two or several fractures, may not be a simple issue, in particular since the information about rock discontinuities often is limited to what can be obtained from drill holes and the ground surface.

In this study it is assumed that the fracture is one single, continuous and planar structure. This is a simpler geometry than most of structures have that will be encountered at a future repository site. But since a single fracture plane is the type of structure that would get the largest and most localized movement, and thus causing the most unfavourable loading condition around the canister, this case is the one that would be most hazardous if it was located at a deposition hole.

The fracture extension is in this two-dimensional study defined by the fracture length, L, along the dip direction of the fracture. The expected shear displacement of a fracture with the length L will depend, not only on the loading situation, but also on the extent of the fracture in other directions, i. e. on the shape of the fracture plane. A 2D-simplification of the problem, such as in the UDEC analyses reported here, will always give some overestimation of the actual shear for a certain load. In cases when the extension of the fracture is expected to be much longer in the direction parallel to the strike, the 2D-assumption would be reasonably accurate. However, if the fracture were considered to be circular, with roughly the same extension in all direction, then the 2D model would give a non-negligible overestimation of the actual shear movement.

To investigate the difference in shear displacement between these two ideal fracture shapes, a fracture with infinite extent in the strike direction (out-of-plane in UDEC models) and a circular fracture, three-dimensional analyses were performed using FLAC3D (Hakami and Olofsson, 2002). The result showed that for the “two-dimensional” case the maximum shear value is 1.4 times larger than for the circular case.

Fracture mechanical properties

Although it is simple to conclude that the friction properties or the shear strength of a fracture will be a main factor determining the shear displacement, it is not easy to determine these parameters for large structures with an extension of several hundreds of metres. In such cases one has to rely on the experience from previous underground construction works, in combination with findings from laboratory and field tests. In the safety assessment analyses it is thus an essential issue to consider the uncertainty or possible range of such parameters, i.e. to perform sensitivity studies.

The approach taken here has been to study the worst case, i.e. a large single fracture plane, although a much more complex geometry of a large structure is more realistic. If a fracture in the large scale is not planar, but stepped or undulating, the overall behaviour of this fracture will be dominated by the character of these steps or undulations.

Unfortunately, there is a general lack of laboratory data for weak infilled fractures. Also, laboratory test results from small samples may be difficult to interpret and applyfor large structures, because of the possible scale effects and sampling biases.

As there will be a design criterion, stating which fractures should be allowed to intersect the deposition holes and which should not, there must nevertheless be established a procedure for how the strength of a discontinuity is to be estimated in the site investigation phase. This study shows that, in order that a considerable thermal-induced displacement takes place, a fracture must have a large size and a very low shear strength, where the friction angle is about 15º or lower. Studying results from discontinuity shear strength tests compiled by Hoek and Bray (1977), only fractures with thick clay fillings could be expected to show such low strength.

Rock mass properties

The rock mass surrounding the single fracture has in this study been simulated as a homogeneous, isotropic and elastic material. This means that the modulus of elasticity, i.e. Young’s modulus, applied for this material should represent the overall deformation properties of the rock mass, consisting in reality of both intact rock blocks and fractures of different order. A reason for large variations in rock mass deformation properties can lie both in the properties of the intact rock type and in the properties of the fractures (faults, joints, fracture zones). Laboratory tests of intact rock samples from a potential repository area showed that the mean Young’s modulus for four rock types tested lied in the range 73 – 78 GPa (Stille and Olsson, 1996). In this study a Young’s modulus for the rock mass of 40 GPa was selected. For this particular study the Young’s modulus is, however, not an important factor (se below).

In general, thermo-mechanical effects will depend both on the thermal expansion coefficient and the elastic modulus of the material, since they determine the deformation and the stress change that result from the thermal expansion. A comparison was therefore made between a UDEC model having 50 GPa Young’s modulus instead of 40 GPa. This comparison showed that the stresses at the fracture ends increase with the higher modulus, but that the maximum shear displacement is almost the same. The reason to this is that in the cases where the fracture is at slip failure, the total displacement is controlled by the total “available” expansion determined by the expansion coefficient, which was in this case held constant.

A comparison was also made between two models with different thermal expansion coefficients, 8.5e-6 and 9.5e-6 respectively. This comparison showed that a 12 % increase in thermal expansion coefficient resulted in a 16 % increase in shear displacement at the centre of the fracture. The uncertainty in the thermal expansion coefficient value is regarded as fairly low, since this parameter may be determined in laboratory. The contribution to the uncertainty in shear displacement due to the thermal expansion coefficient should thus be minor.

The thermal conductivity determines the time for the heat to spread in the surrounding rock. A change in this parameter in a model would thus result in a change in the temperature development with time in an arbitrary point, i.e. the temperature distribution at a certain period of time after deposition would be different. Lower thermal conductivity results in higher maximum temperatures around the repository and accordingly a larger shear

displacement due to the thermal expansion would be expected. The thermal conductivity can be determined on rock samples in the laboratory. According to Sundberg (1988) the average thermal conductivity for granitic and gneissic rocks lies around 3.5 W/mº C. The conductivity decreases slightly with temperature. In this study the fairly conservative value 3.0 W/mº C was used.

Summary and conclusions

Two-dimensional analyses using the UDEC code have been performed. The UDEC model represents a vertical cross section of the repository with a hypothetical planar fracture intersecting a deposition hole at the repository centre. The simulated fracture shear displacements occur due to the thermal expansion of the rock surrounding the heat generating canisters. The initial heat release per unit repository area was assumed to be 8W/m².

The thermo-mechanical analysis shows that the maximum shear is reached after about 200 – 400 years, earlier the more parallel to the repository horizon the fracture plane is.

The largest displacement occurs at the fracture centre, which is in this case located at the repository level, and the magnitude of shear depends on the different assumptions made for the twenty different models analysed. Among the analysed cases, the largest shear values, about 13 cm, was calculated for the cases with about 700 m long fractures with a shear stiffness of 0.005 GPa/m. Also, for large fractures with a higher shear stiffness of 5 GPa/m, but with a low friction angle (15°), the shear displacement reaches similar magnitudes, about 10 cm. As an example of a smaller shear, 4.5 cm displacement was obtained for the case with a fracture of 265 m length, 30° fracture friction and 30° dip angle. A case with a very high friction angle (45°), and 5 GPa/m shear stiffness, resulted in a maximum shear of 0.2 cm.

Fracture extension is the main factor in the estimation of shear displacements. For example, for a fracture with 30° dip angle and about 500 m length in the dip direction, a change of the length by 100 metres, would correspond to maximum 3 cm change in the expected shear displacement in a two-dimensional case.

Also, the shear displacement will depend on the assumed shape of the fracture. A fracture with infinite extent in the strike direction gives 1.4 times larger maximum shear displacement compared to a circular fracture.

For a fracture of given extension, fracture friction angle and fracture shear stiffness are important parameters for the estimation of expected shear displacement. A 10° change in friction angle would imply a change in estimated shear displacement of 3-5 cm, for a fracture with 30° friction. If the fracture shear stiffness is sufficiently low shear displacements are will not depend on friction. The development of a procedure for the estimation (or classification) of fracture friction and fracture shear stiffness, are therefore identified as important tasks for the site investigation phase. A very low friction value is expected only for fractures (or faults) with substantial clay filling material.

For fractures with a friction angle around 30°, the dip angle is an important factor in terms of fracture shear displacement changes. A fracture with a dip angle of 30° instead of 45° results in approximately four times larger maximum shear displacement. This effect is, however, smaller for fractures with lower friction angles.

Factors other than fracture friction angle, shear stiffness, extension and dip angle have less influence on the estimation of maximum shear displacement.

The current safety limit for allowed fracture shear displacements across a deposition hole is ten centimetres. This study shows that it takes fractures of very large extension, several hundred meters, to produce thermally induced shear displacements of this magnitude.

Acknowledgements

This study was initiated and funded by the Swedish Nuclear Waste Management Company (SKB).

References

HAKAMI, E. and S.-O. OLOFSSON (2002) ”Numerical modelling of fracture displacements due to thermal load from a KBS-3 repository” SKB, Technical Report TR 02-08, Stockholm.

HOEK, E. and J. W. BRAY (1977) “Rock Slope Engineering,” The Institution of Mining and Metallurgy, London. ISBN 0 900488 36 0

ITASCA, (2000) “UDEC Users Manual, Vol. I-III,” Itasca Consulting Group, Inc., Minneapolis.

LEIJON, B. (1993) Mechanical properties of fracture zones. SKB Technical Report TR 93-19, Stockholm.

POLLARD, D. D. and SEGALL, P. (1987) “Theoretical displacements and stresses near fractures in rock: with application to faults, joints, veins, dikes, and solution surfaces. Fracture Mechanics of Rock, Academic Press Inc., London.

STILLE, H. and P. OLSSON. (1996) “Summary of rock mechanical experiences from the construction of Äspö Hard Rock Laboratory,” SKB Progress Report PR HRL-96-07, Stockholm.

SUNDBERG, J. (1988) “Thermal properties of soils and rocks,” Doctoral Thesis, Dept. of Geology, Chalmers University of Technology, Gothenburg.

THUNVIK, R. and C. BRAESTER. (1991) ”Heat Propagation From a Radioactive Waste Repository Complementary Calculations for the SKB 91 Reference Canister,” SKB Working Report TR 91-17, Stockholm.

Lanaro, F., Röshoff, K., Jing, L., Christiansson, R. Comparison of different systems for rock mass characterisation
ISRM 2003–Technology roadmap for rock mechanics, South African Institute of Mining and Metallurgy, 2003.

Comparison of different systems for rock mass characterisation and lessons from the Äspö Test Case, Sweden

Lanaro[1], F., Röshoff[1], K., Jing[2], L.,
Christiansson[3], R.

[1]Berg Bygg Konsult AB, Solna, Sweden,
[2]Engineering Geology and Geophysics, Royal Institute of Technology, KTH, Stockholm, Sweden, [3]Swedish Nuclear Fuel and Waste Management Co, SKB, Stockholm, Sweden

This paper presents the results of a project for developing a methodology for empirically determining some of the mechanical properties of the rock mass at the Äspö Hard Rock Laboratory, Southern Sweden. Using the equations available in the literature, the deformation modulus, friction angle, cohesion and unconfined compressive strength of the rock mass were estimated. A comparison of the results using different classification methods (Q, RMR, GSI, RMi, Ramamurthy's) was made to estimate the range of variations in the mechanical properties with the considerations of: i) the quality/quantity of the geological data; ii) the technique for partitioning of the rock mass into homogeneous domains; iii) the sensitivity and subjectivity of the empirical methods; and iv) the need for validating the empirical methods against a test case.

Cet article présente les résultats d'un projet visant à établir une méthodologie, pour déterminer, de façon empirique, les propriétés mécaniques de la masse rocheuse. En utilisant les corrélations disponibles dans la littérature, quelques-unes des propriétés de la masse rocheuse ont pu être déterminées (module de déformation, angle de friction, cohésion, force de compression illimitée). Une comparaison des résultats obtenus par différentes méthodes (Q, RMR, GSI, RMi, de Ramamurthy) a permis d'établir une échelle de variations des propriétés mécaniques et de formuler une série de recommandations concernant : i) la qualité/quantité des données géologiques ; ii) la technique de partition de la masse rocheuse dans des domaines homogènes ; iii) la sensibilité et la subjectivité des méthodes empiriques ; iv) la nécessité de valider les méthodes empiriques à l'aide de nouvelles études de cas.

Dieses Paper präsentiert die Ergebnisse eines Projekts mit dem Ziel, eine Methodik für die empirische Festhellung von mechanischen Eigenschaften im Gesteinmassiv zu etablieren. Durch Verwendung der in der Literatur zugänglichen Korrelationen, wurden einige Eigenschaften des Gesteinmassivs festgestellt (Entstellungsmodul, Reibungswinkel, Kohäsion, unbeschränkte Kompressionsstärke). Ein Vergleich der Ergebnisse unterschiedlicher Methoden (Q, RMR, GSI, RMi, Ramamurthy's) wurde durchgeführt und dies erlaubte die Feststellung der Variationsskala von den mechanischen Eigenschaften, sowie eine Reihe Empfehlungen für: i) Qualität/Quantität der geologischen Dateien; ii) die Technik für Teilung des Gesteinmassivs in homogene Domäne; iii)die Empfindlichkeit und Subjektivität der empirischen Methoden; iv) das Bedarf die empirische Methoden gegen neue Fallgeschichten zu validieren.

Introduction

To estimate the overall properties of fractured rocks during site investigation, design and performance/safety assessment of nuclear waste repositories is a task of major importance. One possible approach is the use of empirical methods. Due to non-existence of closed-form solutions and difficulties in direct large-scale in situ measurements, the rock classification systems are very often used as a means to get a first-hand estimation of the mechanical properties and strength parameters, as applied in many rock engineering projects. This is done without considering issues such as the existence of a representative elementary volume (REV) (Cunha, 1990), reliable constitutive models for fractures and intact rock, and properly defined boundary/initial conditions, which all are required for the numerical schemes.

Characterisation by means of empirical methods has recently been used for predicting the mechanical properties of large-scale rock masses to perform feasibility studies for underground constructions of environmental importance, such as nuclear waste repositories. This is done as a first estimate because more in-depth understanding of the mechanical behaviour and reliable constitutive models of the fractured rocks are not available at the start of site

investigation. Some authors have suggested how to modify the existing classification methods to be applied for the purpose of characterisation of the rock mass (e.g. Barton, 2002).

The object of the work presented in this paper was to develop a methodology of rock characterization with coherent treatment of measurement techniques (geological, geophysical, and laboratory), data sources (boreholes and surface mapping), rating approaches (Q, RMR, etc.) and uncertainty/variations. The developed methodology was applied to a selected rock volume at the Äspö Hard Rock Laboratory (ÄHRL, Southern Sweden), where the Swedish Nuclear Fuel and Waste Management Co (SKB) performs tests and demonstrations for geological disposal for the Swedish nuclear waste isolation programme. The work was carried out within the rock volume of the Äspö Test Case (ÄTC) (Hudson, 2002). The Test Case consisted two large volumes of rock: one volume of size 500×500×550 m, and a smaller portion of it between the depth of 380 and 500 m called the Target Volume (TV). The TV was subdivided into 480 cubes of 30×30×30 m in size. In Figure 1, the rock volumes of the test case are shown in relation to the tunnels of the ÄHRL.

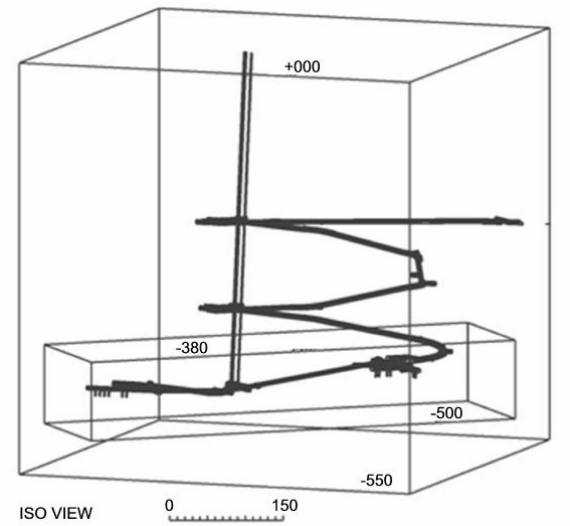

Figure 1. The size and location of the 550 m Model and the Target Volume for the Äspö Test Case.

Review of the empirical classification systems

The aim of a classification system is to describe adequately and as simply as possible rock masses of various complexity. The system should also include meaningful parameters that can easily be measured or determined in the field or from boreholes.

Bieniawski (1989) successively developed the Rock Mass Rating (RMR), a classification system based on six parameters of the intact and fractures rock. Another major classification system is the Tunnelling Quality Index (Q) based on a large amount of case histories of underground excavation in hard rock (Grimstad & Barton, 1993). Both RMR and Q-index have for long time been applied for design of rock tunnels and excavations, estimation of ground support, choice of support system, selection of direction of tunnel axes, however, mainly for shallow excavations.

Recently Palmström (1996) has suggested the Rock Mass Index (RMi), a classification system based on a jointing parameter and on the intact rock strength.

For determining the rock mass strength, the system called Geological Strength Index, GSI, was proposed by Hoek & Brown (1997).

Ramamurthy (1995) suggested that the strength and deformations modulus of a jointed rock mass can be determined from a jointing factor.

Rock mass strength

Hoek and Brown (1997) proposed some relations between GSI index, the strength of the rock mass and RMR. Through those relations, the rock mass strength envelope can be determined according to the Hoek & Brown and Mohr-Coulomb Strength Criterion. By knowing RMR, the cohesion and friction angle of the rock mass can be estimated. The values given by Bieniawski (1989) are determined mainly on soft rock and the values of the cohesion are too low for hard rock.

Rock mass deformation modulus

Grimstad & Barton (1993) gave some relations for determining the rock mass deformation modulus E_m as a function of Q. Based on the Q-index, another correlation was proposed for estimating the mean value of the rock mass deformation modulus (Barton, 1995). The calculation of the deformation modulus using RMR was given by Serafim & Pereira (1983) and is widely applied in practice.

Palmström (1996) provided his system RMi with a relation with the deformation modulus of the rock mass.

Characterisation and classification

The rock mass classification systems were developed mainly for designing tunnels. Later, with different modifications, the systems have been applied for characterisation of fractured rocks. Palmström et al. (2001) have presented a general definition of the differences between “characterisation” and “classification” when using the rock classification systems. “Characterisation” is aimed for interpretation of the geological/mechanical data for site investigations, with focuses on estimating some mechanical properties of the rock mass as a whole. “Classification” is preferably used to classify the rock quality for design and construction of the excavations using empirical rating systems. The requirements for rock characterization and classification are therefore different. The main difference is that some factors reflecting loading conditions (such as stress and water pressure) and excavation layout (such as tunnel orientation with respect to fracture orientation) are considered in classification for excavation designs, but not in characterization for large rock volumes.

In this paper, the use of Q and RMR rating indices was studied for both characterisation and classification purposes. This was achieved by different treatment of the effects of water pressure, stresses, direction of excavation and the orientation of the fracture sets. Similar treatment was also reported in Olsson et al. (1992).

Methodology

For performing the characterisation and classification of the rock mass at the ÄTC, the geological/rock mechanics data have to be treated and organised according to a methodology that would guarantee: i) traceability of the results; ii) identification of the homogeneous areas; iii) treatment of the spatial variability of the parameters; iv) quantification of the uncertainties. In the following paragraphs, a strategy for facing each of the former points is presented.

Division of the drill cores into sections

The length of a borehole in a rock block is divided into a number of core section lengths of approximately homogeneous RQD and fracture frequency. This is usually done in practice for each core box for the classification of the rock mass by RMR and Q. This partition corresponds to a preliminary classification of the rock mass according to Deere (1968) and the differences in rock types are not considered. The number of fracture sets is calculated for each block from all borehole information available in that block. Figure 2 illustrates the technique for dividing the borehole into sections.

Forms were designed for accommodating information needed for the rock mass characterisation. An Input Data Form contains the geological parameters required by Q and RMR. A Data Remark Form reports the comments and the sources of information. Data Processing Forms contain the RMR ratings and Q factors for every core section. These forms are summarized in a Rating Sheet for each block. The statistical analyses of Q and RMR for characterisation and design are given in the Rating Sheet. The Output Parameter Sheet contains the mechanical parameters obtained from the empirical ratings and their histograms.

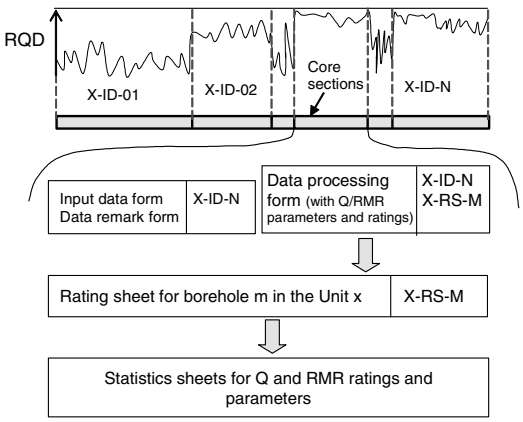

Figure 2. Division of the drill cores into sections for Q and RMR parameterisation.

Statistical treatment of parameters

All parameter values, ratings and properties are treated as statistical populations, since the spatial variability of the data can be significant. For data sets whose mean value and standard deviation do not vary significantly across the zone of interest, it is possible to incorporate the geometrical location in a statistical analysis by means of variograms. If there is some spatial correlation between the values, then the variogram tend to increase usually up to a sill. For distances larger than for the sill the spatial correlation cannot be established.

Quantification of the parameter uncertainty

A technique was created to quantify the uncertainty/confidence on the estimated parameters. The principle of the technique is to rank the confidence in the parameter according to the following influence factors:

- types and quality of the information;
- operational biases (measuring techniques, personal perspectives, etc);
- size of the data population;
- evaluation techniques;
- estimation of difficult parameters (e.g. aperture, roughness, persistence);
- ambiguity in parameter definitions;
- engineering/expert judgment needs;

Data collected by surface mapping, borehole logging, experimental results or no-data-at-all are the possible scenarios of data sources, often available in combination. The confidence on the rating parameters changes consequently. For rock volumes with information from different sources, the borehole data was ranked as the highest level of confidence followed by the surface and shaft/tunnel data. Three classes ware defined regarding the confidence of each rating parameter as:

- *certain*: the rock mass classification is done by using exactly the value of the parameter/rating. All variations in the data are accounted as spatial variation and sampling bias;
- *probable*: The classification is based on engineering judgement and reasoning, because of the very limited support from reliable data sources;
- *guesswork*: the classification is based basically on engineering judgement/reasoning without support from reliable data sources.

The Äspö Test Case

Site geology

The geological model of the ÄTC contains five main fracture zones that divide the rock volume into a number of large-scale blocks. The rock blocks contain different lithotypes: granodiorite, fine grained granite/aplite, metavolcanic rock and mylonite.

The volume of the model can mainly be divided into two domains: one north of and one south of a major fracture zone called EW1. These two domains differ for the number and orientation of fracture sets. Very scarce information was available about some minor fracture zones (EW3 and NE1).

Input data

For ÄTC, a restricted selection of data from Äspö was made available to test the performance of the developed methodology. Borehole logging was the main source of

data and contained records from three diamond-cored boreholes. Surface and shaft mapping with fracture orientation and trace length is also available (Ericsson, 1988). Mechanical testing of samples of intact rock and fractures mainly from the nearby Prototype Repository Test Area was used (Stille & Olsson, 1990; Nordlund et al., 1999; Lanaro & Stephansson, 2001).

The stress field is basically uniform with local changes due to the presence of the fracture zones (Hakami et al., 2002). The vertical stress corresponds to the overburden while the minimum horizontal stress varies between 0.5 and 0.3 times the maximum horizontal stress (Figure 3). The groundwater is assumed to have a hydrostatic pressure field with zero pressure at the ground surface. In reality, water flow is controlled by connected fracture networks and is not uniform, but this cannot be incorporated in the rating systems.

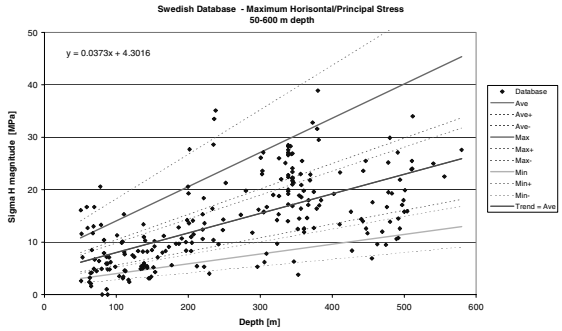

Figure 3. Maximum horizontal stress in Scandinavia (Hakami, 2002).

Parameterisation for Q

RQD is calculated directly for each core section and is most reliable for blocks containing boreholes. The Joint Set Number, Jn, is calculated for each borehole based on the number of fracture sets in the block. The Joint Roughness Number, Jr, comes mainly from three sources: sample JRC, core logging and direct site observations. With the fracture history largely unknown, the Joint Alteration Number, Ja, is determined using the residual frictional angle from laboratory tests and the evidence of coating/infilling conditions in the drill cores. For classification, the Joint Water Reduction Factor, Jw, is estimated based on an assumed hydrostatic water pressure in a saturated condition. For near surface blocks is taken equal to 1. For characterization, Jw is also taken equal to 1. The Stress Reduction Factor, SRF, is perhaps the most difficult parameter to estimate due to subjective descriptive assignation and large stepwise jumps of the classes of SRF. For characterization, SRF is taken equal to 1.

Parameterisation for RMR

The parameterisation for RMR is similar to that for Q. The rating for rock strength is determined for each core section from the uniaxial compressive strength of the rock. The fracture spacing is calculated based on the total frequency of the fractures for each core section. The fracture trace length is obtained from surface and shaft mapping data. The fracture aperture was determined in laboratory. The fracture surface can be described as “slightly rough” (Figure 4). Considering that the apertures of the fractures are generally small, the class of “no infilling” was chosen to estimate the RMR rating. “Slightly weathered” applies throughout the whole model site for describing fracture conditions, and the value of the RMR rating is 5. For characterisation, the RMR parameter for groundwater is taken equal to 15. For classification, this is determined using the assumption of hydrostatic water pressure conditions. The orientation rating considers the relative orientation of fractures with respect to tunnel and cannot be properly estimated without a tunnel layout. For characterisation purposes, a rough estimation is a “good” fracture orientation for the whole model and all blocks.

Figure 4. Photograph of the typical roughness of the fractures.

Main uncertainty issues and their treatment

The main limitations of the empirical approach are:

- The empirical approaches make it impossible to check whether they will obey basic laws of physics, such as conservation laws;
- The strength parameters in RMR are not based on site-specific failure criterion (Mohr-Coulomb) that may or may not meet site-specific rock conditions.
- The deformation modulus obtained from the empirical approaches cannot be explicitly made stress-dependent and fracture-system-geometry-dependent.

The other main uncertainties related to the site conditions considered are: i) uncertain fracture trace length and roughness, especially for blocks with no data (“blank”) blocks; ii) uncertain spatial distribution of strength of intact rocks and fractures; iii) missing information for “blank” blocks; iv) uncertain effect of rock types on rock unit division due to limits in site geological model; v) uncertain fracture orientation relative to tunnel orientation due to lack of a definite tunnel layout; vi) uncertain validity of the empirical equations for site specific conditions.

Stress dependence of the mechanical properties

Due to the complexity of stress effects, the mechanical properties of large volumes of rock cannot be quantified using a single parameter. Therefore, a first estimation of rock mass properties without stress effect should be carried

out using classification systems (Q and RMR) for characterization purposes. For classification, a model for incorporating the stress effects on the mechanical properties was formulated. The strength and deformability of the rock mass depends on the magnitude of confinement stress σ_3 applied. Since the confinement stress in the rock mass often depends on the depth, the strength and the stiffness of the rock mass also increase also with the depth. Fractures are responsible for most of the rock mass deformability and become stiffer with increasing confinement pressure as shown by the experimental results (Figure 5).

The deformation modulus of the rock mass can also easily be calculated according to Li (2000). He assumes a parallel system where the stiffness is given by the contributions from both the intact rock and the fractures. Given that the normal and shear stiffness of the fractures is a function of the normal stress, the variation of the rock mass deformation modulus with the confinement pressure can be assessed.

The stress-dependency of the deformation modulus of the rock mass was estimated along three orthogonal directions, one vertical and two horizontal directions. It can be observed how the deformation modulus increases by increasing the confinement pressure acting on the fractures. Furthermore, the orientation of the fractures with respect to the direction of loading seems to play an important role on the deformation modulus of the rock mass.

The curves in Figure 6 can be approximated by a function of the confinement pressure as:

$$E_m = E_{m0} + c'\sqrt{\sigma_3} \qquad (1)$$

For one of the rock blocks of the ÄTC, the coefficients E_{m0} and c' were evaluated to be 20 GPa and 350 $GPa^{1/2}$, respectively. The deformation modulus of the rock mass obtained by means of RMR (Serafim & Pereira, 1983) was 37 GPa, which is assigned to a confinement pressure of 1 MPa (depth around 50 m).

In the Q-system, the SRF factor is designed for making the rock mass quality to increase stepwise by increasing depth and/or stress. In consequence of this rating choice, the design parameters derived from Q would present a stepwise variation with depth.

Summary of the results

According to the definition of the ÄTC, Q-index, RMR-index, the deformation modulus, cohesion and friction angle, and the unconfined compressive strength of the rock mass were estimated for the rock units and for a certain number of 30 m rock cells at a depth of 380-450 m. The confidence levels were also to be given. To define that, a rule of thumb was defined as below: i) the cells with one or more boreholes passing through will have confidence level 1; ii) the cells at about 30 m distance from a vertical borehole will also have confidence level 1; iii) the cells immediately surrounding the cells of confidence level 1, within the same rock unit, will have confidence level 2; iv) the rest of the cells have confidence 3.

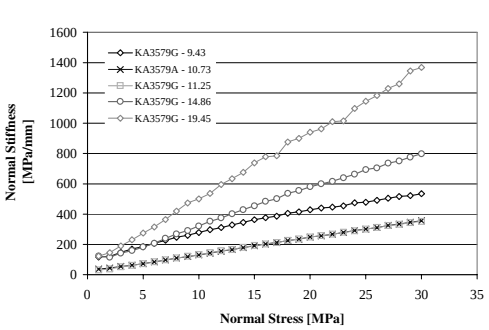

Figure 5. Normal stiffness of fractures versus normal stress for samples from the Prototype Repository (ÄHRL) (Lanaro & Stephansson, 2001).

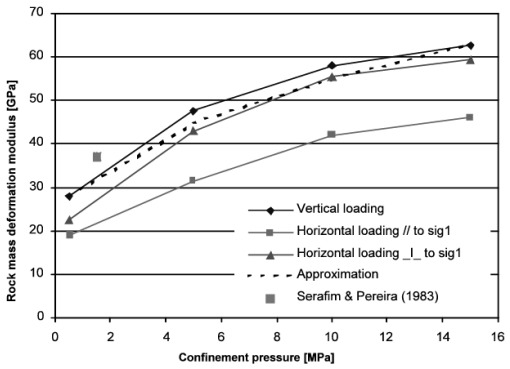

Figure 6. Variation of the rock mass deformation modulus with the direction of loading and the level of confinement pressure (Li, 2001) compared with the deformation modulus for a rock block of the ÄTC.

The Target Area

Q and RMR indices and the correspondent deformation modulus are produced for each cell where there are available geological data (Hudson, 2002). For cells containing both the intact rocks and fracture zones, two sets of values are determined for both cases. The confidence level on the obtained parameter is also determined based on the quality and quantity of the data available for each cell.

Relation between Q and RMR

As described before, Q and RMR indices were independently determined for two purposes: characterisation and classification of the rock mass. For this reason, the ratings obtained for the two purposes do not necessarily coincide. The relation between Q and RMR derived for the Äspö Test Case, for classification purposes, closely resembles the published ones (Figure 8). The relations between RMR and Q determined for characterisation are given in Figure 9. The difference between the results reported in literature and the ÄTC results is due to the treatment of water and stress effects, and to the assumption about tunnel orientation. As Goel et al. (1996) suggested, the published relations between Q and RMR indexes should only apply for “classification” of the rock mass (and design), and different equations need to be developed for “characterisation”.

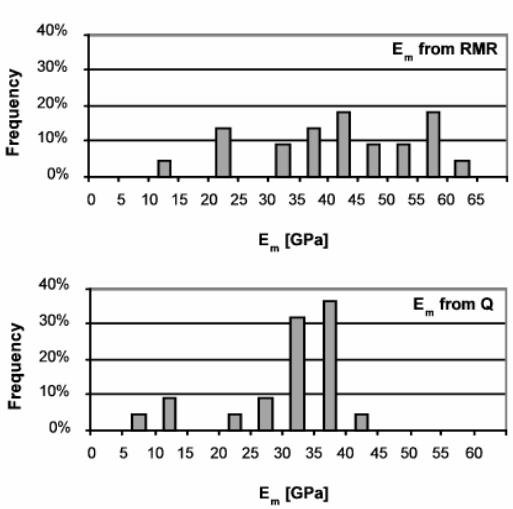

Figure 7. Example of histogram of the deformation modulus for a block of the 550 m Model of the Äspö Test Case (characterisation).

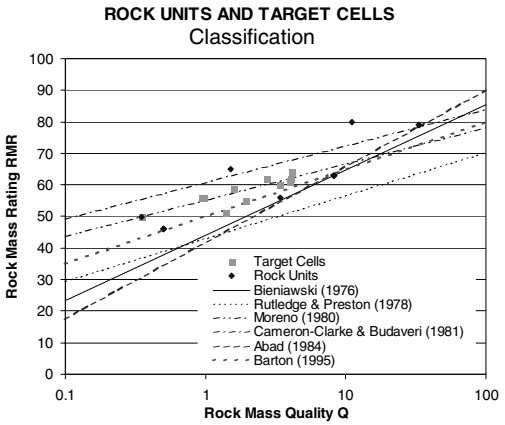

Figure 8. Q versus RMR for the rock blocks and the target cells of the Äspö Test Case (classification).

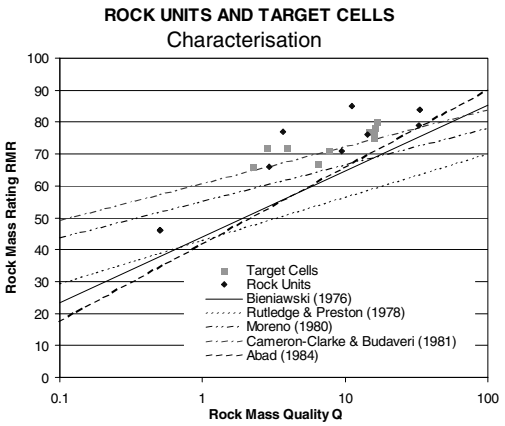

Figure 9. Q versus RMR for the rock blocks and the target cells of the Äspö Test Case (classification).

Deformation modulus

For characterisation, the deformation modulus of the rock mass is obtained according to Bieniawski (1978), Serafim & Pereira (1983), Grimstad & Barton (1993), Ramamurthy (1995) and Palmström (1995) (Figure 10). The spreading of the values is quite wide. Furthermore, all methods based on

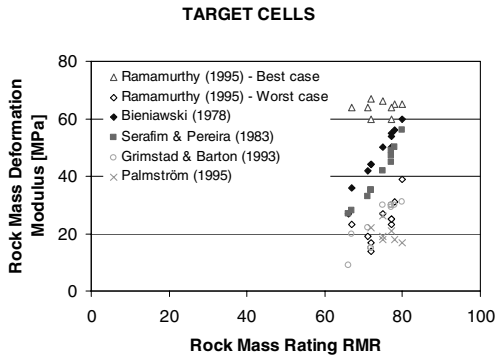

Figure 10. Comparison of the deformation modulus obtained with different relations for the Target Cells of the Äspö Test Case (characterisation).

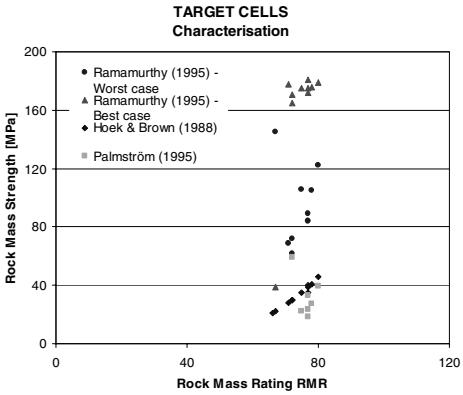

Figure 11. Comparison between the rock mass uniaxial compressive strength obtained with different methods for the Target Cells of the Äspö Test Case (characterisation).

the strength of the rock mass (RMi and Ramamurthy's "best case") do not show any defined function of RMR. The modulus determined by Q is plotted according to a logarithmic curve against RMR. Results from Bieniawski's and Serafim & Pereira's methods are very similar to each other, and they range in between the extreme minimum values provided by Palmström, and the extreme maximum values provided by Ramamurthy ("worse case") (Figure 10).

Rock mass strength

Three relations between ratings and rock mass strength investigated in this study are compared in Figure 11. It can be observed that results by Hoek & Brown's and Palmström's equations are very similar. Concerning Ramamurthy's Criterion, the values of the rock mass strength are almost of the same order of magnitude as the uniaxial compressive strength of the intact rock.

Spatial variability

The characterisation of several hundreds of meters of drill cores makes it possible to recognise some patterns that are useful for the extrapolation of the data to larger volumes of rock with similar geological settings. In this way, the characterisation/classification of the rock mass can become insensitive to the normal variations of geological parameters, as suggested by Stille & Palmström (2002). An

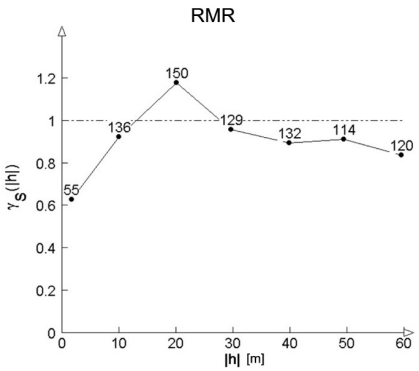

Figure 12. Standard semi-variogram of RMR along a borehole inside one of the blocks of the Äspö Test Case.

attempt of determining the pattern in the variation of RMR inside rather homogeneous blocks was done by means of semi-variograms (Figure 12). Here, a sill is reached for a distance of about 20 m.

Discussion and conclusions

For characterising a large rock volume, which usually spans over several hundred meters in all directions, it is necessary to define representative mechanical properties for both characterization and classification of the rock mass. A set of additional parameters can take into account the influence of stress and water pressure on the strength and deformability of the rock mass. By keeping intrinsic rock mass properties separated from environmental and loading conditions, no safety factors for failure mechanism (rock burst, slabbing, etc.), tunnel layout or depth would affect the determination of the rock quality and mechanical properties.

The geological information available for characterisation is quantitatively different at the different stages of the site investigation. The degree of uncertainty should, in theory, decrease as soon as more geological information is available at the site for detailed investigation and design. By assigning different degrees of confidence to the parameters involved in the characterisation/classification, a method for estimating the quality of the characterisation results was developed. This is a step forward in the development of the existent empirical methods (Stille & Palmström, 2002).

Among the classification systems applied in this paper, Q and RMR were given more attention because: i) they are based on very broad databases of case histories; ii) they are commonly used worldwide; and iii) they provide a variety of empirical relations for rock mass strength and deformation parameters. However, other characterisation and classification methods are also useful, especially for providing the extremes of the possible rock mass properties. The estimated deformability and strength properties for the Äspö Test Case seem to be realistic and representative for the site. This shows that the Q and RMR systems are suitable for identifying volumes of "good rock", as at ÄTC. On the other hand, in small volumes of "extremely good" or "very poor" rock, the results of the two systems differ more. Thus, the empirical methods can be used for localizing volumes of good rock where a repository can be located, and for estimate the large-scale mechanical properties of the rock (Andersson, 2002).

These considerations motivated the suggestion that at least two classification systems should be applied for each site in a completely independent way (Bieniawski, 1988; Palmström, 2001). Each classification systems could be developed into some simplified site-related classification/ characterisation system particularly suited to a certain environment (e.g. Swedish crystalline rocks). Nevertheless, the characterisation must be a robust process where different operators will obtain the same result on the same basis.

The outcomes of the empirical methods need to be validated against in situ measurements. This is possible for instance by determining the in situ deformation modulus of the rock mass using, for example, Goodman-jack testing, hydraulic jacking or pressiometer over large rock volumes, by back-calculation of in situ measurements of displacements in rocks surrounding excavations using numerical simulation.

References

Andersson, J., Christiansson, R., Hudson, J.A. Strategy for rock mechanics descriptive model, Äspö HRL, SKB TR 02-01, Swedish Nuclear Fuel and Waste Management Co, Stockholm, Sweden, 2002.

Barton, N. The influence of joint properties in modelling jointed rock masses, Proc. Int. ISRM Congr. on Rock Mech., Tokyo, Japan, T. Fujii ed., A.A. Balkema: Rotterdam, pp. 1023-1032, 1995.

Barton, N. Some new Q-value correlations to assist in site characterisation and tunnel design, I. J. Rock Mech. & Min. Sci. & Geomech. Abstr., Vol. 39, I. 2, pp. 185-216, 2002.

Bieniawski, Z.T. Determining rock mass deformability, Experience from case histories, I. J. Rock Mech. & Min. Sci. & Geomech. Abstr., Vol. 15, pp. 237-247, 1978.

Bieniawski, Z.T. The Rock Mass Rating (RMR) System (Geomechanics Classification) in engineering practice, in Rock classification systems for engineering purposes, ASTM STP 984 (Kirkaldie L. ed.), American Society for Testing Materials: Philadelphia, USA, pp. 17-34, 1988.

Bieniawski Z.T. Engineering rock mass classifications. John Wiley & Sons, 1989.

Cunha, A.P. Scale effects in rock mechanics, Proc. 1st Int. Workshop on Scale effects in rock messes (Pinto da Cunha ed.), Loen, Norway, AA Balkema: Rotterdam, pp. 3-27, 1990.

Deere, D.U. Geological considerations, Rock Mechanics in Engineering Practice (Stagg R.G. & Zienkiewics eds.), Wiley: New York, pp. 1-20, 1968.

Ericsson, L.O. Fracture mapping study on Äspö Island. SKB PR-25-88-10, 1988.

Grimstad E, Barton, N. Updating the Q-system for NMT. Proc. Int. Symp. On Sprayed Concrete. Fegernes, Norway, Norwegian Concrete Association, Tapis Press: Trondheim, pp. 46-66, 1993.

Goel, R.K, Jethwa, J.L, Paithankar, A.G. Indian experiences with Q and RMR Systems, Tunnelling and

Underground Space Technology, Vol 10, No.1, pp. 97-109, 1995.
Hakami, E., Hakami, H., Cosgrove, J. Strategy for a Rock Mechanics Site Descriptive Model. Development and testing of an approach to modelling the state of stress, SKB R 02-03, Swedish Nuclear Fuel and Waste Management Co, Stockholm, Sweden, 2002.
Hoek, E., Brown, E.T. Practical estimates of rock mass strength. International Journal of Rock Mechanics and Mining Sciences, Vol. 34, No. 8, pp. 1165-1186, 1997.
Hudson, A.J. (ed.). Strategy for a rock mechanics site descriptive model – A Test Case based on data from the Äspö HRL, SKB R 02-04, Swedish Nuclear Fuel and Waste Management Co, Stockholm, Sweden, 2002.
Lanaro F., Stephansson O. Geometrical and mechanical characterisation of rock fractures, Proc. Rock Mech. Meeting "Bergmekanikdag", 14 March 2001, Stockholm, 61-85, 2002, 2001.
Li, C. Deformation modulus of jointed rock masses in three-dimensional space. Proc. Int. Symp. GEOENG 2000, Melbourne, Australia, 2000, Vol. 2, Paper UW1206, 2000.
Markström, I., Stanfors, R., Juhlin, C. RVS-modellering, Ävrö slutrapport, SKB R-01-06, 2001.
Nordlund, E., Li, C., Carlsson, B. Äspö Hard Rock Laboratory: Prototype Repository-mechanical properties of the diorite in the prototype repository at Äspö HRL, SKB IPR-99-25, 1999.
Olsson, L., Rosengren, L., Stille, H. Bergklassificering med hjälp av regressionsanalys (Rock mass classification by means of regression analysis), Swedish Rock Engineering Research Foundation (SveBeFo), BeFo 210:1/92, p. 81 (in Swedish) , 1992.
Palmström, A. Rmi – A system for characterising rock mass strength for use in rock engineering, J. Rock Mech. & Tunneling Tech., Vol. 1, No. 2, pp. 69-108, 1996.
Palmström, A., Milne, D., Peck, W. The reliability of rock mass classification used in underground excavation and support design, ISRM News Journal, Vol. 6, No. 3, pp. 40-41, 2001.
Ramamurthy, T. Bearing capacity of rock foundations, in Rock Foundations (R. Yoshinaka & K. Kikuchi eds) A.A. Balkema: Rotterdam, pp.311-316, 1995.
Serafim, J.L., Pereira, J.P. Consideration of the geomechanics classification of Bieniawski, Proc. Int. Symp. Eng. Geol. & Underground Constr., pp. 1133-1144, 1983.
Stille, H., Olsson, P. Evaluation of rock mechanics, SKB PR 25-90-08, 1990.
Stille, H., Palmström, A. Rock mass classification as tool in engineering geology – Requirements and possibilities, Proc. Rock Mech. Meeting, SveBeFo, Stockholm, pp. 23-42 2003.

Rosengren, L., Brandshaug, T., Andersson, P. and P. Lundman Modeling Effects of Accidental Explosions in Rock Tunnels.
ISRM 2003–Technology roadmap for rock mechanics, South African Institute of Mining and Metallurgy, 2003.

Modeling Effects of Accidental Explosions in Rock Tunnels

L. Rosengren*, T. Brandshaug**, P. Andersson***, P. Lundman****
Rosengren Bergkonsult AB*, GeoTech Consulting**, Swedish National Road Administration***,
Swedish National Rail Administration****

'Tunnel 99', the Swedish National Road Administration´s (SNRA) general technical specification for road tunnels requires that the load bearing system must be designed to withstand specified design explosion loads. This paper presents the results of an SNRA study to provide a perspective of design analyses tailored to comply with the new requirement. The paper provides an example of a design analysis for assumed tunnel conditions using a numerical model. Dynamic predictions of potential damage to the rock mass and ground support system (rock bolts and shotcrete) from the specified explosion loads are presented including the nonlinear response of the shotcrete.

"Tunnel 99", qui fixe les règles de l'Administration nationale suédoise des Routes (Vägverket) concernant la conception et la construction des tunnels routiers, requiert entre autres que la structure porteuse soit capable de résister à certaines contraintes spécifiques résultant d'explosions. Cette étude présente les résultats d'une étude effectuée par Vägverket en vue d'obtenir une perspective d'analyses de conception spécialement élaborées pour se conformer aux nouvelles règles. Il contient un exemple d'analyse en fonction de conditions déterminées, basée sur un modèle numérique. Des prévisions de'études dynamiques de dommages potentiels subis par la masse rocheuse et les systèmes de soutènement (boulons d'ancrage et béton projeté) du fait des contraintes libérées par la force d'explosion spécifiée sont également présentées, y compris dans le cas d'une réaction non linéaire du revêtement en béton.

"Tunnel 99" - die Vorschriften für Strassentunnel der Nationalen Schwedischen Behörde für Straßenwesen - (Vägverket) - fordern vom Tragsystem eine Auslegung in der Form, dass es spezifischen Explosionsbelastungen standhält. Dieser Artikel präsentiert die Ergebnisse einer Studie der Behörde, um einen Ausblick über konstruktive Auslegungen zu geben, die geeignet sind, die neuen Vorschriften zu erfüllen. Der Artikel zeigt ein Beispiel einer konstruktive Auslegung für eine angenommene Tunnelsituation mit Hilfe eines numerischen Modells. Voraussagen unter Beachtung der vollständigen dynamischen Berechnung zu potentiellen Schädigungen des Gebirges und des Ausbaus (Anker und Spritzbetonauskleidung) durch die spezifizierten Explosionsbelastungen, einschließlich des nichtlinearen Verhaltens der Spritzbetonauskleidung, werden gezeigt.

Introduction

The Swedish National Road Administration (SNRA) has updated its general technical specification for road tunnels in 'Tunnel 99'[1]. Several new design requirements were added. One such requirement states that the tunnel load bearing system (i.e., rock mass and ground support) in addition to static loads must be designed for specified accidental explosion loads[a]. This reflects the permission to transport goods of a volatile nature but limited explosive energy in Swedish rock tunnels. The SNRA recognized the unique aspects of the requirement and the possible need to provide a perspective of its compliance. In addition, the effects of particular explosive loads on the general stability of tunnel configurations in 'typical' Swedish rocks were somewhat uncertain. In terms of design analyses, the SNRA anticipated that contributions from numerical models would be needed. To improve understanding of the problem in general, and to demonstrate the behavior of the load bearing system when subjected to explosion loads, the SNRA initiated a study concerning this specific area of tunnel design. The project goals were: (1) to provide a basis for prospective modifications of the specified explosion-load functions in the context of model limitations (e.g., stress wave propagation), (2) to provide a preliminary basis for analyzing the stability consequences of the load bearing system, and (3) to provide guidance in performing tunnel design analyses in the context of explosion loads. The study, which was based on a series of numerical models of a hypothetical (albeit realistic) tunnel system using the two-dimensional finite-difference computer code FLAC (Itasca[3]), is reported by Rosengren and Brandshaug[4,5].

Tunnel Environment and Loading Conditions

The problem geometry is shown in Figure 1 and represents a vertical section through two parallel horseshoe-shaped tunnels located 5 meters below the ground surface. The in-situ rock mass conditions, including stresses, were assumed to be the same as for the Northern Link Project in Stockholm[6], with rock mass quality in terms of the Q-index (Barton et al.[7]) in the range 4 to 10 (i.e., fair). The rock support system used was adopted from the same project, but was modified somewhat to service the assumed loading conditions of this study. The rock support system consists of systematically installed, 25-mm diameter, fully grouted rock bolts at 2-m spacing, and 100-mm thick steel-fiber reinforced shotcrete. The rock bolt length was 4 m in the roof and outside walls, and 3 m in the pillar. The in-situ stresses were:

[a] Also a requirement in the The Swedish National Rail Administration's general technical specification for rail tunnels (BV Tunnel[2])

σ_H=4.5 + 0.075 z [MPa] (normal to the tunnel axis) [1]
σ_h=3.0 + 0.0375 z [MPa] (parallel to the tunnel axis) [2]
σ_v=0.027 z [MPa] (z is depth below surface) [3]

Two explosion loads, P1 and P2, are specified in Tunnel 99 and are defined as the triangular pressure-time pulses shown in Figure 1. The P1 load is a uniformly distributed time-varying pressure over the entire (left) tunnel periphery, with a maximum value of 0.1 MPa and a total duration of 50 ms. The P2 load is a local pressure, uniformly distributed over an area of 4x4 m in the pillar or the roof of the (left) tunnel, with a maximum value of 5 MPa and a total duration of 2 ms. In both cases, the pressure rise time is 10 percent of the total pulse duration. The two pressure pulses are based on theoretical studies (Ahlenius[8]) and engineering experience of air blasts, and represent, for example, the air-blast effects from an accidental explosion of 30 kg Dynamex during transportation in the tunnel. Only the effect of the P2 load is considered in this paper.

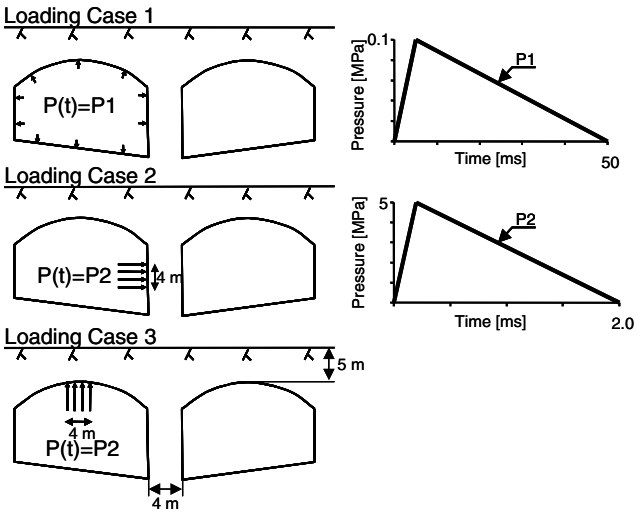

Figure 1: Tunnel Geometry and Load Cases Studied

Material Characteristics

Rock Mass

Because all rock masses are more-or-less fractured, choosing the 'best' analysis approach has important implications for the design of stable underground openings. Although general guidelines (e.g., Hoek and Brown[9]) exist for determining whether it is reasonable to characterize a rock mass as a continuum or discontinuum, the choice should be decided based on the prevailing rock mass conditions and the configuration of the underground openings. Regardless of the analysis method, the reliability of a prediction depends strongly on the characterization of the rock mass (e.g., degree of rock mass homogeneity and isotropy, intact rock strength and stiffness, fracture frequency, orientation and strength) and on local environmental factors (e.g., the magnitude and orientation of in-situ stresses, presence of groundwater, seismicity potential).

A continuum analysis was used in the current work; hence, conditions of a well-fractured rock mass of multiple joint sets are assumed, which is often the case for shallow excavations. The rock mass properties from the Northern Link Project (Rosengren and Olofsson[6]) were used in a traditional elasto-plastic Mohr-Coulomb (M-C) material model. The properties were estimated using an engineering approach by means of rock classification systems. In some cases, the rock mass was also considered to exhibit the behavior of a strain-softening (S-S) material, through the loss of some of its cohesive and frictional strengths as a function of accumulated plastic shear strain (ε^{PS} in Table I). This response appeals to the notion that the rock mass becomes disturbed, or damaged, to some degree from the construction of the underground opening (through stress relief and rotation, and possibly from excavation blasting), resulting in a finite reduction in strength. A recent update of the Hoek-Brown failure criterion (Hoek et al.[10]) discusses the addition of a disturbance factor, 'D', which modifies the rock mass strength. The concept of the disturbance factor is used in this work, although somewhat differently than intended by Hoek et al.[10]. Rather than pre-assigning a disturbance level to the whole or parts of the rock mass, only areas that exceed the peak strength become disturbed or weakened. A linear reduction in strength as a function of accumulated plastic shear strain then follows until the disturbed strength is reached. Thus, the disturbed rock-mass conditions are equated to the post-peak conditions as they evolve. Estimating the post-peak properties involve the following five steps: (1) transformation of Q to GSI; (2) determination of the maximum confining stress; (3) establishing Hoek-Brown[10,11] failure criterion for undisturbed conditions i.e., D=0; (4) estimation of the damage factor, D; and (5) estimation of M-C post-peak properties for disturbed conditions. To provide a reasonable range of properties for the S-S model, the disturbance factor was chosen to be 0.5 and 0.8, and the post-peak rock mass behavior to be semi-brittle and strain-softening. The S-S response was implemented using the standard S-S model in the FLAC code, while an associated reduction in rock mass stiffness was implemented via FLAC's macro-language 'FISH' (**F**LAC-**ish**). Table I summarizes the material parameters used for the M-C and S-S models, while Figure 2 shows a schematic of the stress-strain relations used for the S-S models.

Rock Bolts and Shotcrete

The rock bolts were modeled using FLAC's bolt structural elements. These are 1D elements of elastic-perfectly-plastic response that also allow for bond failure between the bolts and the rock. Table II lists the rock bolt parameters used in these analyses. The shotcrete was modeled using FLAC's beam structural element, and modified to include the nonlinear response associated with local failure from the combined axial and flexural loads in Eq. 4:

$$\sigma^{\text{compression / tension}} = \frac{N}{A} \pm \frac{Mc}{I} \qquad [4]$$

where, for the shotcrete, N is the normal force, A is the cross-sectional area, M is the moment, c is half the thickness and I is the second moment of inertia. The modifications, which were implemented using FISH allow failure to occur in compression, tension, or transverse shear. Failure in either tension or compression is determined from the outer-fiber stresses in the shotcrete. The model is based on the assumption that a crack develops across the entire shotcrete thickness when the transverse shear, tensile or

Table I: Summary of M-C and S-S Material Parameters

Parameter	**M-C**	**S-S**			
		Set #1 (D=0.5)	Set #2 (D=0.8)	Set #3 (D=0.8)	Set #4 (D=0.8)
ρ_m [kg/m^3]	2700	2700	2700	2700	2700
E_m [GPa]	14	10.3	8.2	8.2	8.2
ν_m	0.25	0.25	0.25	0.25	0.25
c_m [MPa]	1.8	1.25	0.95	0.95	0.95
ϕ_m [°]	40	37.1	33.5	33.5	33.5
ψ_m [°]	7	7	7	7	7
σ_{tm} [MPa]	0.26	0.26	0.26	0.26	0.26
ε^{PS} [%]	-	0	0	0.5	0.05

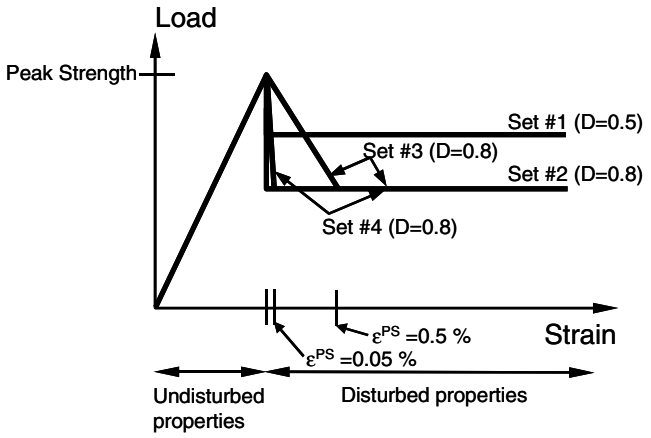

Figure 2: Illustration of S-S Stress-Strain Relations Used

compressive load exceeds the corresponding shotcrete strength. If any of these failure modes occur, the structural segment looses its capacity to sustain a bending moment and an axial tensile load, but will sustain an axial compressive load limited to the compressive strength. The transverse shear force capacity is limited to the lesser of F_{axial} x tan ϕ_c and the shear strength, τ_d, where F_{axial} is the axial compression force and ϕ_c is the friction angle of the crack. As implemented, the shotcrete model is brittle, which is somewhat conservative as the shotcrete is reinforced with steel fibers. A full description of the inelastic shotcrete model is given in Rosengren and Brandshaug[4]. Table III lists the shotcrete parameters used in these analyses.

The contact between the rock mass and the shotcrete was considered to be an interface to allow for bonding failure. For all models this interface was characterized by its normal and shears stiffnesses (40 GPa/m), cohesion (1.8 MPa), friction angle (40°), and bond strength (0.5 MPa).

Table II: Rock Bolt Parameters

Parameter	Value
Density, ρ_s [kg/m^3]	7800
Young´s modulus, E_s [GPa]	200
Tensile strength, f_{yk} [MPa]	500
Tensile strain capacity, ε_{gd} [%]	3.62[a)] 5.00[b)]
Stiffness of grout, K_{bond} [GN/m/m]	9.62
Shear strength capacity of grout, S_{bond} [kN/m]	40

Table III: Fiber Reinforced Shotcrete Parameters

Parameter	Value
Density, ρ_c [kg/m^3]	2300
Young´s modulus, E_c [GPa]	16
Second moment of inertia, I [m^4]	8.33E-5
Tensile strength, f_{flcr} [MPa]	2.8[a)] 3.9[b)]
Compressive strength, f_{ccd} [MPa]	15.8[a)] 26.1[b)]
Shear strength, τ_d [MPa]	2
Friction angle in shotcrete crack, ϕ_c [°]	40

a) Values used for static conditions; b) Values used for dynamic conditions.

Dynamic Modeling Considerations

Evaluating effects of tunnel explosions in the context of the specified P1 and P2 pulses is a two-step process. The first is a determination of the static equilibrium conditions associated with the tunnel excavation, and the second is the application and propagation of the stress wave through the model. Hence, the static solution represents the initial conditions for the dynamic part. In the static part, a gradual excavation of the two tunnels was used with ground support (bolts and shotcrete) installed at the time of 80 precent tunnel wall displacements. The gradual excavation is implemented readily with FISH and minimizes the inertial effects that an instantaneous excavation can have on the development of rock mass damage or plasticity. This is particularly important when using the S-S model because of its sensitive nature, which can lead to artificially unstable conditions. The overall dimensions of the model in this study (40x100 m height x width) were determined primarily to minimize the effects of boundary conditions on the stress state in the vicinity of the tunnels. Roller boundaries were used in the static model with the exception of the ground surface, which was free. In the dynamic part of the problem, the roller boundaries were changed to non-reflecting boundaries through the use of FLAC's viscous boundary conditions.

Although the dynamic effect is considered in the second part of the problem, it must also be considered during the initial construction of the model, when the spatial discritization is decided. Ensuring an accurate propagation of the dynamic stress wave through the model imposes a limit on the maximum spatial discretization (i.e., zone or element size) that should be used. This is not unique to FLAC; it is a general restriction common to numerical models of discretized media. For accurate wave propagation through a model, Kuhlemeyer and Lysmer[12] have shown that the element size, Δl, must be less than approximately 1/8-1/10 of the wave length associated with the highest frequency of the input wave. This implies that the criterion in Eq. 5 must be satisfied to avoid numerical dispersion of the wave:

$$\Delta l \leq \frac{C}{10 f^{max}} \qquad [5]$$

where C is the speed of propagation associated with the mode of oscillation (i.e., the P- or S-wave velocity of the medium), and f^{max} is the highest frequency of the wave. Hence, to ensure accurate propagation of the waves associated with pulses P1 and P2, their frequency content must be known. This was achieved by means of FFT-analyses (Fast Fourier Transform) of the two pressure-time

pulses. The maximum frequency content of the P1 pulse was found to be 80 Hz. The frequency content versus Fourier amplitude for the P2 pulse is shown in Figure 3 and indicates a maximum frequency of 2000 Hz. Thus, according to Eq. 5, the maximum zone size is controlled by the P2 pulse. However, Figure 3 also indicates that most of the energy contained in the P2 pulse is associated with frequencies of less than 750 Hz. Therefore, the higher frequencies could be removed by filtering without a significant change to the total power of the pulse. For comparison, Figure 3 also shows the Fourier amplitude versus frequency for the P2 pulse filtered at 750 Hz, while Figure 4 compares the specified and filtered pressure-time relations of the P2 pulse. The total power of the filtered pulse is 93 percent of the specified pulse.

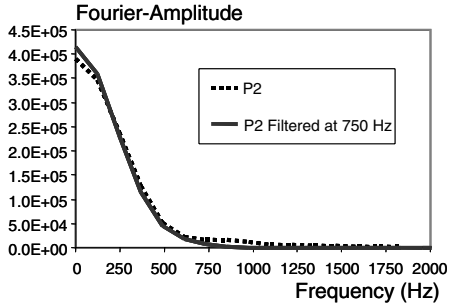

Figure 3: Frequency Content of the P2 Pulse

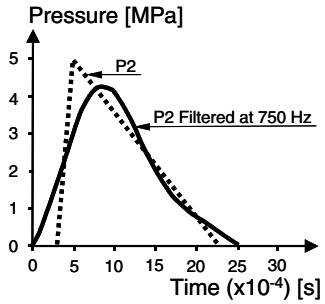

Figure 4: P2 and Filtered P2 Pulse

Depending on whether the P-wave or the S-wave is considered at the filtered 750 Hz maximum frequency, and 8 or 10 is used in the denominator in Eq. 5, the estimated maximum zone size ranges from 0.15 m to 0.32 m. Based on one-dimensional (i.e., plane-wave) elastic wave propagation tests of the filtered P2 pulse, a maximum zone size of 0.25 m was selected and applied uniformly throughout the model.

Artificial damping can be applied in FLAC, but it was not used in this work. In these analyses, any damping of the kinetic energy occurs strictly through the capacity of the strain-softening plasticity model to dissipate energy and the transmission of the waves through the non-reflecting boundaries of the model.

Analysis Results

The analyses focused on the predicted response of the tunnel environment, such as the loads in the shotcrete and rock bolts, and the extent to which the rock mass yields. In the following, unless expressed otherwise, results shown are for the S-S model using property Set #1 in Table I and Loading Case 2 in Figure 1 for the explosion directed toward the pillar. Figure 5 illustrates the predicted region of the plastically yielded rock mass resulting from the gradual excavation of the tunnel system (i.e., the static part of the problem). The yielded region is also the region of the rock mass that has become disturbed, as discussed earlier. As a result of the relatively high in-situ horizontal stress and the strain-softening response of the rock mass, localization of shear failure occurs above as well as below the tunnels. Note that because the tunnels are excavated simultaneously and at the same rate in this analysis, the pillar between the tunnels remains substantially intact. A design analysis in this case should give consideration to the sequence and rate at which the tunnels are excavated as this will affect the rock mass response (e.g., amount and location of yield).

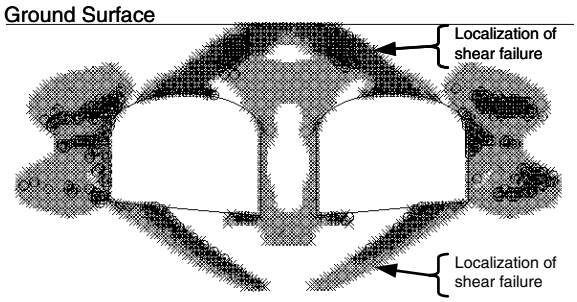

Figure 5: Regions of Plastic Yield for Static Conditions

The rock bolts and shotcrete respond to the static load without exceeding their load capacity. Only two roof bolts (in each tunnel) carry a significant load of approximately 30 percent of the yield strength. The stresses in the shotcrete are well below the yield strength with the exception of two locations in the outer walls (close to the floor and close to the roof) where tensile stresses develop with magnitudes below but close to the yield strength. The tunnels are stable for the static conditions.

In the dynamic analysis, application of the P2 pulse in the pillar of the left tunnel results in predicted final rock-mass displacements (i.e., after the stress wave has passed through the model), as shown in Figure 6. Note that these displacements are only a result of the dynamic load. The displacements are small (maximum 3.2 mm) and relatively local to the pillar wall of the right tunnel. Results from monitoring the particle velocity at the mid-height of this wall are shown in Figure 7 and indicate a peak velocity of about 1 m/s for both the M-C and S-S models. The figure also indicates the greater capacity of the S-S model to dissipate kinetic energy. The corresponding estimated region of rock mass yielding is shown in Figure 8. The effect of the P2 explosive load in this case causes slightly more yielding of the rock mass than predicted from the result of excavation (Figure 5). As shown in Figure 9, only the pillar rock bolts are affected significantly by the explosive load in this case. The bolts in the right tunnel are subjected to higher extension than those in the left, which is consistent with the predicted displacements in Figure 6. The bolts are near yield in this case. Only when using property sets #3 and #4 in Table I do the pillar bolts in the right tunnel slightly exceed the yield strength of 246 kN, but for bolt strains far below the strain capacity. The predicted total damage to the shotcrete from the P2 explosive load toward the pillar is shown in Figure 10 as the 'tabs' along the periphery of the tunnel. Each tab represents failure (i.e.,

a crack) in a shotcrete element. Failure was caused exclusively by the shotcrete outer-fibers exceeding the tensile strength. For the other cases investigated, the predicted shotcrete failure differed only marginally from that shown in Figure 10. The explosion did not affect the contact bond between the shotcrete and the rock. By increasing the thickness of the shotcrete from 100 mm to 150 mm, the amount of damage predicted virtually disappeared.

To assess the consequence of the shotcrete failure, it is necessary to understand its function as a ground support member. The purpose of the shotcrete is not to be the main component of ground support but, rather, to contribute a kinematic restraint to the blocky rock system adjacent to the tunnel surface, thereby preventing an unlocking of this sytem that may cause a sudden roof or wall fall.

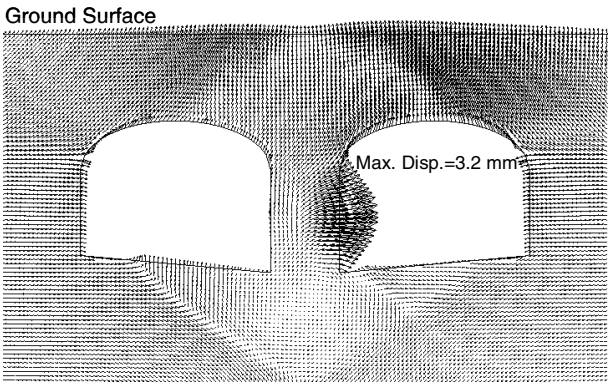

Figure 6: Displacement Vectors for Dynamic Conditions

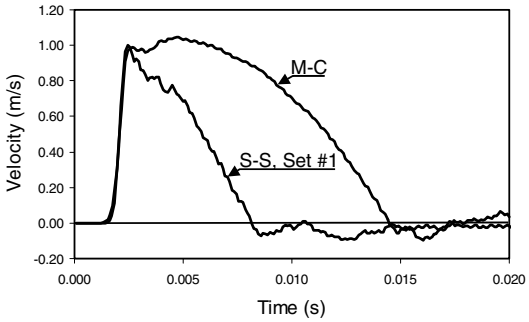

Figure 7: History of Horizontal Velocity

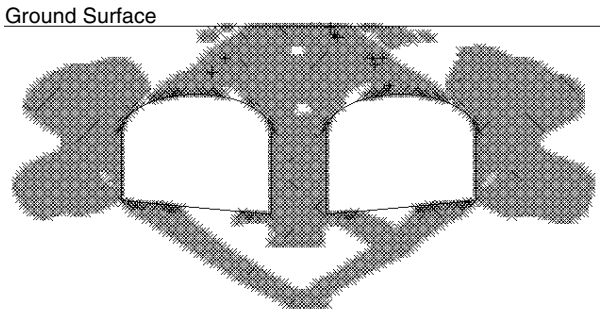

Figure 8: Regions of Plastic Yield for Dynamic Conditions

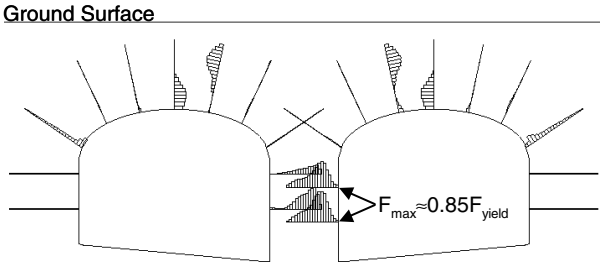

Figure 9: Forces in the Rock Bolts for Dynamic Conditions

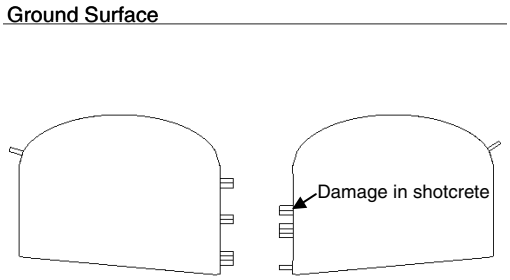

Figure 10: Damage in Shotcrete for Dynamic Conditions

To serve this function does not require a significant amount of back-pressure from the shotcrete toward the tunnel surface. Therefore, the shotcrete can be relatively thin. Even if the shotcrete capacity is diminished by the damage predicted in Figure 10, the effect is relatively local and could be readily repaired. Hence, the consequence of the damage as predicted is expected to be limited, and the tunnels are considered to remain stable.

Conclusions

Concerned with public safety and disruption to roadway infrastructure, the SNRA issued updated requirements regarding the design and construction of rock tunnels in publication Tunnel 99[1]. One new requirement expresses that the tunnel load bearing system must be designed to withstand specified design explosion loads. The SNRA recognized the uniqueness of this requirement and a need to provide a compliance perspective. This paper has addressed this need in the context of a rock-tunnel design analysis based on a fully dynamic nonlinear numerical model using the FLAC (Itasca[3]) computer code. Although assumed tunnel conditions were analyzed, they are considered a realistic case for which the rock mass quality in terms of the Q-system is fair. In conducting the analyses, observations were made that address the objectives set forth in the Introduction of this paper:

- Ensuring accurate wave propagation in analyses of discretized media puts limits on the maximum zone size that should be used. The maximum frequency of the propagating wave affects this limit. Tunnel 99 should consider allowing filtering of the specified P2 pulse, as was done in this analysis, to remove higher frequencies associated with little transfer of energy but which cause a stricter requirement to maximum zone size. Tractable numerical-design analyses depend, to some extent, on the maximum allowable zone size. For rock mass conditions different than those considered in this work (e.g., lower stiffness), some analyses may not be possible.

- These analyses have shown that a system of parallel rock tunnels in fair crystalline rock (according to the Q-system) are stable when subjected to an explosive load that closely matches the specified P2 load in Tunnel 99. Minor local damage can be expected in a 100-mm thick shotcrete, but it is likely to be of limited consequence to the tunnel stability.

- This paper is a brief summary of the work described by Rosengren and Brandshaug[4,5], which gives a detailed outline of the process, steps and concerns associated with conducting fully dynamic nonlinear design analyses in the context of the Tunnel 99 requirement.

Acknowledgements

The authors wish to express their appreciation to the Swedish National Road Administration and the Swedish National Rail Administration for funding this work and for alowing this paper to be published.

References

[1] Vägverket (1999): *General Technical Specification For Road Tunnels – Tunnel 99*. (in Swedish) Publ. 1999:138, Vägverket, Enheten för statlig väghållning.

[2] Banverket (2002): *General Technical Specification For Rail Tunnels – BV Tunnel*. (in Swedish), Standard BVS 585.40, 2002-07-01.

[3] Itasca Consulting Group, Inc. (2000): FLAC (Fast Lagrangian Analysis of Continua), Version 4.0. Minneapolis: ICG.

[4] Rosengren, L. and T. Brandshaug (2001): *Numerical Analysis of Explosion Loads in Rock Tunnels*. (in Swedish) Rosengren Bergkonsult report to Vägverket, December 2001.

[5] Rosengren, L. and T. Brandshaug (2002): *Numerical Analysis of Explosion Loads in Rock Tunnels – Phase 2*. (in Swedish) Rosengren Bergkonsult AB report to Vägverket, December 2002.

[6] Rosengren, L. and S-O. Olofsson (1997): Design of Rock Reinforcements for Contracts Roslagstull and Värtan According to Tunnel 95. *Proceedings of the Swedish Rock Mechanics Day.* Ed. C. Bachman, Stockholm 1997, pp. 65-84 SveBeFo.

[7] Barton, N.R., Lien, R. and J. Lunde (1974): Engineering classification of rock masses for the design of tunnel support. *Rock Mech.* 6(4), pp. 189-239.

[8] Ahlenius, E. (1999): *Explosion Loads And Fundamental Structures – Risks, Evaluations And Costs.* (in Swedish) Licentiate Thesis, ISRN KTH/BKN/B-47-SE, Royal Institute of Technology, Stockholm.

[9] Hoek, E. and E.T. Brown (1980): *Underground Excavations in Rock*. The Institution of Mining and Metallurgy, London 1980.

[10] Hoek, E., Carranza-Torres, C.T., and B. Corkum (2002): Hoek-Brown failure criterion – 2002 Edition. *Proceedings of the NARMS-TAC 2002,* Toronto, Canada – July 7 to 10, 2002. Eds. R. Hammah, W. Bawden, J. Curran and M. Telesnicki. Vol. 1 pp. 267-271. University of Toronto.

[11] Hoek, E. and E.T. Brown (1997): Practical estimates of rock mass strength. *Int. J. Rock Mech. & Mining Sci. & Geomech. Abstr.* 34(8), pp.1165-1186.

[12] Kuhlemeyer, R. L., and J. Lysmer. (1973): Finite Element Method Accuracy for Wave Propagation Problems. *J. Soil Mech. & Foundations*, Div. ASCE, 99(SM5), pp. 421-427 (May).

Sjöberg, J., Lundman, P., Nordlund, E., Quinteiro, C. Stability analysis of ore passes in the Kiirunavaara mine
ISRM 2003–Technology roadmap for rock mechanics, South African Institute of Mining and Metallurgy, 2003.

Stability analysis of ore passes in the Kiirunavaara mine

Jonny Sjöberg *, Peter Lundman **,
Erling Nordlund ***, Carlos Quinteiro ****
SwedPower AB *, Banverket HK **,
Luleå University of Technology ***, LKAB ****

Abstract

In the Kiirunavaara underground mine, crude ore is transported through ore passes from the production levels to the main haulage level. Failure and stability problems have occurred in some of these ore passes, with increasing frequency as mining depths increase. In this paper, selected results are presented from a research project run by LKAB. The presentation focuses specifically on stability analysis. Numerical models were used to identify failure mechanisms, in conjunction with empirical data and engineering judgment. The most important controlling factors governing failure and damage in ore passes were quantified. A causative model was established in which failure mechanisms and failure development were described. This model was used to formulate a prognosis of future ore pass stability, and for recommending remedial measures.

Résumé

Le transport du minerai entre les niveaux de production et le niveau principal de transport, à la mine de fer de Kiruna, se fait par des passes à minerai. Avec la profondeur d'extraction grandissante, les problèmes de stabilité au niveau de ces passes à minerai se sont multipliés. Les résultats d'un programme de recherche sur la stabilité des passes à minerai à la mine de fer de Kiruna sont présentés dans cet article. Les mécanismes de rupture ont été identifiés à l'aide de modèles numériques, de données de terrain et du jugement empirique des ingénieurs. Les facteurs principaux controllant l'instabilité des passes à minerai ont aussi été quantifiés. Un modèle a été établi dans lequel les mécanismes de rupture et le développement des dommages ont été décrits. Ce modèle a été utilisé à fins prédictives et remédiatives.

Zusammenfassung

In der Grube Kiirunavaara wird das gewonnene Erz über Sturzschächte von den Abbauebenen zu der Hauptförderebene gefördert. Mit zunehmender Tiefe des Abbaus sind vermehrt Standsicherheitsprobleme in den Sturzschächten aufgetreten, die teilweise zu Verbrüchen geführt haben. In dem vorliegenden Beitrag werden ausgewählte Ergebnisse einer Forschungsarbeit des LKAB präsentiert. Dabei wird der Schwerpunkt auf die Standsicherheitsuntersuchungen gelegt. Zur Ermittlung der Bruchmechanismen wurden numerische Modelle in Verbindung mit empirischen Daten angewendet. Die wichtigsten Einflußfaktoren für das Versagen der Sturzschächte wurden ermittelt. Es wurde ein Modell zur Beschreibung der Bruchmechanismen und des Versagensablaufs aufgestellt. Dieses Modell wurde verwendet, um die Standsicherheit zukünftiger Sturzschächte zu prognostizieren und um Sanierungsmaßnahmen zu erarbeiten.

Introduction

In the Kiirunavaara underground mine (owned and operated by LKAB), some 23 million metric tons of iron ore is mined annually using sublevel caving. The crude ore is transported underground through ore passes from the production levels to the main haulage level. The ore passes constitute a critical link in the production chain and high availability is required. There are currently eight groups of ore passes comprising four ore passes each, and two additional groups with three ore passes each (Figure 1).

Failure and stability problems have occurred in some of these ore passes, with increasing frequency and extent as mining depths increase. There are examples of ore passes that have increased in cross-sectional area from the original 7 m^2 to over 100 m^2, although these had only been in operation for a fraction of their intended life. These damages have necessitated extensive and costly renovations. However, there are also ore passes with very little damage despite large tonnages being transported. It has not been possible to identify the governing factors behind the initiation and propagation of failures, or to describe the failure mechanisms for these.

In this paper, selected results are presented from a research project run by LKAB. The project was aimed at improving ore pass stability and, eventually, reduce costs and increase availability. The project comprised collection and compilation of all pertinent data on ore passes, literature review of similar problems in other mines, identification of controlling factors for failures and stability problems, identification of failure mechanisms, and prognosis of future stability conditions in ore passes.

This paper focuses specifically on stability analysis of the ore passes, including numerical modeling used in conjunction with empirical data and engineering judgment. Methodology, input data and calibration of models is described as well as practical application of the results.

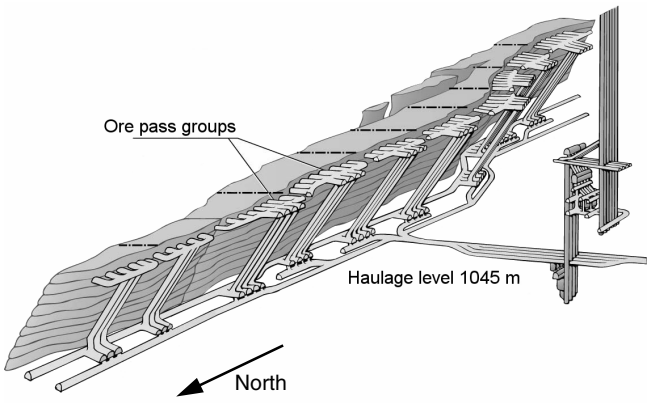

Figure 1 Ore passes for the current main haulage level in the LKAB Kiirunavaara mine.

Ore passes in Kiirunavaara

Ore pass data

The tabular Kiirunavaara orebody is more than 4000 meter long, with an average width of 80 meters. The orebody dips approximately 60° toward east and strikes almost north-south. All mining is currently conducted using sublevel caving. During the time of the project, mining was conducted between levels 765 and 820 meter (with the ground surface located between levels 50 and 150 meter).

All ore passes for the current main haulage level were full-face drilled with a 3 m diameter and a total length of about 260 m. Drilling was carried out in two stages with an intermediate level at 910 m (Figure 2). The chutes connecting each production level with the ore pass are constructed using conventional drilling-and-blasting. These are developed consecutively as mining progresses downward. The dip of the ore passes varies between 60° and 70°. The horizontal distance between the orebody and the ore passes is around 70 m. Some, but not all, of the ore passes have been reinforced using cable bolting in fans at 5 meter vertical distance. Cable bolt lengths are normally between 3 and 6 m. A few of the ore passes are fitted with grizzlies (to reduce boulder size). The ore pass geometry is defined according to Figure 2, where the hangingwall is termed "roof" and the footwall defined as "floor" of the ore pass. Hence, the "width" is defined as the distance between the ore pass walls (north-south) and the "height" as the distance between roof and floor (east-west) in the plane perpendicular to the ore pass axis.

The rock mass quality in Kiirunavaara is generally good (*RMR* = 60 on average for the footwall). Rock conditions do, however, vary from high-strength, brittle rock to altered, slightly weathered rock with numerous clay- and chlorite-filled discontinuities. Dominating joint orientations are north-south (parallel to the orebody) and east-west. Both these joint sets are steeply dipping.

Core drilling has been conducted for each ore pass group before full-face drilling. Only two of these holes were placed in the actual position of an ore pass—all the others are at a distance of 30 m or more from the ore pass. However, nearly all ore passes were mapped immediately after full-face drilling (Dahnér, 2000). The mapping comprised rough geological characterization and mapping of discontinuities and zones of poor rock. Unfortunately, some portions of the ore passes could not be mapped due to rock bursts, poor rock conditions, or time constraints. Consequently, detailed knowledge of the geology and the geomechanical conditions along and around every ore pass is not available.

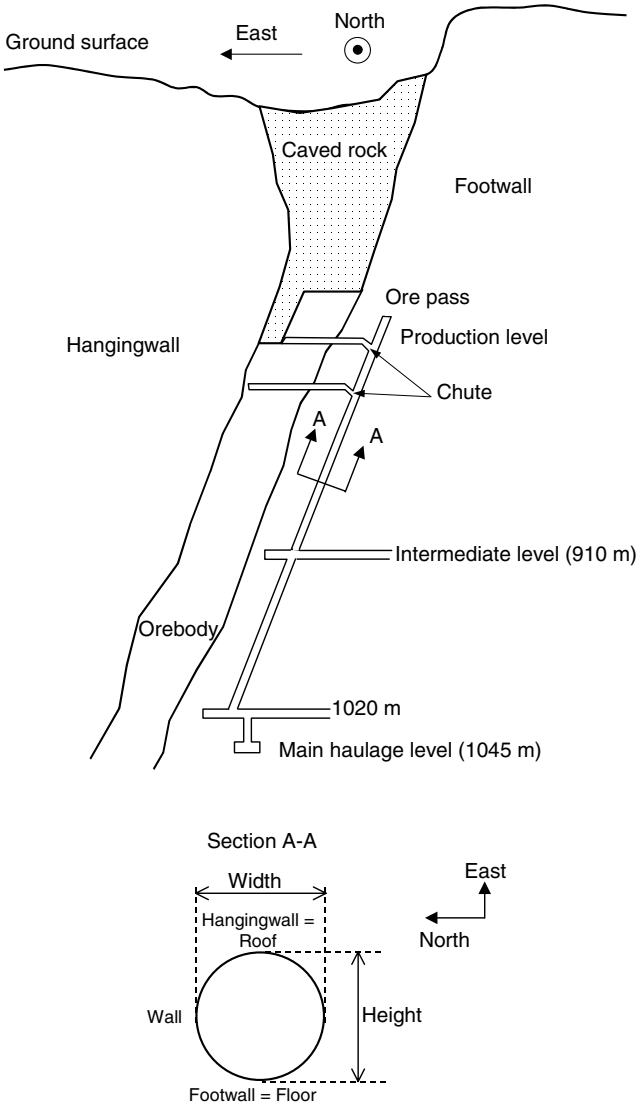

Figure 2 Typical ore pass geometry from level 790 to 1045 meter (looking south) and definition of ore pass geometry (figure not to scale).

After the ore passes were taken into production, ore pass inspections have been conducted annually (or more often if dictated by conditions). Inspections are performed using a special ore pass "buggy" fitted with a video camera. The buggy is lowered into the ore pass with video recording being done continuously. The video camera is also equipped with a laser for approximate length measurements (on the video monitor). Ore pass dimensions are measured every 5 meter along the ore pass. Due to the challenging field conditions (dust, poor lighting, etc.) and the measurement method itself, the measurement errors are fairly large, up to an estimated ± 20%.

Failure modes in ore passes

Based on inspection data, mapping, and information from LKAB staff, seven primary failure modes were identified: (1) width increase, (2) groove in the floor of the ore pass, (3) fall-outs on the intermediate level, (4) height increase, (5) increase in width and height, (6) fall-outs in the chute, and (7) wedge failures (block fall-outs) in the ore pass.

The most common of these was the increase in width in the north-south direction (parallel to the orebody). An example is shown in Figure 3. Height increase (in the east-west direction) is less common, with the exception of the forming of a groove in the floor of an ore pass—most likely an effect of wear and boulder impact. The groove varies in depth from about 0.1 m to over 2 m. Purely structurally controlled failures are less frequent, except for failures near the intermediate level, where the increased free surface (ore pass and drifts, cf. Figure 2) allows larger wedge and block failures.

An increase in both width and height was observed in several cases (cf. Figure 3). This failure mode has sometimes resulted in very large fall-outs. The failure development, from initial damage to large fall-outs has not been possible to follow due to the relatively large time interval between the inspections.

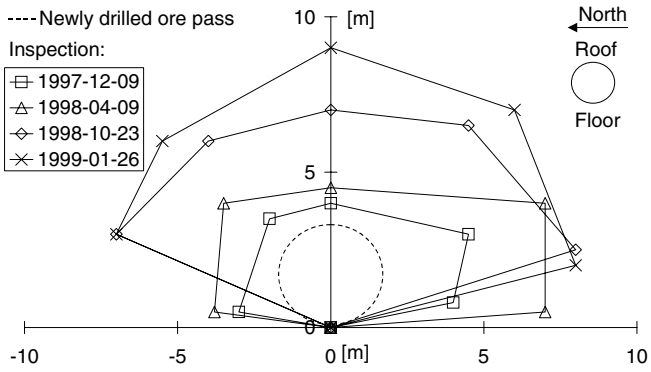

Figure 3 Increase in ore pass width as measured from ore pass inspections.

Analysis

Approach

Analyses have been used in conjunction with ore pass data and observations to identify and quantify failure mechanisms and governing factors for rock failures in ore passes. The analyses were focused on the primary failure mechanisms—i.e., those that cause the initial failure modes—but continued failure development was also studied using numerical modeling. Calculations were conducted for typical ore pass geometries and for a set of parameter combinations representing different geology and rock conditions to cover the varying site conditions in the different groups of ore passes. The conducted analyses were:

- analysis of stresses around ore passes,
- analysis of failure development,
- analysis of structurally controlled failures, and
- analysis of wear and boulder impact in ore passes.

In this paper, results from the stress analysis and the analysis of failure development are presented.

Stress analysis

Stress-inducted failures were analyzed using a global-local modeling approach. A global model was used to calculate the stresses induced by sublevel caving. Neither ore passes, nor drifts or cross-cuts, were included in the global model (Figure 4). The calculated stresses from the global model were used as input data to a local model in which the ore pass geometry was simulated.

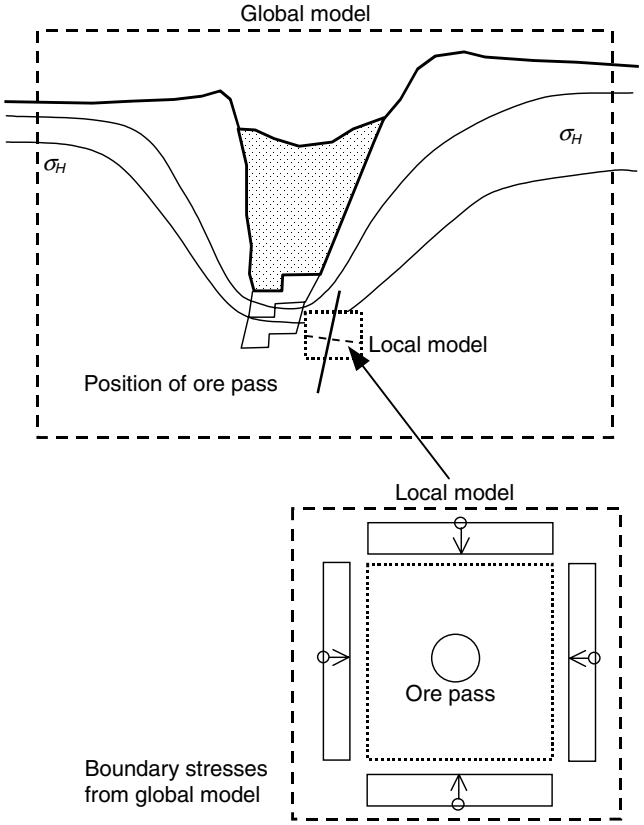

Figure 4 Global-local stress analysis.

The global model was constructed for a vertical cross-section perpendicular to the orebody strike, using the two-dimensional finite-difference program *FLAC* (Itasca, 2000). Stresses were calculated for nine mining steps, corresponding to different positions (depths) of the sublevel caving front, from level 713 m to level 993 m. Both linear-elastic and elastic-plastic analyses were performed. However, calculated stresses in the position of the ore passes showed only small differences between the two types of analyses. Only results from the linear-elastic model were thus used as input to the local model.

In the local model, a two-dimensional cross-section perpendicular to the ore pass axis was studied. The circular geometry enabled the use of an analytical model, under the assumption of complete plane strain conditions. This

assumption is valid along the ore pass, with the exception of the areas closest to the active mining level and around the intermediate level (cf. Figure 2). Using the analytical model, stresses were calculated for the critical points on the ore pass boundary: (i) in the center of the ore pass wall, and (ii) in the center of the ore pass roof. These calculations were carried out along the entire ore pass (for an average orientation) and for all analyzed mining steps (from the global model).

The calculated stresses were consistently highest in the ore pass walls. An example is shown in Figure 5. This finding is as expected, since the largest stress redistribution occurs perpendicular to the orebody (stresses being forced under the sublevel caving area), which, in turn, result in stress concentrations on the opposite sides of a circular cross-section. Furthermore, the stress increase due to the construction of the ore pass is dramatic, compared to both the virgin (pre-mining) stress and the stress change solely due to sublevel caving (cf. Figure 5).

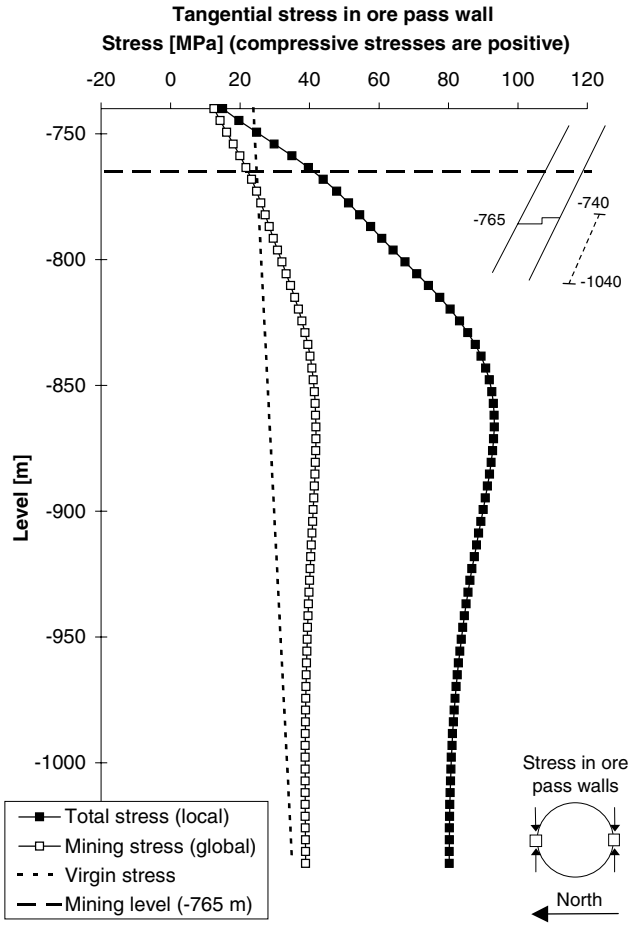

Figure 5 Calculated tangential stress in ore pass walls, compared with virgin stress and induced stress from sublevel caving only, for mining to the 765 m level.

The stress redistribution due to the sublevel caving results in the largest stresses occurring at a relatively large distance from the active mining level. In general, the largest stresses were found at approximately 100 m vertical distance from the mining level. Taking Figure 5 as an example, the largest stress in the ore pass wall occurs around the 850 m level, while active mining still at the 765 m level. These observations are also in good agreement with observations showing at what level (in the ore pass) the first instabilities occurred.

Calculated stresses were also compared with failure criteria for the rock mass. Both the Hoek-Brown criterion (Hoek & Brown, 1997) and the extension strain criterion (Stacey, 1981) were used**.** These comparisons showed that stress-induced failures could be expected in the ore pass walls even for rock of good quality and high strength. When mining continues downward, the high-stressed areas are de-stressed, which facilitates fall-outs of failed and damaged rock.

Analysis of failure development

The development of failure in the ore passes was studied in a local model using *FLAC* and for a cross-section perpendicular to the ore pass axis. Only elastic-plastic calculations were performed with strength parameters (cohesion and friction angle) determined through linear regression of the Hoek-Brown failure criterion (Hoek & Brown, 1997) and with input data from rock mass classification and laboratory tests. Two sets of strength data were used, corresponding to different rock types in the mine. Analyses were conducted both for an initially intact ore pass, as well as for an ore pass with a groove in the floor. Boundary stresses were taken from the global model.

The calculations showed that for high-strength rock, only a very thin failed zone developed around the ore pass. This damaged portion can, however, result in slabbing and minor fall-outs, in particular when rock is being transported in the ore pass. For low-strength rock, extensive shear failure can be expected in the ore pass walls.

For the case when a groove has formed in the floor of the ore pass (due to wear and boulder impact), the extent of shear failure is significantly increased. The groove functions as a kerf and facilitates new failures in the ore pass walls (Figure 6). Simulation of the continued failure development showed that this failure is highly progressive with no stable geometry being achieved.

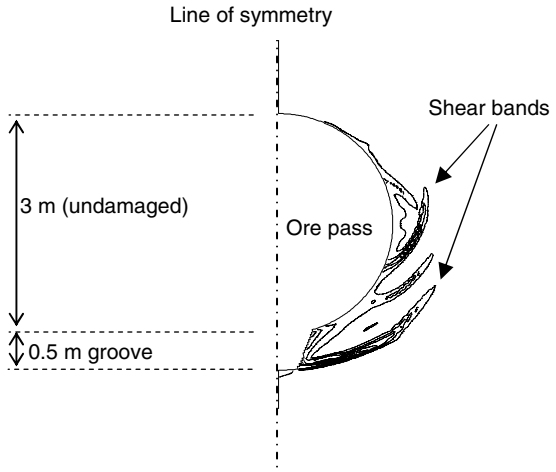

Figure 6 Calculated shear strains around an ore pass with a groove (model is symmetric with respect to the vertical axis).

Causative model

Failure mechanisms and controlling factors governing failure and damage were identified from observations and analysis. The most important controlling factors were found to be: (i) rock conditions, (ii) stress state, and (iii) wear and impact from boulders. The dominating failure modes as well as the failure mechanisms and controlling factors governing these are summarized in Table 1.

Table 1 Failure modes, failure mechanisms, and controlling factors for failures and damages in ore passes.

Failure mode	Mechanism	Controlling factors
Slabbing Width increase	Spalling	High stress High-strength, brittle rock
Groove in floor Height increase	Wear and impact from transported rock	Wear Boulder impact
Width increase Increase in width and height	Groove and shear failure in ore pass walls	Stress state Wear and impact Non-brittle rock
Block fall-outs Height increase	Wedge failures along joints	Pre-existing joints Stress state
Fall-outs on the intermediate level	Wedge failures along joints Boulder impact	Pre-existing joints Geometry and construction of intermediate level

Several potentially influencing factors were judged to have very little effect on the ore pass stability. This included e.g., installed cable bolting, vibrations from discharging of rock into the ore pass, and vibrations from nearby blasting. It should also be noted that for existing ore passes, only the action of wear and boulders impact is possible to control (e.g., by reducing boulder size).

Based on these findings, the failure modes were grouped by controlling factors, as shown in Figure 7. In this case, the effect of wear and boulder impact is expressed as tonnage transported through the ore pass. In addition to the failure modes shown in Figure 7, fall-outs on the intermediate level can occur for all rock conditions. The lack of continuous follow-up of ore pass conditions inhibited a more quantitative assessment of the influence of each controlling factor.

The failure development, from initial instabilities to extensive fall-outs and damage to ore passes, was found to be complex and governed by several controlling factors. In some cases, several failure mechanisms interacted, thus resulting in several simultaneously occurring failure modes. One example is the initiation of a groove in the floor of the ore pass, which, in turn, act as a kerf for shear failure in the ore pass walls, as well as tensile failure around the groove. The failure development is highly progressive. In this case, the observed failure modes change from an initial height increase to a width increase and/or simultaneous increase in height and width.

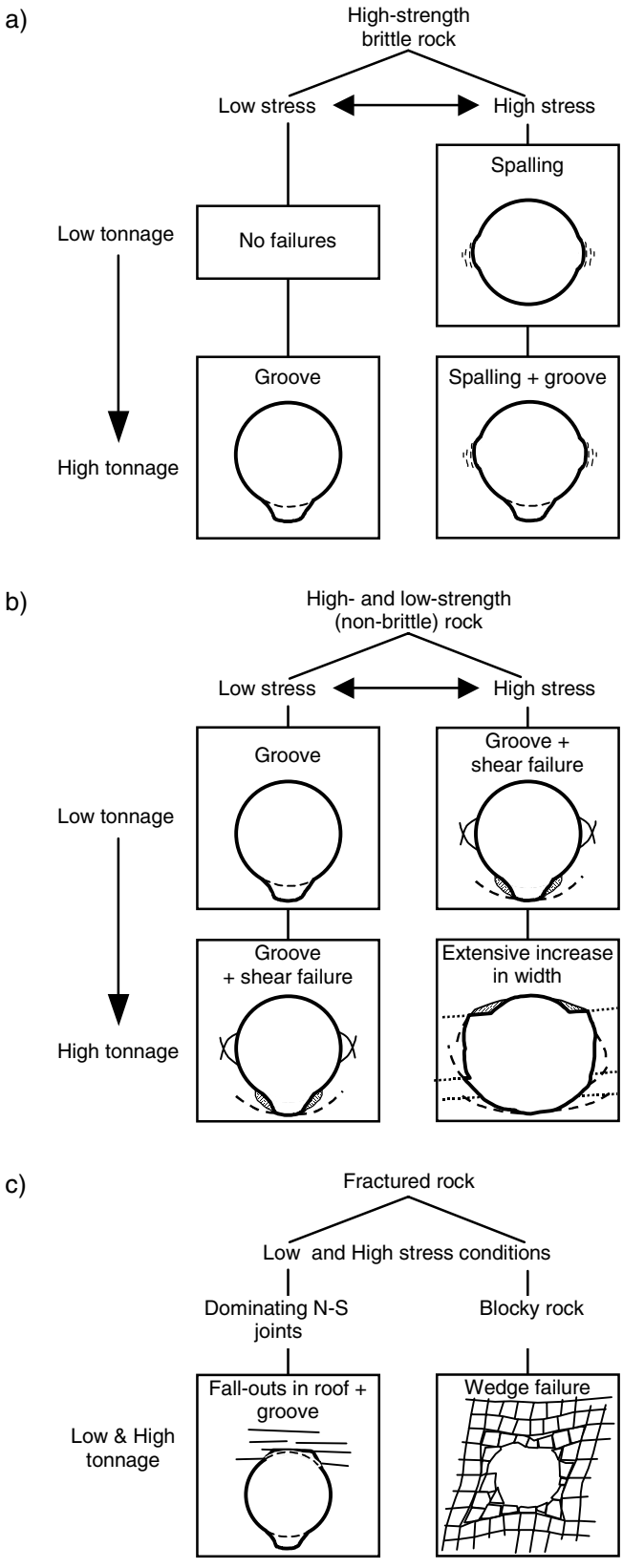

Figure 7 Failure modes grouped by controlling factors; a) high-strength, brittle rock conditions, b) non-brittle rock conditions, and c) fractured rock conditions.

The extent of failure is thus governed by both the stress state and the amount of transported rock in the ore pass. For high-strength rock, shear failure does not develop in the ore pass walls and the ore pass only exhibits damage in the form of the groove in the floor. Minor spalling and slabbing failure may also occur for these rock conditions. Structurally controlled wedge failures may, or may not, become progressive depending of rock conditions and stress state. The high compressive stress in the ore pass walls "clamp" blocks, thus reducing the possibilities of fall-outs in sparsely jointed rocks. However, once the rock is destressed and confinement is reduced (close to the active mining level or at the intermediate level) larger fall-outs may occur. Larger structurally controlled failures also occur in heavily jointed rock masses.

The causative model (Table 1, Figure 7) was used for developing a prognosis of future ore pass stability, and for making recommendations on remedial measures to improve stability conditions. The prognosis showed that further failures can be expected in a number of ore passes. The reliability of the prognosis varies, depending on available input data. Higher reliability in failure predictions can be achieved through improved follow-up of ore pass conditions.

Conclusions and recommendations

The following conclusions could be drawn:

- Compilation of ore pass and inspection data enabled identification of the most common failure modes in the ore passes.
- Stress analysis using a global-local modeling approach worked satisfactorily. The approach allowed quantification of stress level for different mining stages and at every point along the ore pass, with exception for the area close to the active mining level and the chute.
- Five failure mechanisms were identified, which describe the majority of the observed failure modes. The failure development is often complicated and highly progressive. The initiation of the groove in the floor is an important factor, since the change in geometry facilitates the initiation of new failures, which can result in progressive, large, failures.

Based on the project results, the following recommendations were formulated:

- Improved follow-up of ore pass stability is required to better resolve the impact of controlling factors and failure development. This can be achieved through more frequent ore pass inspections, improved measurement method, and systematic compilation of measurement data and observations.
- To improve the stability of drilled ore passes the following is suggested: (1) additional rock reinforcement of the intermediate level, (2) installation of grizzlies for all ore passes, and (3) maintaining a high ore pass balance (ore pass filled with rock). These proposals are judged cost-effective and simple to implement, and should result in longer life (before total renovation) of the ore passes.
- Future work should focus on (1) improving the knowledge on geological and geomechanical conditions around the ore passes, (2) quantifying the influence of wear and impact, and (3) studying alternative methods for ore pass stabilization, e.g., de-stressing.

Acknowledgements

The work presented in this paper is part of a larger project concerned with ore passes for the KUJ 1045 main level in Kiirunavaara. The project was run and financed in full by LKAB with hired consultants for different stages of the project. Mr. Daniel Hrafnkelsson was project chief with Dr. Carlos Quinteiro as project manager. The project group also comprised Mr. Börje Johansson, Mr. Lars Malmgren, Mr. Bert-Ola Sundkvist and Mr. Thomas Savilahti (all with LKAB). All project members are hereby gratefully acknowledged for fruitful cooperation. The authors also wish to acknowledge Mrs. Christina Dahnér of LKAB for supplying a large portion of the fundamental data for this work. Finally, the translation of abstracts to French and German by Mr. Emmanuel Henry and Mrs. Bettina Wittke-Schmitt, respectively, are thankfully acknowledged. Mr. Peter Lundman was with the consulting company Petro Bloc AB during the project, which is hereby acknowledged.

References

DAHNÉR, C. 2000. Bergschakt KUJ 1045: Statusrapport. LKAB internal report, 2000-09-28 (in Swedish),

HOEK, E. & BROWN, E. T. 1997. Practical estimates of rock mass strength. Int. J. Rock Mech. Min. Sci., Vol. 34, pp. 1165-1186.

ITASCA. 2000. FLAC Version 4.0. Manual. Minneapolis: ICG.

STACEY, T. R. 1981. A simple extension strain criterion for fracture of brittle rock. Int. J. Rock Mech. Min. Sci. & Geomech. Abstr., Vol. 18, pp. 469-474.

Equation Chapter 1 Section 1Staub, I., Fredriksson, F., Christiansson, R. A theoretical model for the characterisation of rock mass mechanical properties ISRM 2003–Technology roadmap for rock mechanics, South African Institute of Mining and Metallurgy, 2003.

A theoretical model for the characterisation of rock mass mechanical properties – Application at the Äspö HRL, Sweden

Isabelle Staub*, Anders Fredriksson*, Rolf Christiansson**
Golder Associates*, SKB**

A theoretical model based on DFN models and 2D DEM numerical modelling has been developed for evaluating the rock mass mechanical properties. The description of the methodology is non-site related and can be applied in any site for this type of characterisation. The methodology was developed in the frame of the Site Investigation programmes for a Deep Repository for spent fuel in Sweden, and validated on sets of data coming from the Äspö Hard Rock Laboratory.

Un modèle théorique base sur des modèles probabilistiques de réseaux de fractures et sur un modèle numérique DEM 2D a été développé dans le but de déterminer les propriétés mécaniques de la masse rocheuse. La méthodologie développée peut être appliquée à tout type de site pour ce genre de caractérisation. Le modèle a été élaboré dans le cadre des programmes de recherche d'un site d'enfouissement des déchets nucléaires en Suède, et validé par une application au laboratoire de recherche souterrain à Äspö.

Ausgehend von DFN-Modellen und 2D DEM numerischen Modellierungen wurde ein theoretisches Modell für die Auswertung von mechanischen Eigenschaften von Fels entwickelt. Die Methodikbeschreibung ist nicht standortspecifisch sondern kan überall für diesen Typ von Standordkarakteriserung angewendet werden. Die Methodik wurde in Schweden im Rahmen der Standortuntersuchungsprogramme für die Endlagerung von verbrauchten Brennelementen entwickelt und ist mit Hilfe von Daten des Äspö Hard Rock Laboratory validiert worden

Introduction

The methodology is developed in the frame of SKB's site investigation programmes for a Deep Repository for spent fuel and meant to be used for the rock mass mechanical characterisation of the sites. The model shall describe the initial stresses and the distribution of rock mechanical properties such as deformation and strength properties for the intact rock, for the fractures, for the deformation zones and for the rock mass viewed as a unit consisting of intact rock and fractures. The strategy established for the development of a Rock Mechanics Site Descriptive Model is presented in Andersson et al., 2002.

The basis of the theoretical approach is to determine the mechanical properties of the rock mass, in any potential site. The methodology is based on Discrete Element Method for the modelling of behaviour of rock masses. The rock mass is modelled as a discontinuous geometry in which contacts between blocks are fractures. The input parameters required for the model are the fracture geometry, and the mechanical properties of fractures and intact rock.

Overview of the methodology

Definition of the fracture network

A Discrete Fracture Network (DFN) model was chosen to simulate the fracture network, and the FracMan® software is used for generating fractures in three dimensions within a given rock volume. The definition of input parameters and the theoretical background of DFN models as developed in FracMan® are presented in Dershowitz *et al.*, 1998.

Considering the large number of fractures that are generated in a DFN volume (from 1000 to more than 15000 for a 30-m cube) it is at the moment technically difficult to do 3D simulations with a realistic network of discrete disc-shaped fractures. However it was determined fully possible to realise the modelling of the mechanical behaviour of a fractured rock mass in two dimensions considering rock sections of different directions. For this purpose, the 2D numerical code UDEC was selected as calculation tool.

This implies that the three-dimensional Discrete Fracture Network generated by FracMan® is transferred to tow-dimensional fracture trace sections to fit UDEC. An example of a 2D section is presented in Figure 1.

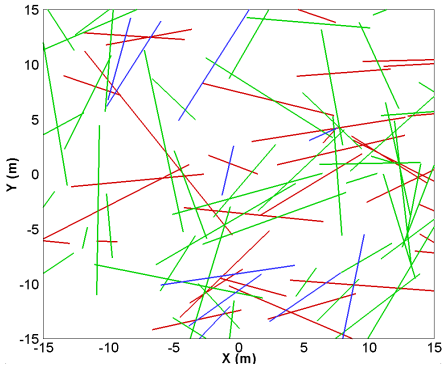

Figure 1. 2D fracture trace sections; 3 fracture sets

The DFN model size must be set large enough to avoid any truncation of the fracture trace at the boundaries of the trace planes.
To avoid shear stresses in the numerical model the fracture traces are obtained in planes aligned with the in situ principal stresses at the investigated site.
The 2D fracture traces are integrated in the single rock block model. The numerical coding of UDEC implies that parts of fractures that terminate in the rock after intersection with another fracture, and fractures that are isolated in the rock mass, are removed from the model during the meshing and the generation of the blocks. The block model resulting from the processing of the 2D fracture trace section presented in Figure 1 is illustrated in Figure 2.

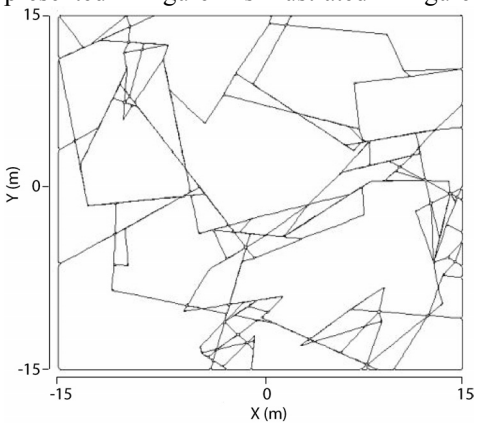

Figure 2. Block model built in UDEC from the 2D fracture trace section shown in figure 1

When the block is generated, mechanical properties are assigned to the intact rock and to the fractures. The constitutive models chosen to simulate the behaviour of the material are the Mohr-Coulomb plasticity model for the intact rock, and the Barton-Bandis model for the fractures. Specific mechanical properties can be assigned for each identified fracture set.

The numerical model

Description of the loading test

The numerical model simulates a plain strain-loading test of the rock mass with constant confining stresses during testing (Figure 3). The vertical loading is applied to the model beyond the elastic behaviour of the components of the model (rock material and fractures) so that the estimation of the rock mass strength can be assessed. First, the in situ stress conditions are reproduced in the UDEC model by means of the IN SITU command, with consideration to the actual intensity of stresses. The State of Stress is considered in 3D in the model, as in situ stresses in the out-of-plane direction must be taken into account to avoid failure in this plane (Figure 3). Then confining stresses are applied during the loading test. Different values of confining stresses were applied for the same set-up of parameters, simulating (Figure 4):

- (I) Plain strain loading test on the undisturbed rock mass,
- (II) Plain strain loading test at the proximity of a tunnel.

In the latest case an intermediate unloading numerical step is required to reach a confining stress of 75% of the in situ horizontal stress (Figure 3).

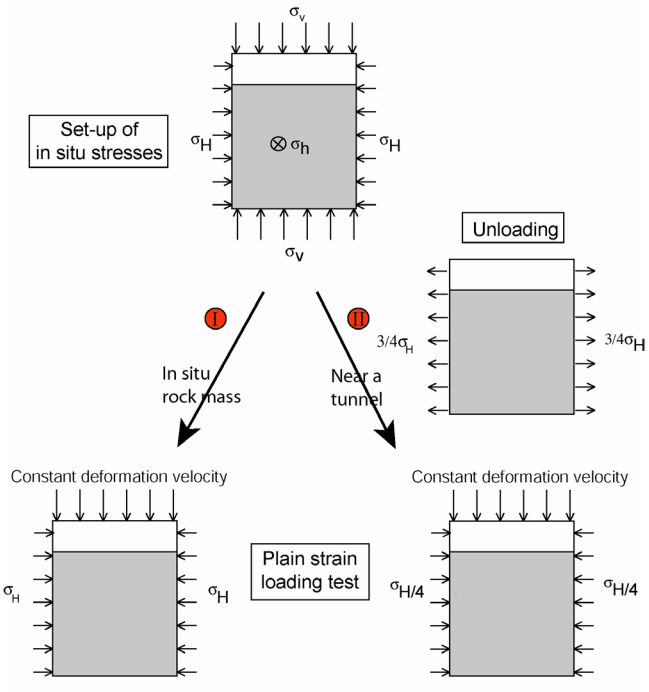

Figure 3. State of Stress for the plain strain loading test

Even if the stress boundary conditions are such that the model is in an initial force-equilibrium state before alteration, the equilibrium state is checked before performing vertical loading.

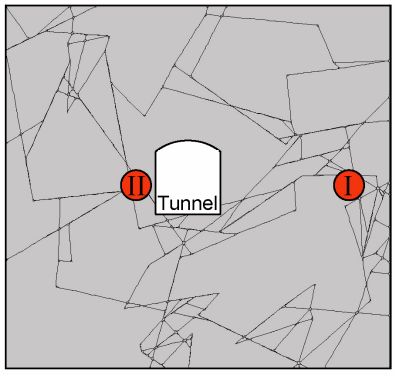

Figure 4. General stress state in the rock mass in relation to an excavation; (I) undisturbed rock mass, (II) rock mass at the proximity of the tunnel

The rock mass is loaded by means of a top loading block that is pushed down with a constant velocity (Figure 3). Applying the vertical loading by means of a top block generates a better distribution of stresses and deformation for measurements in the model under testing. If not using a top block, several monitoring profiles in the 30-m rock blocks had been required. The deformation modulus of the top loading block is set about 1000 times greater than the

deformation modulus of the intact rock in order to make it stiff and non deformable. The interface between the loading block and the rock mass block is assumed to have no friction.
Applying loading by means of computational cycles limits the influence of deformation velocity on the results.
Two different set-ups are used for applying confining stresses:

- Confining stresses are applied on both vertical sides (Figure 5-a), and one point is fixed on the bottom boundary; this set-up simulates conditions valid for the characterisation of the undisturbed rock mass in the in situ conditions.
- Confining stresses are applied on one vertical side (Figure 5-b), the other vertical side is fixed in the horizontal direction, and the bottom boundary is fixed in the vertical direction. This set-up represents conditions around a tunnel.

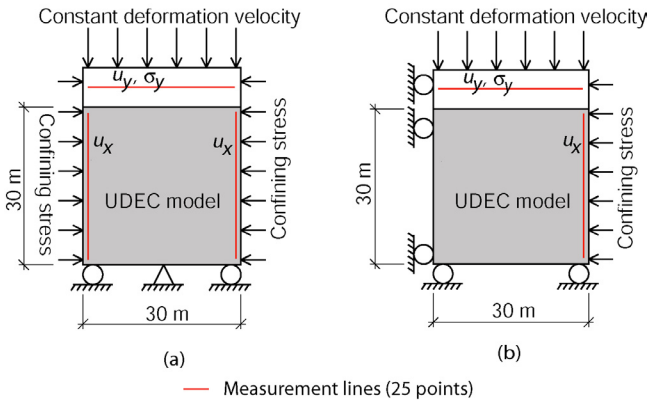

Figure 5 Set-up of the numerical UDEC model

Estimation of the rock mass mechanical properties

The vertical stress, σ_y, and horizontal deformation, u_x, are recorded as a function of the vertical deformation, u_y, at the end of each computational cycle. The parameters are monitored along profiles consisting of 25 monitoring points that are equally distributed along measurement lines (Figure 5). The value at a computing node is attributed to the nearest monitoring point on the reference lines, and the mean value of the monitored variable on the 25 points is then calculated at each loading step. The Poisson's ratio, ν_m, and the deformation modulus, E_m, of the rock mass are calculated according to the following equations:

$$\nu_m = \frac{1}{1+\left(L_x \cdot u_y\right)/\left(L_y \cdot u_x\right)} \quad [1]$$

$$E_m = \left(1-\nu_m^2\right)\cdot \Delta\sigma_y \cdot L_y/u_y \quad [2]$$

where L_x and L_y are the length over which u_x and u_y are monitored. Equations [1] and [2] are derived from Hooke's law for plain strain loading.
The rock mass strength has been determined following the Mohr-Coulomb linear failure criterion expressed as:

$$\sigma_1 = \sigma_3 \cdot \left(1+\sin\phi\right)/\left(1-\sin\phi\right) + 2\cdot c\cdot \cos\phi/\left(1-\sin\phi\right) \quad [3]$$

where ϕ is the friction angle and c the cohesion of the intact rock.
The Mohr-Coulomb envelope is defined by the pair of principal stresses at failure, σ_{1a}/σ_{1b} and σ_{3a}/σ_{3b}, obtained for the two states of confining stresses referred as to a and b.
With respect to the Mohr-Coulomb failure criterion, the friction angle, ϕ_m, the uniaxial strength, σ_{cm}, and the cohesion, c_m, of the rock mass are calculated. The following equations are used (from Hoek and Brown, 1997):

$$\phi_m = \arcsin\left(k-1/k+1\right) \quad [4]$$

$$\sigma_{cm} = \sigma_{1b} - k\sigma_{3b} \quad [5]$$

$$c_m = \sigma_{cm} \cdot \left(1-\sin\phi_m\right)/2\cos\phi_m \quad [6]$$

$$\text{where } k = \left(\sigma_{1a}-\sigma_{1b}\right)/\left(\sigma_{3a}-\sigma_{3b}\right) \quad [7]$$

Computation strategy

Sensitivity analysis on the model

The validity of the model was checked by running some benchmark tests. Moreover, sensibility analysis have been conducted on some rock block models for studying the dependency of mechanical properties to the in situ stresses, the influence of boundary conditions, rock material and joint constitutive models used to simulate the behaviour of intact rock and fractures, domain size and anisotropy. The influence of the automatically discarded fractures has also been studied.
2D and 3D numerical simulations were also carried out on a simplified model for determining the influence of evaluating the mechanical properties of the rock mass in 2D. These calculations show that the 2D numerical model presents a very good agreement with the 3D model (Figure 6) when the 2D sections are in the axis of the most unfavourable stability situation and of the most important deformation in 3D.

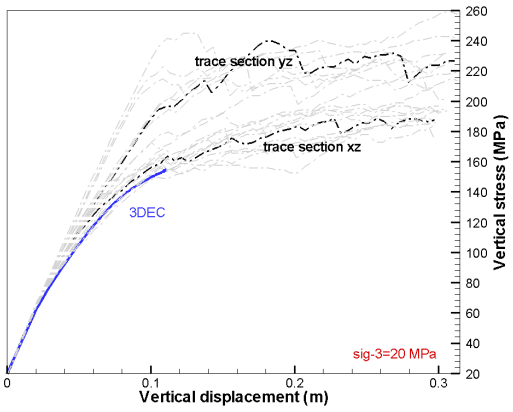

Figure 6 Calculated vertical stress–vertical deformation curves. *The 3DEC curve is for a triaxial loading situation, and the UDEC curves for plain strain loading*

Data uncertainty and spatial variability

The spatial variability can be separated into the spatial variability of the geometry of the fractures, the spatial variability of the rock type, and into the data uncertainty and spatial variability of the parameters describing the properties of the intact rock and the fractures.
The data uncertainty of the input parameters for the DFN model is managed through means and standard deviation of statistical functions. The data uncertainty and spatial variability of the material parameters for a specific rock type are expressed by the measured mean value and the standard deviation. A normal distribution is assumed.
A handy way to get the statistical parameters for a model with many input parameters that can be expressed in statistical terms is to run Monte Carlo simulations. One set of parameters is randomly chosen according to the statistical distributions of the parameters and the response of the model with these parameters is calculated. By running a lot of simulations and by treating the outcome in a statistical way the mean and standard deviation of the outcome from the model can be estimated.
In order to minimise the number of numerical calculations with UDEC a simplified way of doing Monte Carlo simulations has been used according the following (Staub et al., 2002):

- The influence of the spatial variability in the 3D DFN model is estimated by running 20 Monte Carlo simulations on the input parameters for the model. 20 different 3D models are then created, and the 2D trace section files are extracted for each of these models. The variability is then statistically determined from the results of the computations.
- The influence of one specific mechanical parameter on the outcome from the model is calculated by keeping all other parameters constant. Using the calculated influence of the parameter on the outcome of the model in a simple Monte Carlo simulation in Excel, the influence of the specific parameter distribution can be added to the influence of all parameters.
- By using the calculated distributions of the properties for each rock type and then combining the different rock types with respect to their measured percentage, the statistical parameters for the "combination" are estimated.

Application to SKB site investigation programme

In order to enlighten the assets and potential limitations / needs to improvements of the methodology, the theoretical approach was tested on a limited set of data on two models designed at the Äspö Hard Rock Laboratory (HRL) in Sweden. The description of the Test Case is presented in Hudson ed., 2002.

Presentation of the domains of application

The large model is a box of 550-m sides from 50 m above the surface down to 500 m, and the detailed model is defined by a box located at depth -380 to -500 m. In the large model the units were delimited by major deformation zones identified in the model. The detailed model was screened in 30·30·30 m cubes, which divide the box in 4 depth layers and 420 cubes. The scale of the cubes is defined to capture the processes around the excavation. In the following focus is made on the detailed model.

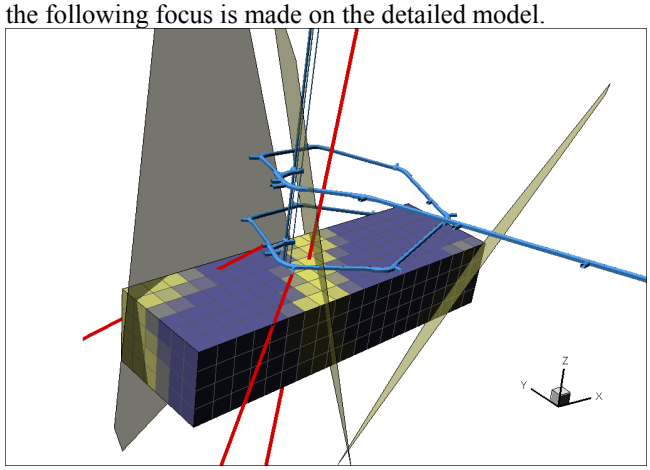

Figure 7. The detailed model, with fracture zones, boreholes and tunnel system, and the 30 ·30·30 m cubes

Two different types of "rock units" were defined: 1) the "ordinary rock units" identifying the fractured rock mass, and (2) the "deformation zone units" identifying the deformation zones. Three major deformation zones cut through the model (Figure 7). Due to the uncertainty of the width and undulation of deformation zones both unit types might be assigned to one cube. The potential "deformation zone units" appear in lighter grey tones in Figure 7.

Specific assumptions made for the Test Case

Specific assumptions related to data availability and model definition for the Test Case need to be determined.
Assumptions are to be made on the geometrical model and for the assignment of intact rock and fracture mechanical properties used as input to the numerical model. The confidence in input data varies in the model and is high where predictions are supported by local data (a borehole goes through a cube) and low when the predictions are the results of guesswork (all other cubes).
The same DFN model is assigned to all cubes, but adjustments might be made in the cubes with high confidence as regards to data provided by the borehole in the referred cubes. The mechanical properties of intact rock are considered constant for one rock type in the 30-m cube volume. Mechanical properties of fractures are constant on the whole fracture plane, and kept constant for each fracture set whatever the rock type. Special assumptions on fracture networks and mechanical properties were made for the determination of mechanical properties in deformation zones. The rock type distribution assigned to low confidence cubes is determined from a statistic analysis of rock type distribution along the boreholes inside the large model. The rock type distribution for high confidence cubes is determined from boreholes data inside the 30-m cube.

Input data

The sets of data used for the Test Case are mainly coming from 3 boreholes, one subvertical and two inclined boreholes (Figure 7). Data from laboratory tests, geological surface mapping and geophysical measurements were also available.

Intact rock

Table 1 presents the mean value of input parameters used to model the behaviour of intact rock in UDEC.

Table 1. Input parameters for the intact rock, according to the Mohr-Coulomb material model; mean value

	D (kg/m^3)	K (MPa)	G (MPa)	c (MPa)	ϕ (°)	ψ (°)	σ_{ti} (MPa)
Småland granite	2.64	39e3	25e3	37.7	45	0	12.8
Aplite	2.67	38e3	26e3	47.2	45	0	15
Greenstones	2.96	31e3	21e3	23.8	45	0	8
Granodiorite	2.75	52e3	28e3	31	49	0	14.8

with D: density, K: bulk modulus, G: shear modulus, c: cohesion, ϕ friction angle, ψ dilation angle and σ_{ti} tensile strength of the intact rock.

Fractures

Fracture statistics used for the DFN model are extracted from Hermansson et al., 1998 (Table 2). A truncation length of 2m has been defined for the DFN model as small fractures are discarded in UDEC.

Table 2. Input parameters used for the DFN model

Parameter		Value	Comments
Set 1			
Orientation	Mean pole trend and plunge (°), dispersion	348.2, 4.2, K=8.69	Fisher model
Intensity (P32, m^2/m^3)		0.23	
Fracture size, radius (m)	Mean, Std deviation	4 / 2	Lognormal distribution
Set 2			
Orientation	Mean pole trend and plunge (°), dispersion	46.4,7.4, K=10.50	Fisher model
Intensity (P32, m^2/m^3)		0.7	
Fracture size, radius (m)	Mean, Std deviation	5 / 1	Lognormal distribution
Set 3			
Orientation	Mean pole trend and plunge (°), dispersion	142.8, 63.7, K=8.99	Fisher model
Intensity (P32, m^2/m^3)		0.11	
Fracture size, radius (m)	Mean, Std deviation	4 / 2	Lognormal distribution

Table 3 presents the mean value of input parameters assigned to fractures in UDEC. 3 different values are given for the friction angle, which correspond to the values used for the sensitivity analysis.

Table 3. Input parameters for the fractures, according to the Barton-Bandis joint constitutive model

	K_n (MPa/m)	K_s (MPa/m)	ϕ_r (°)	σ_c (MPa)	JRC_0	JCS_0 (MPa)	L_0 (m)	a_{jn} (mm)
Greenstones	44e3	29.9e3	25/30/35	115	12	92	5.51e-2	0.58
Granodiorite	44e3	29.9e3	25/30/35	214	9.3	170	5.51e-2	0.58
Småland granite	44e3	29.9e3	25/30/35	182	8.2	146	5.51e-2	0.58
Aplite	44e3	29.9e3	25/30/35	228	9.1	180	5.51e-2	0.58

with K_n joint normal stiffness at σ_n=23 MPa, K_s joint shear stiffness at σ_n=23 MPa, ϕ_r residual friction angle, σ_c intact rock uniaxial compressive strength, JRC_0 Lab-scale Joint Roughness Coefficient, JCS_0 Lab-scale Joint Compressive Strength, L_0 Lab-scale joint length, and a_{jn} joint aperture at zero normal stress. σ_n=23 MPa is the normal stress applied during the plain strain loading and is expected to be valid at the deepest level in the detailed model (-470/-500 m).

In situ stresses

The state of in situ stresses is analysed in Hakami et al., 2002, and given in Table 4. Orientation of in situ stresses is assumed to be constant with depth.

Table 4. Magnitude and orientation of in situ stresses

		σ_H (MPa)	σ_h (MPa)	σ_v (MPa)
Magnitude in relation to depth	Level 1 (-380/-410m)	19	10.7	10.2
	Level 2 (-410/-440m)	20.2	11.5	10.7
	Level 3 (-440/-470m)	21.3	12.3	11.2
	Level 4 (-470/-500m)	22.4	13.1	11.7
Orientation	Strike (°)	136	226	0
	Dip (°)	0	0	90

Modelling

The simulations have been run applying the general methodology as described above. In the following a description of the application of the numerical modelling strategy to the Test Case is given.

Computations and data uncertainty

The simulations were first carried out on rock block models constituted of homogeneous rock types. The variation of the in situ and confining stresses in the numerical model accounted for the different depth levels in the 30-m model. To assess the influence of variation of the fracture friction angle on the outcome of the model, at one depth level, 20 simulations were run on ϕ_r=30° and then 1 simulation for respectively ϕ_r 25 and 35°. The 20 simulations represent the 20 realisations of the DFN model. Using the calculated influence of the parameter on the outcome of the model in simplified Monte Carlo simulations, the influence of all parameters on the output data can be combined.
Then for the same depth level, the same set-up of variation of parameters and number of simulations has been applied to conduct loading tests at a reduced horizontal stress (state II).

Estimation of rock mass mechanical properties of the model cubes

The rock models in UDEC were run assuming 100% of the same rock type, and the rock mass mechanical properties determined for homogeneous cubes. However, the cubes are lithologically heterogeneous, and the percentage of occurrence of each rock type in a cube is estimated from borehole core mapping. This distribution is then used in a simplified Monte Carlo simulation using a combination of Probability Density Functions to calculate the output from the lithologically homogeneous models in a way to represent the probability of occurrence of the different rock types in the cubes (Figure 8).

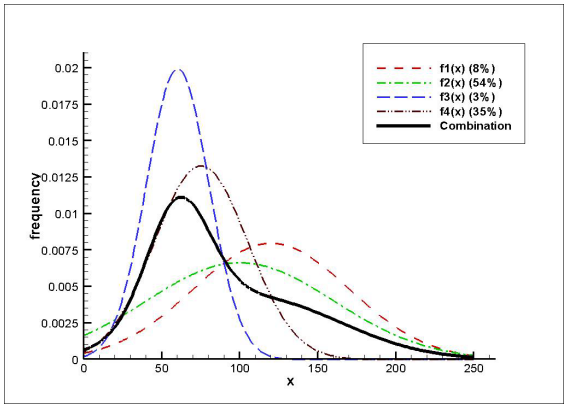

Figure 8. Model used for combination of parameter distribution for heterogeneous rock blocks

f1(x) to f4(x) are the distributions for four different rock types, x being the mechanical parameter to be determined for the heterogeneous cube. Into brackets are the proportions of each rock type in a specific cube. This methodology provides a good integration of the volumetric occurrence of rock types. Nevertheless the mechanical behaviour is subjected to the spatial distribution of rock types, which is very difficult to assess especially for igneous rocks.

Deformation modulus, Poisson's ratio, uniaxial compressive strength, friction angle and cohesion of the rock mass are determined in each cube of the model, for the 4 depth levels. The results will be different for the 9 cubes of high confidence but will be identical for all other cubes at a same depth level. The rock mass mechanical parameters will also be affected if the cubes are identified as "deformation zone units". Table 5 illustrates the Young's modulus determined for cubes of low confidence. Complete modelling results are presented in Staub et al., 2002.

Table 5. Young's modulus for cubes of low confidence

		E_m (GPa)			
		σ_H [2]		$\sigma_{H/4}$	
Cube ID	Rock unit Type[1]	Mean	Std Dev.	Mean	Std Dev.
Cubes without zones	1				
Depth level 1 (-395 m)	1	40.3	4.57	18.8	5.7
Depth level 2 (-425 m)	1	41	4.82	23.3	5.9
Depth level 3 (-455 m)	1	41.7	5	27.6	6.3
Depth level 4 (-485 m)	1	42.5	5.08	31.6	6.66
Cubes with zone EW-1	2	13	1.56	6.8	1.43
Cubes with zone NE-1	2	4.5	0.4	2.4	0.5
Cubes with zone NE-2	2	35.4	4.35	24.5	5.15

[1] 1: "ordinary rock unit"; 2: "deformation zone unit"

[2] The values of σ_H are related to the depth level of each cube

Discussions and conclusions

The theoretical approach developed in this study provides a near-field rock mechanical model for rock masses that can be applied in the undisturbed rock mass or at the proximity of an excavation. The model is based on generic site investigation Discrete Fracture Network models and on a 2D Discrete Element Method numerical code. The spatial variability of input parameters and its influence on the outcome of the model is accounted for by means of Monte Carlo simulations.

The computations of the mechanical properties of the rock mass are based on multiple stochastic realisations in order to reflect the variability and possible distribution of input parameters to the model and permit a statistical analysis of the results.

The Test Case provided an opportunity to test the methodology and improve the theoretical approach by smoothing out problems that might appear when applying a general approach to a specific site.

The Test Case especially enlightened the need of better understanding of fracture patterns in deformation zones, and of focus on data analysis. Method of dealing with spatial variability and data uncertainty need to be further developed.

References

ANDERSSON, J., CHRISTIANSSON, R. and HUDSON, J. Site Investigations. Strategy for Rock Mechanics Site Descriptive Model. SKB, TR-02-01, Stockholm, dated May 2002.

DERSHOWITZ, W.S., LEE, G., GEIER, J., FOXFORD, T., LAPOINTE, P. and THOMAS, A. FracMan Version 2.6 Interactive Discrete Feature data Analysis, Geometric Modeling, and Exploration Simulation, user documentation, Report 923-1089, Golder Associates Inc., Seattle, Washington, dated 1998.

HAKAMI, E., HAKAMI, H. and COSGROVE, J. Strategy for Development of a Descriptive Rock Mechanics model, Development and testing of an approach to modelling the State of Stresses. SKB, R-02-03, Stockholm, dated May 2002.

HERMANSSON, J., STIGSSON, M. and WEI, L. A Discrete Fracture Network model for the Äspö Zedex tunnel section. SKB, PR HRL-98-29, Stockholm, dated 1998.

HOEK, E. and BROWN E.T. Practical estimates of rock mass strength. Int. Jl of Rock Mech. And Min. Sc. Vol. 34, No 8, pp.1165-1186, dated 1997.

HUDSON, J. A. ed. Strategy for a Rock Mechanics Site Descriptive Model. A test case based on data from the Äspö HRL. SKB, R-02-04, Stockholm, dated June 2002.

STAUB, I., FREDRIKSSON, A. and OUTTERS, N. Strategy for a Rock Mechanics Site Descriptive Model. Development and testing of the theoretical approach. SKB, R-02-02, Stockholm, dated May 2002.